Combined EFD and CFD Approach using the Form Factor for Full Scale Ship Powering Prognosis

Auteur : Quintuña Rodríguez, María Tadea
Promoteur(s) : Rigo, Philippe
Faculté : Faculté des Sciences appliquées
Diplôme : Master : ingénieur civil mécanicien, à finalité spécialisée en "Advanced Ship Design"
Année académique : 2022-2023
URI/URL : http://hdl.handle.net/2268.2/18058

With the support of the Erasmus+ Programme of the European Union

Combined EFD and CFD Approach using the Form Factor for Full Scale Ship Powering Prognosis

Name:	María Tadea Quintuña Rodríguez
Student ID:	222202278
Subject:	Advanced Design of Ships and Offshore Structures
E-Mail:	maria.rodriguez@uni-rostock.de
Chair:	Ship Design
Faculty:	Faculty of mechanical engineering and marine technology
Thesis schedule:	20 weeks
Submission:	07.08.2023

First Reviewer:
Prof. Dr.-Ing. Florian Sprenger
Professor, Chair Holder in Ship Design
University of Rostock
Albert-Einstein-Str.2
18059 Rostock
Germany

Second Reviewer:
Dip.-Ing. Peter Horn
Project Manager, Researcher Ships
Hamburgische Shiffbau-Versuchsanstalt
Bramfelder Str. 164
22305 Hamburg
Germany

EMship+ Advanced Design

Master's Thesis

University of Rostock

María Tadea Quintuña Rodríguez
maria.rodriguez@uni-rostock.de

This document was set with LaTeXon July 31, 2023.

Abstract

In this study, the investigation of the form factor determination as part of the 1978 ITTC power prediction method is performed with the objective to find suggestions to improve the ship power prediction. This study follows a combined CFD/EFD approach, where the extrapolated resistance from the towing tank tests is calculated with the form factor obtained from a CFD based method. In the present thesis two ship models are analysed, the MO5500 (a multipurpose vessel) and MO4500 (a container ship), these models correspond to HSVA benchmark models from which the experimental resistance is obtained from towing tank tests performed at the HSVA facilities.

The CFD based form factors are obtained from the viscous resistance of double body numerical simulations divided by the frictional resistance of a flat plate. In this study, numerical simulations are used to obtain the flat plate frictional resistance curve, using two different turbulence models, the $k-\omega$ standard and the $k-\omega$ SST. The obtained numerical friction curves predict C_F values at low Reynolds below the ones predicted analytically, following the same behaviour of other existing numeral friction lines, where for example the difference between them decreases as the Reynolds number increases.

In order to have a better understanding of the behaviour of the form factor, it was determined for both ship types at model and full scale. The results confirm the dependence of the form factor on Reynolds number because of the different values obtained at both scales. The difference between the numerical form factors at different scales present an average percentage of 10.4% for the ones obtained with the ITTC'57 correlation line. While the average difference with the numerical line of $k-\omega$ SSt is 6.4%, these results corroborate the scale effects of the ITTC'57 line and the decrease with the use of numerical friction lines.

Full scale resistance predictions were performed following the ITTC'78 method (which applies the ITTC'57 correlation line) using the model resistance results from the towing tank tests, and also extrapolating from the results of the CFD model scale simulations. The extrapolation process was done with 4 different form factors, the experimental one and 3 based CFD form factors obtained with the ITTC'57 curve, and with the 2 numerical friction lines derived in this study. In addition, the power predictions for the two ship models were also performed following the standard HSVA correlation method which does not contain form factors.

The full scale resistance predictions for the 2 ship models were compared with the results of the CFD resistance simulations at full scale. It was found that the extrapolation made with the form factor derived from the numerical friction line $k-\omega$ SST presented the smallest difference from the CFD full scale resistance values, while the highest difference was obtained with the form factor based on the ITTC'57 curve.

Contents

List of Figures

List of Tables

List of Abbreviations

Abbreviation	Meaning
EFD	Experimental Fluid Dynamics
CFD	Computational Fluid Dynamics
HSVA	Hamburgische Schiffbau-Versuchsanstalt
ITTC	International Towing Tank Conference
RANS	Reynolds Averaged Navier-Stokes
SST	Shear Stress Transport

List of Formulas

Symbol	Unit	Meaning
C_A	$[-]$	Correlation allowance
C_{AA_S}	$[-]$	Ship air resistance coefficient
C_F	$[-]$	Ship fictional resistance coefficient
C_T	$[-]$	Total resistance coefficient
C_v	$[-]$	Viscous resistance coefficient
C_W	$[-]$	Wave resistance coefficient
ΔC_F	$[-]$	Roughness allowance
U^+	$[-]$	Non-dimensional wall velocity
y^+	$[-]$	Non-dimensional wall distance
y	$[m]$	Wall normal coordinate
τ_w	$[Pa]$	Wall shear stress
ω	$[1/s]$	Specific turbulence dissipation rate
ϵ	$[m^2/s^3]$	Turbulence dissipation
k	$[m^2/s^2]$	Turbulent kinetic energy
R_F	$[N]$	Frictional resistance
R_P	$[N]$	Pressure resistance
R_T	$[N]$	Total resistance
R_V	$[N]$	Viscous resistance
R_W	$[N]$	Wave resistance
T	$[m]$	Draft
T_{aft}	$[m]$	Draft at the aft perpendicular
T_{fore}	$[m]$	Draft at the forward perpendicular
S	$[m^2]$	Wetted surface area
V	$[m/s]$	Ship velocity
L	$[m]$	Length
L_{WL}	$[m]$	Length of waterline
L_{PP}	$[m]$	Length between perpendiculars
λ	$[-]$	Scale factor
Fr	$[-]$	Froude number

Symbol	**Unit**	**Meaning**
Re	$[-]$	Reynolds number
g	$[m/s^2]$	Force of gravity
ρ	$[kg/m^3]$	Density
ν	$[m^2/s]$	Kinematic viscosity
ν_t	$[m^2/s]$	Eddy viscosity
μ	$[Pa.s]$	Dynamic viscosity
$(1+k)$	$[-]$	Form factor
x	$[m]$	x-coordinate

1. Introduction

1.1. Motivation

The power prediction of a ship is one of the most important steps in the design process as the ship should reach the speed requested by the owner in a good relation to the fuel consumption and a good operational cost, this power prediction requires higher accuracy each day [36]. Model testing from the experimental fluid dynamics EFD, is used to determine ship powering performance, where the measurements of the model tests are extrapolated to full scale ship following the recommendation of the "1978 ITTC Performance Prediction Method for Single Screw Ships"[1][37]. Model tank tests, despite being the recommended method for resistance prediction during ship design, is costly and time consuming. Therefore, it has been preferred to focus the research on the computational fluid dynamics CFD, as numerical simulations are currently put into practice for the design of ships, as well as for hydrodynamic analysis, behavior of the ship at sea, form optimization, and other problems part of the ship life. Over time, numerical methods have been studied to improve the prediction of the resistance in order to have a better performance of ships [28].

When towing tank tests have been carried out, the model resistance results have to be scaled to a full size ship. In practice to extrapolate the model measurements, the frictional resistance is obtained from the "ITTC'57 correlation line"[2], which is derived from the skin-friction of a flat plate. But its validity over the years was questioned and other friction lines were proposed by Grigson [15], Katsui [25], among others. Recently the resistance of a flat plate can be obtained computationally with numerical methods which might result in more reliable estimations [2].

In this extrapolation process there exists another important source of uncertainty, that is the determination of the form factor used in the ITTC 1978 method. In practice, this is determined with model tests at low Froude numbers, but at those speeds it is difficult to measure the resistance accurately, becoming a source of uncertainty. In the last years, the CFD has become a method of obtaining the form factor by using double body calculations. However, there are no general recommendations for the form factor calculation using CFD [28].

The aim of this thesis is to improve the extrapolation methods by using a form factor determined numerically. First, a numerical friction line is obtained by CFD simulations with different turbulence models and compared with the existing ones. Second, the form factor is obtained for the two ship models at different drafts by CFD double body simulations. The validity is checked

[1] Referred to as "ITTC 1978 method" or simply "ITTC'78" in the remainder of this thesis.
[2] Referred to as "ITTC 1957 line" or simply "ITTC'57" in the course of this thesis.

with the form factors obtained from the model tests. Finally, the extrapolation procedure is exemplarily tested with this combined EFD and CFD approach at two of HSVA reference models. Based on this evaluation suggestions could be given to HSVA standard calculation of the form factor.

1.2. Thesis Structure

Chapter 2 contains all the theory used for the development of this thesis, starting from obtaining the power prediction of a ship, going through the existing frictional lines in the literature as well as the numerical ones, the ways of determining the form factor, and all the theory that numerical simulations entail. Chapter 3 contains the prediction of the numerical friction line. The frictional resistance of a flat plate, regardless of being a simple concept, has been analyzed over the years and despite this, the ITTC'57 line continues to be used. In this chapter proposals for friction lines are obtained with two different turbulence models. A flat plate is simulated in a range of Reynolds number that covers the model and full scale size of a ship. The uncertainty of these numerical simulations is analyzed so that the friction results of the flat plate simulations can be used and derived in a friction line. At the end of the chapter, the friction lines obtained are compared with some existing ones, either numerical or proposed by the literature, including the ITTC'57 curve.

In Chapter 4, the form factor is determined. This factor also has a large uncertainty when derived experimentally with the Prohaska method, however it also continues to be implemented for resistance extrapolation. This chapter is based on obtaining form factors with the results of numerical simulations applying numerical frictional lines. In order compare both methods, first, the experimental form factor is calculated with the Prohaska method using the model tests results from the towing tank. Second, CFD based form factors are calculated by total resistance simulations of the ship models in model scale and full scale. For the calculation of the numerical form factors, the numerical friction lines obtained in the previous chapter are used. Finally, the comparison between the form factors obtained experimentally (EFD approach) and those obtained with numerical simulations (CFD approach) is presented.

In chapter 5, the resistance of the model tests and the CFD results at model scale are extrapolated to full scale ship resistance using the standard HSVA correlation method (also known as the 2D-method) which has no form factors included. The same is done using the ITTC'78 approach (also known as the 3D-method) which uses the numerical form factors obtained in the previous chapter and the experimental form factor by Prohaska method. Finally, the ship resistance extrapolated with these two methods is compared with the total resistance obtained with the CFD full scale numerical simulations of the two ship models. A work flow of the main body of the thesis is presented in fig 1.1. Finally conclusions and suggestions for improvements of the HSVA CFD standard calculations are presented.

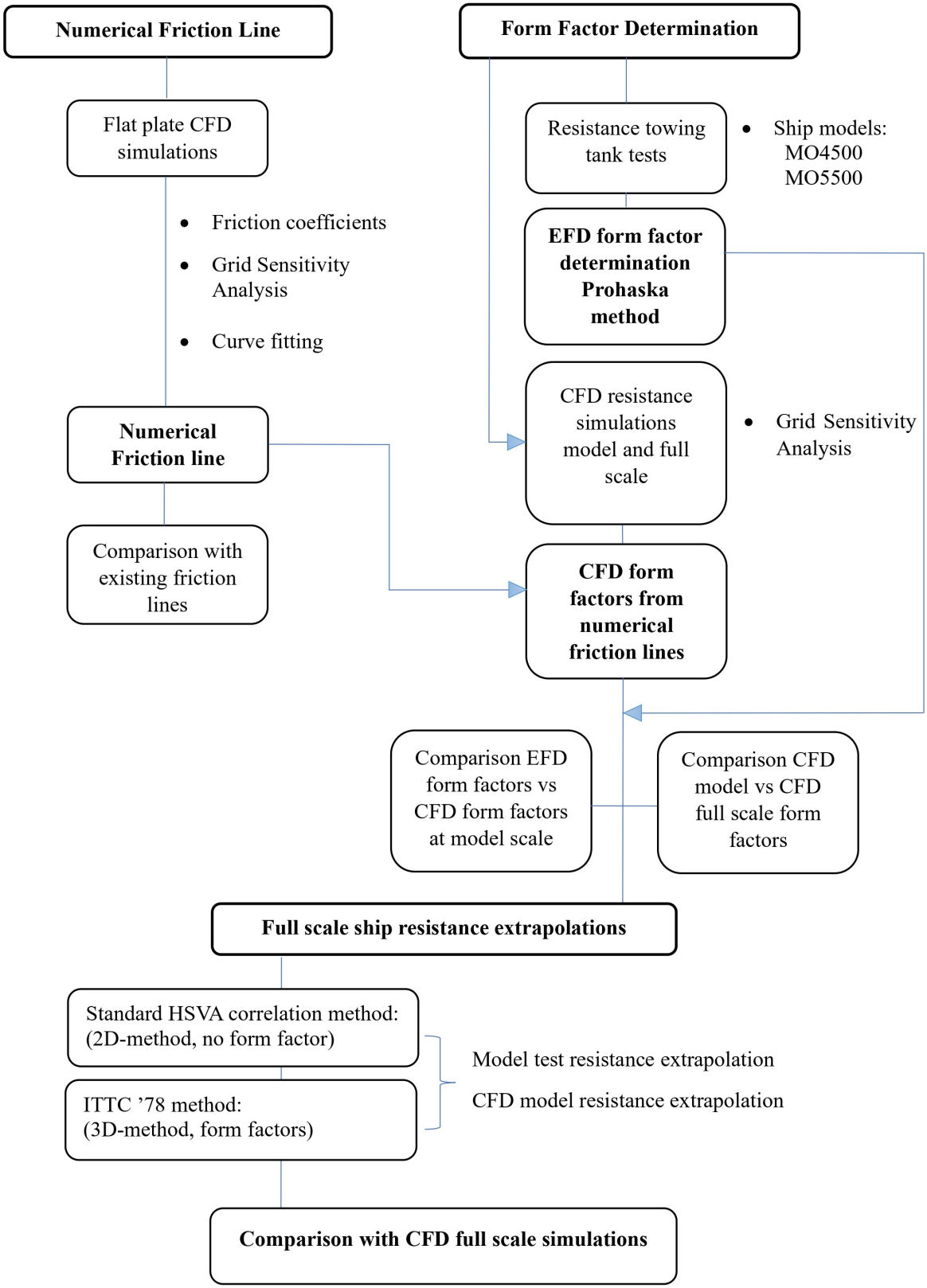

Figure 1.1.: Body thesis structure

2. Theoretical Background

2.1. Ship Resistance

This section introduces the theory of ship resistance for the understanding of the resistance components because of their importance in the power prediction of a ship. In literature there exists two common ways of dividing the forces, by the frictional resistance R_F generated by the tangential shear forces acting on the ship hull and the pressure resistance R_P that consists on the pressure force acting on the ship surface. In this definition, the pressure drag doesn't arise purely, it contains viscous effects and hull wave making. Resulting the total resistance R_T in the following expression:

$$R_T = R_F + R_P \tag{2.1}$$

The other alternative is to divide the resistance in the total viscous resistance R_V that includes the skin frictional resistance and part of the pressure force. The other component is the total wave resistance R_W due to the generation of water waves and water spray. Resulting in the alternative expression:

$$R_T = R_V + R_W \tag{2.2}$$

The typical form of presenting the ship resistance is through the ITTC form of coefficient, given by:

$$C_T = \frac{R_T}{\frac{1}{2}\,\rho\,S\,V^2} \tag{2.3}$$

where:

C_T = total resistance coefficient,
R_T = total resistance force,
ρ = water density,
S = wetted surface area,
V = ship speed.

Model testing is used to estimate the resistance of a ship by extrapolating the results to full scale. For the model tests there exists some requirements and assumptions to ensure the similarity in forces. The geometric similarity has the requirement that the model and full scale are geometrically similar given by the scale factor λ defined as the ratio between the ship length, L_S and the model scale length L_M (the subscript 'S' signifies the full scale ship and the subscript 'M' the model scale ship) :

$$\lambda = \frac{L_S}{L_M} \tag{2.4}$$

This scaling factor is also used for scaling the surface area, the displacement, and other environmental parameters as the waves, water depth, among others. The other criteria for the model tests is the dynamic similarity at which the ratio between forces should be the same as for the full scale. There exists the requirement of the dimensionless number that characterise the flow, this is the Froude number Fr, which needs the same ratio between the inertia and gravity forces.

$$Fr = \frac{V_M}{\sqrt{g\,L_M}} = \frac{V_S}{\sqrt{g\,L_S}} \tag{2.5}$$

Where g = force of gravity. This similarity assure that the wave pattern of the model and full scale will be equal, and its importance relies on the assumption that the residual resistance coefficient C_R, is the same in both cases.
The other criteria that the model tests should follow is the similarity of the Reynolds number Re, where the relation of the inertial forces to viscous forces should be the same for model and full scale. In the following equation ν corresponds to the kinematic viscosity:

$$Re = \frac{V_M\,L_M}{\nu_M} = \frac{V_S\,L_S}{\nu_S} \tag{2.6}$$

The characteristics of the model and full scale should fulfill the Froude and Reynolds number similarities, however this is practically impossible and in practice for the model tests just the Froude number is identical.

2.2. The resistance test

The resistance test is used to determine the total ship resistance of a ship at different speeds and different drafts. This test is performed without a propeller and the model is attached to a moving carriage and towed along the tank. The resistance is measured for a constant velocity during a period of time. The towing force in the horizontal direction is measured by a load cell, this value with the vessel speed correspond to the input data for the scaling procedure to calculate the propulsive power for the full scale ship. During the experiment, the temperature of the water should be measured and used for the resistance calculation, the viscosity is also dependent on the water temperature. The typical layout of a resistance test is presented in the figure 2.1.

The size of the ship model is chosen in order to prevent the wall interference with the towing tank and at the same time should be as large as possible to minimise the scale effects. The models should have a good material strength, geometry accuracy and surface finish. In the past, models were made from paraffin wax, nowadays some materials include wood, foam and fibre reinforced plastic, models in this study are made of wood [36] [23].

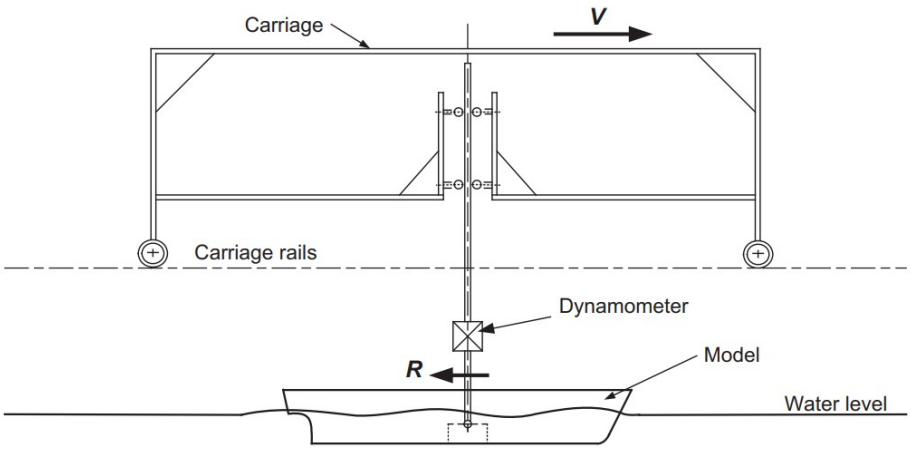

Figure 2.1.: Layout of model towing test [36]

2.3. Computational Fluid Dynamics CFD

Computational fluid dynamics has become the methodology used today to solve complex problems in all fields of engineering. CFD simulations in advantage provide detailed hydrodynamic characteristics that are difficult to obtain from model tests, such as streamlines, the distribution of forces on the hull and any other hydrodynamic parameter in any zone without affecting the flow. Numerical simulations are a good alternative to make improvements to the design of a ship, also they are faster, and less expensive than performing an experimental analysis. In our context, CFD simulations are an alternative to fulfill the Froude and Reynolds number similarity that model tests are not able to follow at the same time. Nowadays, the accuracy of the numerical simulations continue to be investigated, especially at full scale ship computations where the availability of real data is limited [42].

2.4. The extrapolation method

Nowadays, the ITTC'78 Method gives an analytical procedure to predict delivered power of ships from model test results. The total resistance coefficient of a ship is [22]:

$$C_{T_S} = (1+k)C_{F_S} + \Delta C_F + C_A + C_W + C_{AA_S} \tag{2.7}$$

where

- k[1]: the form factor determined from the model resistance test.
- C_{F_S}: the frictional resistance of the ship following the ITTC 1957 model-ship correlation line.
- ΔC_F: the roughness allowance.
- C_A: the correlation allowance.

[1]In this thesis the expression $(1+k)$ is considered as the form factor

- C_{AA_S}: the air resistance coefficient in full scale.
- C_W: the wave resistance coefficient obtained from the resistance tests by the formula:

$$C_W = C_{T_M} - C_{F_M}(1+k) \tag{2.8}$$

where

- C_{F_M} the model frictional resistance coefficient is derived from the ITTC 1957 correlation line.
- C_{T_M} is the total resistance coefficient of the model test.

The correlation factor C_A considers the effects not taken into account in the prediction method, like the uncertainties of the model tests, and the assumptions made in the prediction method. It is preferred that each towing tank institution build up its own correlation factor because each one may have different equipment. If calculated the recommended C_A is given by the formula:

$$C_A = (5.68 - 0.6\,log(Re)) * 10^{-3} \tag{2.9}$$

The roughness allowance ΔC_F contains the effects on the resistance made by the roughness of the hull. The formula for ΔC_F is given by:

$$\Delta C_F = 0.444 \left[\left(\frac{k_S}{L_{WL}} \right)^{\frac{1}{3}} - 10\,Re^{-\frac{1}{3}} \right] + 0.000125 \tag{2.10}$$

where k_S is the roughness of the hull, with a standard value of $150E-6$ when a measure data does not exist.

The ITTC'78 method separates the total resistance into the viscous and the wave resistance and the concept of the form factor is introduced to consider the resistance caused by the hull geometry as part of the viscous resistance. The ITTC introduced this component with the assumption that the form factor of a ship is the same for the model scale and full scale, being independent of the ship speed. In the present work, the study will focus on the frictional resistance and the form factor determination in order to numerically investigate the scale effects to could improve the quality of power predictions, and to reduce the uncertainties of the form factor in comparison with the ones obtained experimentally.

2.5. Friction Line

From the formulation of the ship resistance, the viscous component C_V is proportional to the skin friction coefficient C_F, which assumes that the hull is a flat plate moving through the water as shown in the equation (2.11). Therefore, the form factor k contains the information of the hull form for the viscous resistance.

$$C_V = (1+k)C_F \tag{2.11}$$

Flow over a Flat Plate

The flow over a flat plate in the x direction with a velocity V, forms a boundary layer with a thickness δ, where the particles at the plate surface have zero velocity in relation to the plate, and then reducing the velocity of the adjacent particles reaching the 99 percent of the free-stream velocity at the edge of the boundary layer. The boundary layer is the region near the wall where the viscous forces and the rotationality of the flow become important. It is a function of the velocity V, position at the flat plate x, and fluid properties as density, ρ and dynamic viscosity, μ [9].

The behaviour of the flow over the flat plate begins laminar but as the flow moves down the plate increasing the Reynolds number at an x position (Re_x), the boundary layer can not remain laminar and start the transition region until reaching the fully turbulent boundary layer as shown in the figure 2.2.

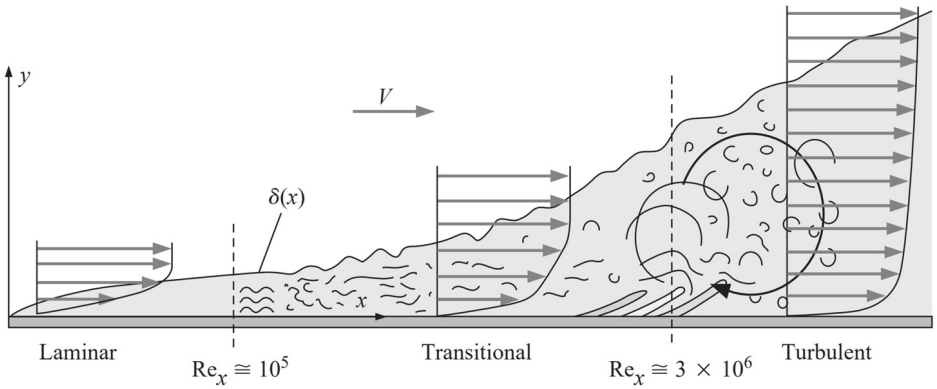

Figure 2.2.: Boundary layer profile of the flow over a flat plate [9]

The expressions to calculate the laminar and turbulent boundary layers on a smooth flat plate are the followings [9]:

- Laminar boundary layer on a flat plate. The flow is considered laminar until a Re_x=1x10^5 for which δ is defined as:

$$\delta = \frac{4.91x}{(Re_x)^{1/2}} \tag{2.12}$$

- Turbulent boundary layer on a flat plate. The flow is considered turbulent from a Re_x=3x10^6 for which δ is defined as:

$$\delta = \frac{0.16x}{(Re_x)^{1/7}} \tag{2.13}$$

  where:

$$Re_x = \frac{Vx}{v} \tag{2.14}$$

Re_x corresponds to the Reynolds number along a flat plate.

For a parallel flow over a flat plate, there is no pressure drag, thus the total resistance is equal to the frictional coefficient. The friction coefficient for the entire plate is determined by the integral of the local friction coefficient along the surface of the flat plate which varies due to the changes in the velocity boundary layer [9]. There exists analytical equations to calculate the friction coefficient as a function of the Reynolds number, for the laminar and turbulent flows, [21], this last equation is referred as "Theory Flat Plate" in the plots :

$$C_{F_{laminar}} = \frac{1.328}{Re^{1/2}} \qquad Re < 5\text{x}10^5 \tag{2.15}$$

$$C_{F_{turbulent}} = \frac{0.455}{[log(Re)]^{1/5}} \qquad 5\text{x}10^5 < Re < 10^7 \tag{2.16}$$

Where Re is the Reynolds number and it is used to predict whether a fluid flow is laminar or turbulent based in the fluid properties as the velocity V, viscosity ν and a characteristic length L. A low Reynolds number indicates a laminar flow, the fluid is dominated by viscous forces while the turbulent flow occurs at high Reynolds numbers where the inertial forces are dominant and the fluid is characterized to be chaotic and irregular. Between these two flow types, there is a region called the transitional range where the laminar flow experience periodic and after that fully random turbulent fluctuations.[40]

The ITTC 1957, also known as model-ship correlation line has developed a friction line for typical hull forms prior to 1957, which may affect the prediction of modern hulls that have evolved over time. This fact causes this correlation line to be questioned when extrapolating the resistance of a model ship. Also this friction line is a function of the turbulent flat plate friction values which come from experiments and contain uncertainty. This correlation lines was based on Hughes flat plate friction line. [23]

Hughes Flat Plate friction line

Hughes [17] proposed a pure two dimensional friction line of a smooth plane surface in turbulent flow:

$$C_F = \frac{0.067}{(\log_{10} Re - 2)^2} \tag{2.17}$$

ITTC 1957 friction line:

The ITTC'57 correlation line [22] is based in the proposal by Hughes, but incorporates three-dimensional friction effects from the hull curvature [36] and is defined as:

$$C_{F_{ITTC57}} = \frac{0.075}{(\log_{10} Re - 2)^2} = C_F = (1 + 0.1194)\,\frac{0.067}{(\log_{10} Re - 2)^2} \tag{2.18}$$

There exists other friction lines proposed by Grigson and Katsui as follows:

Grigson Formula:

Grigson [15] gave some corrections to the ITTC'57 line, and in general seems to be physically more correct, even though it is not adopted for the model-ship extrapolation as the differences are not significant [36]. Grigson suggested further refinements to his proposal. It uses polynomials as multipliers of the ITTC line, Grigson formula is given by:

$$C_F = C_{F_{ITTC57}} G_1 \tag{2.19}$$

with

- 1.5 x 10^6 < Rn < 2 x 10^7
  $x = log_{10}(Re) - 6.3$
  $G_1 = 0.9335 + 0.147x^2 - 0.071x^3$
- 2 x 10^7 < Re < 6 x 10^9
  $x = log_{10}(Re) - 7.3$
  $G_1 = 1.0096 + 0.0456x - 0.013944x^2 + 0.0019444x^3$

Katsui Formula:

Katsui [25] also proposed a frictional line, this formula is given in the ITTC report [19] which mentions that "Grigson's Line and Katsui's Line are obtained by the numerical integration of local friction in the boundary layer". The formula is given by:

$$C_F = \frac{0.0066577}{(\log_{10} Re - 4.3762)^a} \qquad for \qquad 1\text{x}10^6 \leq Re \leq 7\text{x}10^9 \tag{2.20}$$

with $a = 0.042612 \log_{10}(Re) + 0.56725$

The numerical friction line

The friction line contains the frictional resistance values of a flat plate and is used in the ITTC 1978 method for the extrapolation of the resistance of a ship. It has been shown at [14] that it is possible to obtain the values of the resistance of a flat plate for a wide range of the Reynolds numbers from model to full scale using numerical simulations. Eca and Hoekstra [2] have performed this analysis with 7 different turbulence models and obtained very good results, where the differences between these 7 numerical lines are smaller than the differences between the existing curves in the literature. They have concluded that the use of the numerical friction lines in the extrapolation of the resistance is still to be investigated, even though, those numerical friction lines can be very useful for the determination of the numerical form factor.

Nowadays, some numerical friction lines have also been proposed in addition to the ones from Eça and Hoekstra [2], for example the one from Wang et al. [6] and Korkmaz et al. [27]. Figure 2.3 shows the difference between these numerical friction lines and the ones from literature.

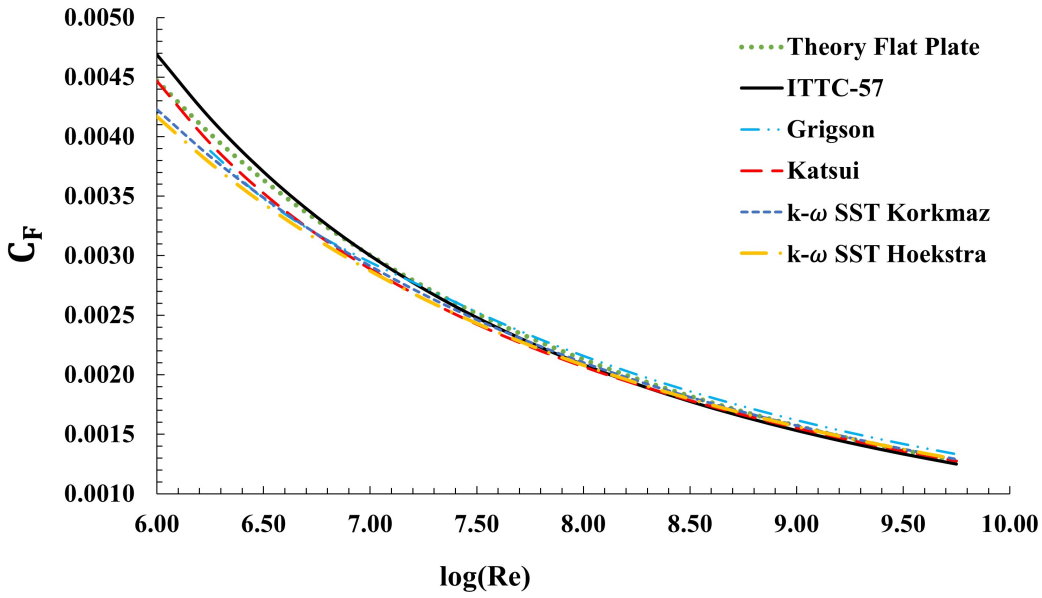

Figure 2.3.: Friction lines from literature and numerical references

2.6. Form Factor determination

The friction resistance of a vessel is related to the viscous resistance with the form factor, which contains the additional resistance due to the shape and curves of the hull. The form factor is a very important component of the ship resistance determination, as it is used in the extrapolation method from the model test data to the full ship scale resistance. The form factor is determined following the 1978 ITTC Performance Prediction Method [22] that uses the Prohaska approach.

Prohaska Method

Prohaska proposed a method to obtain the form factor from the model tests resistance. When if not separation is present, the total resistance coefficient is expressed as:

$$C_T = (1+k)C_F + C_W \tag{2.21}$$

And the wave resistance coefficient at low speeds is proportional to the Froude number as:

$$C_W = a\, Fr^4 \tag{2.22}$$

Where a is a coefficient. Dividing the equation (2.21) by the friction resistance coefficient results in:

$$\frac{C_T}{C_F} = (1+k) + \frac{C_W}{C_F} = (1+k) + a\,\frac{Fr^4}{C_F} \tag{2.23}$$

The assumption of Prohaska is based on model tests at low speeds, Froude numbers between 0.1 and 0.2 are needed in order to have the wave resistance component proportional to Fr^4

and a straight line plot of C_T/C_F versus Fr^4/C_F as shown in figure 2.4. From the graph the intersection with the ordinate ($Fr = 0$) corresponds to the form factor $(1 + k)$.

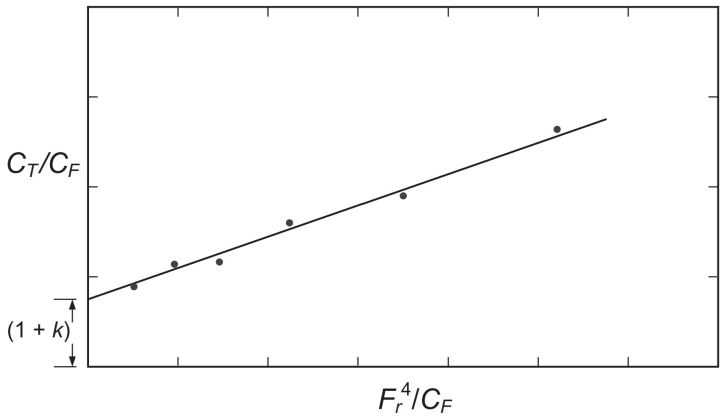

Figure 2.4.: Prohaska Mesthod [36]

The determination of the form factor has been questioned and its influence in the power prediction of a ship. The shortcomings lie on the difficulty to measure the resistance with accuracy at low speeds at the towing tanks, even the total resistance measurements vary from basin to basin.

CFD form factor prediction

The CFD based form factor determination method follows the assumptions of Hughes [17] and is obtained by:

$$(1 + k) = \frac{C_F + C_{PV}}{C_{F0}} = \frac{C_V}{C_{F0}} \tag{2.24}$$

where:

The viscous coefficient C_V is obtained by double body CFD numerical simulations. (C_{PV} corresponds to the viscous pressure coefficient). The C_{F0} coefficient at the denominator is the flat plate frictional resistance calculated at the same Reynolds number. In this thesis, this flat plate frictional resistance is also obtained from the numerical friction lines.

Combined EFD/CFD based form factor determination: background

The form factor during the extrapolation method of the ITTC'78 is calculated using the Prohaska method which has been questioned for many decades. Studies have been carried out using the CFD approach, showing the dependence of the form factor on the Reynolds number [41] and the existence of scale effects [13], [39], [6], it was found that the main cause the the scale effects is the ITTC'57 correlation line serving as the friction line. One of the last investigations on the CFD based form factor determination [43], found that the results of this method have a better correlation with sea trials than the experimental Prohaska method for form factor determination.

The combination of CFD and EFD method for the estimation of the form factor has already been studied for the well known ship benchmark cases KVLCC2 and KCS where the form factors were calculated by CFD double body numerical simulations and compared with the experimental values. In this study done by Korkmaz [28] it was found that the resistance values extrapolated to full scale using the results of the combined EFD/CFD approach show significantly less dispersion and therefore make it a preferable method. A similar study was carried out in [29] where 14 common cargo vessels were analyzed thanks to the availability of model test results and full scale speed trials, the same conclusion was found, saying that the use of CFD based form factor improves the predictions of the resistance.

All this gives a good encouragement for this thesis that is based on the study of EFD/CFD form factor determination method for the analysis of the power extrapolation using the HSVA ship benchmark models, the calculation of an own friction line using the FRESCO+ RANS solver, the comparison with the results of the experimental tests of these ship models performed at the HSVA large towing tank and the numerical simulations also using the same CFD solver.

2.7. Turbulence Models

The majority of fluid flows that occur in life, in nature as well as in engineering, are turbulent. For example, the atmosphere, ocean currents, flow of water in rivers; flow through turbines and pipes; the wake of air-crafts, cars and ships. However due to the difficulty of defining turbulence, it is described by a number of characteristics [5] [12]:

- **Irregularity**. Turbulence flows are irregular and stochastic. The flow contains different eddy sizes, ones in the order of the boundary layer thickness, and smallest eddies that dissipates into internal energy.
- **Diffusivity**. It causes the increase rate of momentum in boundary layers and delays its separation such as on cylinders and airfoils. Diffusivity produces the increase of resistance in pipelines.
- **Large Reynolds numbers**. Turbulent flows occur at high Reynolds number, originated as an instability of laminar flows.
- **Three-dimensional vorticity fluctuations**. Turbulence is three dimensional, because of its high levels of fluctuating vorticity. However, it can be treated as two dimensional when the equations are time averaged.
- **Dissipation**. Turbulent flows are dissipative, the kinetic energy of the small eddies is transformed into internal energy.
- **Continuum**. As in a turbulent flow, any smallest scales are larger than the molecular scale, the flow can be treated as continuum.

The most used approach to solve turbulent flows is to follow the Reynolds Averaged Navier-Stokes (RANS) equation (2.25), where the flow instantaneous variables are decomposed into a

mean and a fluctuating value, as in equations(2.26), (2.27). This decomposition is because the interest lies in the mean values of the flow quantities and the need of numerical fine resolution in grid and time to solve all turbulent scales.

$$\frac{\delta\rho\overline{U}_i}{\delta t} + (\rho\overline{U}_i\overline{U}_j)_{,j} = -\overline{P}_{,i} + [\mu(\overline{U}_{i,j} + \overline{U}_{j,i}) - \rho\overline{u_i u_j}], j. \tag{2.25}$$

$$U_i = \overline{U}_i + u_i \tag{2.26}$$

$$P = \overline{P} + p \tag{2.27}$$

Where:
U_i: the instantaneous velocity in x_i direction.
$\overline{U}_i$: the time-averaged velocity in x_i direction.
u_i: the fluctuating velocity in x_i direction.
P: the instantaneous pressure.
$\overline{P}$: the time-averaged pressure.
p: the fluctuating pressure.
μ: the dynamic viscosity.

This Reynolds averaging results in an additional term in the right hand side, $\overline{u_i u_j}$, called the Reynolds stress tensor that contains the mean of the fluctuating velocities, and it is an unknown for which we need a model to close the RANS equations system because the number of unknowns is larger than the number of equations. There are for example the algebraic models, one-equation models, two-equation models and Reynolds stress models. In this study two-equation models are chosen as they include two extra transport equations that represent the transport of two scalars, that can be the turbulent kinetic energy, k, turbulent dissipation, ϵ, or the specific turbulence dissipation rate, ω. The two equation models were selected as those considers two variables to solve the flow problem providing a better visualization of the flow and the history effects of the turbulent energy as the convection and diffusion [10], [35], these models have shown accurate prediction in ship hydrodynamics and are given as a recommendation within the ITTC Practical Guidelines for Ship CFD Applications [21]. The most common two equation models are the k-epsilon model and the k-omega model. These models are based on the Boussinesq Assumption, that replace the Reynolds stress tensor by the turbulent viscosity μ_t (eddy viscosity) multiplied by the velocity gradients, see equation (2.28). This new eddy viscosity factor needs to be calculated by one of the turbulence models chosen ($k-\epsilon$ or $k-\omega$).

$$\rho\overline{u_i u_j} = -\mu_t(\overline{U}_{i,j} + \overline{U}_{j,i}) + \frac{2}{3}\delta_{ij}\rho k \tag{2.28}$$

The $k-\epsilon$ Model

The standard $k-\epsilon$ model is based on modelling the transport equations for the tubulence kinetic energy k, and its dissipation rate, ϵ. In this model there is the assumption that the flow is fully turbulent and the effects of molecular viscosity are negligible [8]. But, if it is necessity to solve the equations into the viscous sublayer, damping functions need to be applied to the

model. Even though, the k-epsilon model is recommended for fully turbulent flows, high-Re applications [45].

The $k-\omega$ Model

This model was proposed by Wilcox [44]. The standar k equation is solved as the length scale determining quantity ω is used, usually called $specific dissipation$. In contrary to the $k-\epsilon$ model, $k-\omega$ has the advantage of the near wall treatment, it can be used as a low-Re number model to analyze the flows very close to the wall as in the viscous sublayer. Therefore, the $k-\omega$ turbulence model is gaining populatiry because is generally more robust for those flow conditions. [12] A major problem of the standard $k-\omega$ method is being too sensitive to the inlet free stream turbulence properties, not being adequate to the turbulence interface treatment. However, a solution was proposed by Menter. [33] [26]

The Menter SST $k-\omega$ model

The shear stress transport, SST $k-\omega$ combines the best of the two models. It uses the $k-\omega$ formulation near the wall for the inner parts of the boundary layer and the $k-\epsilon$ model for the free stream treatment. [38]

2.8. Wall Modeling

The presence of walls imply boundary layers that needs very fine grids to solve the sharp gradients, consequently too much computational power. A good alternative is to use wall functions that can model the region near the wall by applying boundary conditions and assuming that the flow near the wall behaves as fully developed turbulent boundary layer. The wall functions allow to use a larger mesh near to the walls because they do not need to resolve the boundary layer which yields in a reduction of the mesh size and computational time. [32]

The near wall region

There are important parameters that can help to describe the near wall region, like the kinematic viscosity ν and the wall shear stress τ_w. From these quantities it comes the definition of the friction velocity u_τ:

$$u_\tau = \sqrt{\frac{\tau_w}{\rho}} \tag{2.29}$$

The distance from the wall is given by:

$$y^+ = \frac{u_\tau y}{\nu} \tag{2.30}$$

Where y^+ is the non-dimensional distance from the wall to the first grid point. y is the dimensional distance from the wall.
Finally these relations allows to define the dimensionless velocity U^+:

$$U^+ = \frac{u}{u_\tau} \tag{2.31}$$

Where u is the local velocity and U_τ the friction velocity.

The wall functions are empirical formulations that need to fit the behaviour of the velocity profile near the wall. Figure 2.5 shows the relationship between y^+ and U^+ with a log-law velocity profile where three zones are noticed:

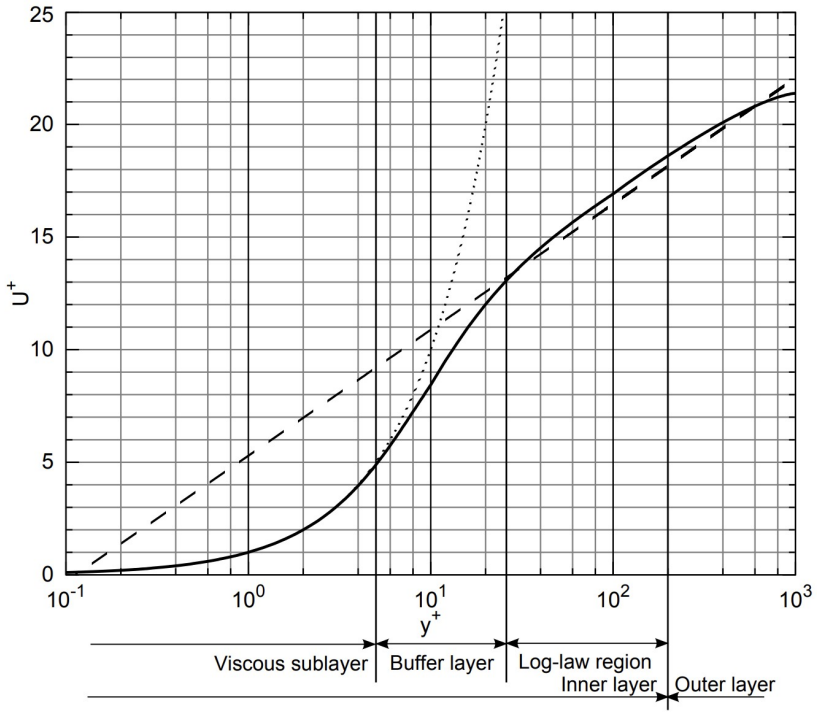

Figure 2.5.: Log-law velocity profile. Dotted line: $U^+ = y^+$, striped line: $U^+ = \frac{1}{k}log(y^+) + B$, solid line: experimental data [38]

- Viscous sublayer ($y^+ < 5$) where the Reynolds stresses are negligible and the viscous effects are dominant. The normalized velocity profile (U^+) has a linear relationship with the Y+. $U^+ = y^+$
- Buffer layer ($5 < y^+ < 30$). No law is hold in this region.
- Fully turbulent or log-law region ($y^+ > 30$) where the viscous stresses are negligible. The velocity profile varies slowly with a logarithmic function where k and B are constants.

$$U^+ = \frac{1}{k}log(y^+) + B \tag{2.32}$$

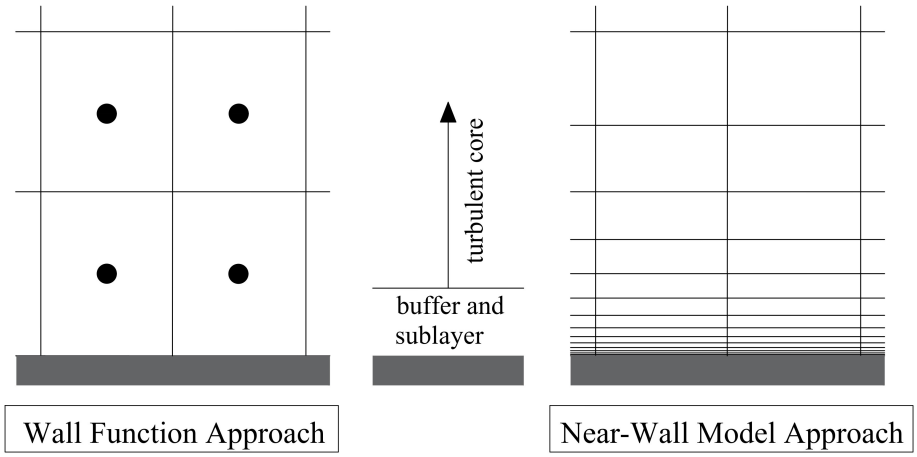

Figure 2.6.: Near Wall treatment [7]

There exists two approaches to model the bounded turbulent flow (Figure 2.6):

- Wall Functions: semi-empirical equations to link the turbulent flow and the wall region where the viscous sublayer and buffer layer are not resolved [30].
- Near wall model: needs to resolve all the way down to the wall, solving the fully turbulence region and the viscous region. Simulations where the flow near the wall is important use this model with an adequate grid size that can describe all the boundary layer.

The choice of the use of wall functions influence directly to the value of the y^+ [21]:

- Wall functions: $30 < y^+ < 100$
- Near wall: $y^+ < 1$

2.9. Computational domain and Mesh Generation

The computation domain is the space at which the simulation is performed, it is the first step in any numerical simulation. The domain should be big enough to avoid interference with the body in study, assuming an undisturbed far field velocity and to allow the flow dynamics to be fully developed across the computational domain. The ITTC [20] gave an example of this application, where the inlet boundary is located at 1 L_{PP} from the bow, the outlet at 2 L_{PP} from the stern, a side boundary at 1 L_{PP} from the symmetry plane and the bottom boundary at 1 L_{PP} from the keel. These positions can be taken as a guide for the computational domain for ship numerical simulations.

Mesh generation

In CFD the mesh is the discretization of the space under analysis. This is modeled by small cells in which the mathematical equations are applied. The mesh is one of the most important parts of a numerical simulation, a good quality mesh can guarantee stability in the results, which means that the results do not present exponential growth or oscillatory features. The generation

of the grid has some important requirements. The cells should have a smooth distribution in the entire space and there should be refined in the regions of large flow gradients. In the case of the flat plate simulations, to resolve the boundary layer and the y^+ concept without wall functions, the grid should have a good resolution in the normal direction to the plate, but as those cells are extremely thin, the rest of the domain should have coarser cells to be able to run the simulation with an acceptable computational effort and time [31]. The mesh generation is an important task and involves decisions to take according of the domain in analysis, as for example the type of connectivity that can be structured or unstructured (see Figure 2.7).

- **Structured Mesh**: A structured mesh is characterized by the regular connectivity of the cell points in 2 or 3 dimensions with quadrilaterals or hexahedral elements respectively. For simple problems as for flat plate simulation are in general more accurate than unstructured grids. The calculations take less computational time because the existing algorithms behaves more efficiently in the structured grids [1].

- **Unstructured Mesh**:An unstructured mesh has irregular connectivity between the elements, that can be 2D triangles or 3D tetrahedral or polyhedral. The grid generation is usually much faster than the structured one. For complex flows, unstructured meshes can lead to more accurate results due to the adaptive capacity [1].

In some CFD simulations as for example the flow around a ship, there is the need of the combination of the two types of meshes, the structured mesh for the stretched cells in the viscous boundary layer, and the unstructured one for the adaptation of the cells to the geometry and the domain size.

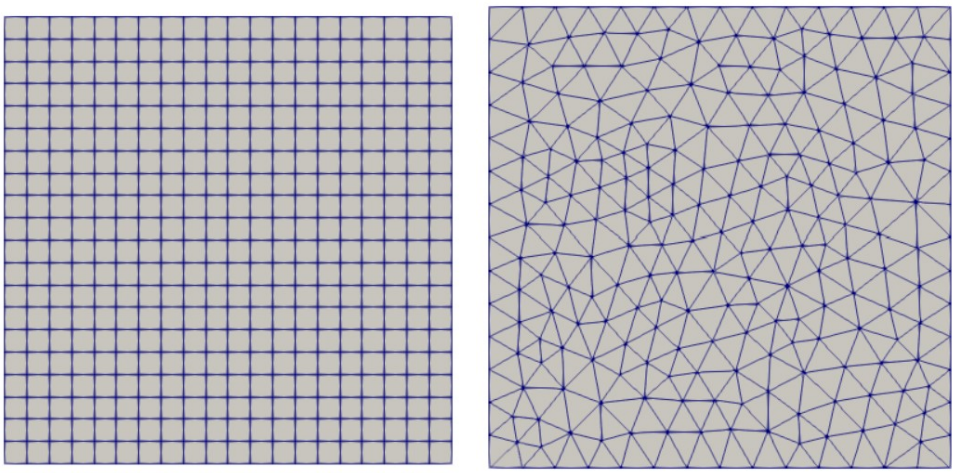

(a) Structured mesh (orthogonal) (b) Unstructured mesh (triangular)

Figure 2.7.: Mesh types [4]

Boundary layer grid resolution

In order to describe correctly the boundary layer in the CFD simulations, prism layers are needed at the flat plate. Those are characterized by:

- First layer thickness Y_H. With the value of desired y^+, the dimensional distance y can be obtained. It corresponds to the distance from the wall to the first point (middle of the cell). $Y_H = 2y$

$$y = \frac{y^+ L}{Re_L \sqrt{\frac{C_f}{2}}} \tag{2.33}$$

- Inflation factor: is the size relation of adjacent cells within the boundary layer.
- Number of layers: the boundary layer thickness needs to be contained by these inflation layers.

2.10. Converge of numerical solution

Convergence limits the process of fluid dynamics, in a CFD problem the exact solution is not known, and the systems of equations are solved iteratively. A precision of the desired solution is established for the problem, which limits the numerical process when the discretized equations reach the specified tolerance. An iterative convergence also occurs when the numerical solution no longer changes with the iterations. The residuals are the imbalances of the discretized equations and are used to monitor a numerical simulation which finishes when the process reaches a specific tolerance. The residuals are a guide to determine if a numerical simulation has convergent or divergent behavior. In a convergence behaviour the residuals tend to decrease as the numerical process evolves. But if the imbalances grow, that means the residuals increase, then the numerical simulation can be qualified as divergent. The iterative error normally is negligible compared with the discretization error explained in the following section, then it is not taken into consideration for the estimation of the error of a numerical simulation. [42].

2.11. Grid Sensitivity

In order to asses the quality of the results in CFD simulations, verification and validation procedures are needed by the users. Verification intends to answer the question if solving the equations is done correctly while the validation analysis deals with if the right equations are being solved. [3]. Following the paper done by Eça and Hoekstra [3], the analysis is focused on estimating the error or uncertainty of a numerical simulation when the exact solution is unknown. In the present section, the work done by Eça and Hoesktra is summarized and applied to the present thesis.

Error estimation

The error estimation of numerical simulations is based only in the calculation of the discretization error, as the iterative and round-off errors are considered to be negligible in comparison with this one.
The estimation of the discretization error, ε_ϕ, uses power series expansions with the equation:

$$\varepsilon_\phi \simeq \delta_{RE} = \phi_i - \phi_0 = \alpha h_i^p \tag{2.34}$$

Where:

δ_{RE} is called the "standard" error estimator. ϕ_i represents any integral, in this study it corresponds either to the frictional resistance coefficient or the total resistance coefficient.
ϕ_0 is the estimate of the exact solution.
α a constant to determine.
h_i is the parameter that characterize the difference between grids, typically the cell size, in this work it corresponds to the Y+ value.
p the observed order of grid convergence.

The minimum number of grids (n_g) needed to apply the error estimation is three, even though in order to follow the least-squares sense, four or more grids are expected. The refinement ratio, between the consecutive grids are constant as for example, ($h_2/h_1 = h_3/h_2$), corresponding h_1 to the finest grid. When the refinements ratios are the same, it is possible to estimate the discriminating ratio, R, with the equation (2.35)and the order of grid convergence with the equation (2.36):

$$R = \frac{\phi_1 - \phi_2}{\phi_2 - \phi_3} \tag{2.35}$$

Where:

- Monotonic convergence for 0<R<1
- Monotonic divergence for R>1
- Oscillatory convergence for R<0 and |R|<1
- Oscillatory divergence for R<0 and |R|>1

$$log(R) = p\, log(\frac{h_1}{h_2}) \tag{2.36}$$

When the data arrives in the region of monotonic convergence, it is possible to calculate the error estimate ε_ϕ with the equation (2.34), but in complex geometries or complex equations, the scatter data appears, additional equations for the error estimate are needed.
The steps to obtain the discretization error, ε_ϕ, for all cases are the following:

1. First, to determine the order of grid covergence, p, by solving the equation (2.37) in terms of the least-squares sense with and without weights of the truncated power series expansions.

   $$\delta_{RE} = \alpha\, h_i^p \tag{2.37}$$

   The parameters α, p and ϕ_0 are calculated from the minimum of S_{RE} (2.40) with and without weights (2.38), (2.39):

   - Non-weighted approach

     $$w_i = 1 \quad and \quad nw_i = 1 \tag{2.38}$$

- Weighted approach

$$w_i = \frac{\frac{1}{h_i}}{\sum_{i=1}^{n_g} \frac{1}{h_i}} \quad and \quad nwi = n_g w_i \tag{2.39}$$

From the minimum of the function (2.40), it leads to a system of non-linear equations, (2.41),(2.42),(2.43).

$$S_{RE}(\phi_0, \alpha, p) = \sqrt{\sum_{i=1}^{n_g} w_i(\phi_i - (\phi_0 + \alpha h_i^p))^2} \tag{2.40}$$

$$\phi_0 = \sum_{i=1}^{n_g} w_i \phi_i - \alpha \sum_{i=1}^{n_g} w_i h_i^p \tag{2.41}$$

$$\alpha = \frac{\sum_{i=1}^{n_g} w_i \phi_i h_i^p - (\sum_{i=1}^{n_g} w_i \phi_i)(\sum_{i=1}^{n_g} w_i h_i^p)}{\sum_{i=1}^{n_g} w_i h_i^{2p} - (\sum_{i=1}^{n_g} w_i h_i^p)(\sum_{i=1}^{n_g} w_i h_i^p)} \tag{2.42}$$

$$\sum_{i=1}^{n_g} w_i \phi_i h_i^p log(h_i) - \phi_0 \sum_{i=1}^{n_g} w_i h_i^p log(h_i) - \alpha \sum_{i=1}^{n_g} w_i h_i^{2p} log(h_i) = 0 \tag{2.43}$$

and its standard deviation:

$$\sigma_{RE} = \sqrt{\frac{\sum_{i=1}^{n_g} nw_i(\phi_i - (\phi_0 + \alpha h_i^p))^2}{(n_g - 3)}} \tag{2.44}$$

From here it is possible to calculate the discretizacion error, (2.34), (2.37).

- If any of fits has the order of grid convergence between $0.5 \leqslant p \leqslant 2$, the error is estimated from $\varepsilon_\phi = \delta_{RE}$ (2.37). In the case of both fits with $0.5 \leqslant p \leqslant 2, \delta_{RE}$ corresponds the fit with the smallest standard deviation, σ.

- If p is grater than 2, p>2, this can produce too small error estimates. That is why the error is calculated with other equations with fixed exponents δ_1(2.45), δ_2 (2.46). The best of the four fits is chosen by the one with the smallest standard deviation

$$\delta_1 = \alpha h_i \tag{2.45}$$

$$\delta_2 = \alpha h_i^2 \tag{2.46}$$

The parameters ϕ_0, α and the standard deviation, σ are obtained from the following equations:

$$S_1(\phi_0, \alpha) = \sqrt{\sum_{i=1}^{n_g} w_i(\phi_i - (\phi_0 + \alpha h_i))^2} \tag{2.47}$$

$$\phi_0 + \alpha \sum_{i=1}^{n_g} w_i h_i = \sum_{i=1}^{n_g} w_i \phi_i \tag{2.48}$$

$$\phi_0 \sum_{i=1}^{n_g} w_i h_i + \alpha \sum_{i=1}^{n_g} w_i h_i^2 = \sum_{i=1}^{n_g} w_i \phi_i h_i \tag{2.49}$$

and its standard deviation:

$$\sigma_1 = \sqrt{\frac{\sum_{i=1}^{n_g} n w_i (\phi_i - (\phi_0 + \alpha h_i))^2}{(n_g - 2)}} \tag{2.50}$$

For a single term expansion with second-order term

$$S_2(\phi_0, \alpha) = \sqrt{\sum_{i=1}^{n_g} w_i (\phi_i - (\phi_0 + \alpha h_i^2))^2} \tag{2.51}$$

$$\phi_0 + \alpha \sum_{i=1}^{n_g} w_i h_i^2 = \sum_{i=1}^{n_g} w_i \phi_i \tag{2.52}$$

$$\phi_0 \sum_{i=1}^{n_g} w_i h_i^2 + \alpha \sum_{i=1}^{n_g} w_i h_i^4 = \sum_{i=1}^{n_g} w_i \phi_i h_i^2 \tag{2.53}$$

and its standard deviation:

$$\sigma_2 = \sqrt{\frac{\sum_{i=1}^{n_g} n w_i (\phi_i - (\phi_0 + \alpha h_i^2))^2}{(n_g - 2)}} \tag{2.54}$$

- If p<0.5, the error estimate can become too conservative and again the error is estimated with the equations with fixed exponents, (2.45), (2.46), and additional the equation (2.55):

$$\delta_{12} = \alpha_1 h_i + \alpha_2 h_i^2 \tag{2.55}$$

From the least-squares solutions, the ε_ϕ is obtained form the fit that has the smallest standard deviation from the 6 fits needed to be calculated, following:

$$S_{12}(\phi_0, \alpha_1, \alpha_2) = \sqrt{\sum_{i=1}^{n_g} w_i (\phi_i - (\phi_0 + \alpha_1 h_i + \alpha_2 h_i^2))^2} \tag{2.56}$$

$$\phi_0 + \alpha_1 \sum_{i=1}^{n_g} w_i h_i + \alpha_2 \sum_{i=1}^{n_g} w_i h_i^2 = \sum_{i=1}^{n_g} w_i \phi_i \tag{2.57}$$

$$\phi_0 \sum_{i=1}^{n_g} w_i h_i + \alpha_1 \sum_{i=1}^{n_g} w_i h_i^2 {}_{\alpha 2} \sum_{i=1}^{n_g} w_i h_i^3 = \sum_{i=1}^{n_g} w_i \phi_i h_i \tag{2.58}$$

$$\phi_0 \sum_{i=1}^{n_g} w_i h_i^2 + \alpha_1 \sum_{i=1}^{n_g} w_i h_i^3 {}_{\alpha 2} \sum_{i=1}^{n_g} w_i h_i^4 = \sum_{i=1}^{n_g} w_i \phi_i h_i^2 \tag{2.59}$$

and its standard deviation:

$$\sigma_{12} \sqrt{\frac{\sum_{i=1}^{n_g} n w_i (\phi_i - (\phi_0 + \alpha_1 h_i + \alpha_2 h_i^2))^2}{(n_g - 3)}} \tag{2.60}$$

2. Once the estimation of the discretization error ε_ϕ is obtained, and the quality of this estimation is calculated with the standard deviation of the fits. It is possible to estimate the uncertainty U_ϕ. To start defining the quality of the fit, a data range parameter is calculated as:

$$\Delta_\phi = \frac{(\phi_i)_{max} - (\phi_i)_{min}}{n_g - 1} \tag{2.61}$$

3. To calculate the Uncertainty, a safety factor is designated depending on how good or bad is the error estimation, which is characterized as reliable if the solution is monotonically convergent with 0.5<p<2.1 and the standard deviation is less than the data range parameter (2.61) ($\sigma < \Delta_\phi$), being in this scenario the safety factor of F_S=1.25. Otherwise F_S=3. Finally it is possible to calculate the uncertainty with:

   - For $\sigma < \Delta_\phi$:

   $$U_\phi(\phi_i) = F_S \varepsilon_\phi(\phi_i) + \sigma + |\phi_i - \phi_{fit}| \tag{2.62}$$

   - For $\sigma \geqslant \Delta_\phi$:

   $$U_\phi(\phi_i) = 3\frac{\sigma}{\Delta_\phi}(\varepsilon_\phi(\phi_i) + \sigma + |\phi_i - \phi_{fit}|) \tag{2.63}$$

3. Numerical Friction line

3.1. Flat Plate CFD Simulations Set Up

The range of Reynolds numbers used to determine the numerical friction line, $log(Re) = 6$ to $log(Re) = 9.75$, is selected based on the Reynolds numbers at which models tests are usually run and the ones that reach the modern big ships in length and speed. To simulate flat plate throughout all this Reynolds range, the plate properties must be adjusted. In this study it is decided to vary the length of the plate and keep the velocity of the fluid constant. However, the Reynolds range is so wide that it is necessary to also vary the speed after a certain Reynolds number. Table 3.1 shows the velocity and lengths for each Reynolds number. As a result, 16 different flat plates with length of 2.85 m to 446 m are generated and run at speeds from 0.4 to 15 m/s. The fresh water density and molecular viscosity are used for flat plate simulations at low Reynolds numbers, and the properties of salt water are used for the high Reynolds numbers simulations. The characteristics of each flat plate from the corresponding Reynolds number are shown in the table 3.1:

Table 3.1.: Flat plate characteristics for numerical simulations

Flat Plate #	**log10(Re)**	**Reynolds Number**	**Density [kg/m3]**	**Molecular Viscosity [Pa.s]**	**Velocity [m/s]**	**Length [m]**
1	6.00	1.00E+06	999.01	1.14E-03	0.4	2.85
2	6.25	1.78E+06	999.01	1.14E-03	0.4	5.06
3	6.50	3.16E+06	999.01	1.14E-03	1.0	3.60
4	6.75	5.62E+06	999.01	1.14E-03	1.0	6.40
5	7.00	1.00E+07	1026.20	1.22E-03	4.0	2.97
6	7.25	1.78E+07	1026.20	1.22E-03	4.0	5.29
7	7.50	3.16E+07	1026.20	1.22E-03	4.0	9.40
8	7.75	5.62E+07	1026.20	1.22E-03	4.0	16.71
9	8.00	1.00E+08	1026.20	1.22E-03	4.0	29.72
10	8.25	1.78E+08	1026.20	1.22E-03	8.0	26.43
11	8.50	3.16E+08	1026.20	1.22E-03	8.0	46.99
12	8.75	5.62E+08	1026.20	1.22E-03	8.0	83.56
13	9.00	1.00E+09	1026.20	1.22E-03	8.0	148.60
14	9.25	1.78E+09	1026.20	1.22E-03	8.0	264.25
15	9.50	3.16E+09	1026.20	1.22E-03	15.0	250.62
16	9.75	5.62E+09	1026.20	1.22E-03	15.0	445.67

Computational domain

For the numerical calculation of the friction resistance of the flow over a flat plate, the computational domain is structured as a prismatic grid where the x direction, corresponds to the flow direction parallel to the flat plate, z the normal direction to the plate, and y out of the page with one cell thick. Considering the length of the plate as L, the upstream extent is $0.25L$ of the leading edge, the top boundary located $0.5L$ away from the plate. The upstream extend is needed before the flat plate to allow the fluid to develop and not cause disturbances due to the presence of this body. The dimensions of the computational domain were based on the "2D Zero Pressure Gradient Flat Plate Validation Case" from NASA technical report [24] and the numerical friction line study made by Eça and Hoekstra [2]. The origin of the coordinate system $x, y, z = 0, 0, 0$ is set at the start of the flat plate at the red point in the Figure 3.1.

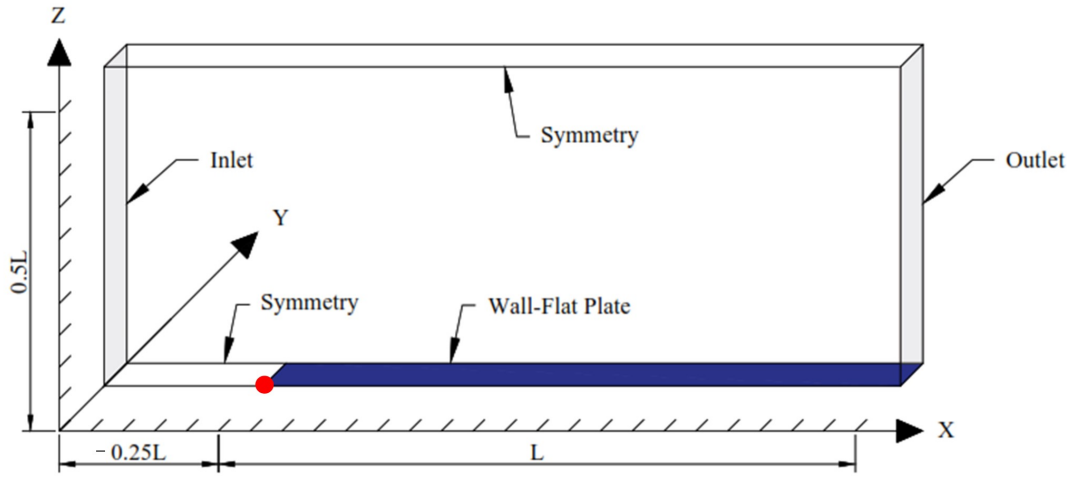

Figure 3.1.: Flat plate computational domain

Turbulence model

For the numerical simulations of the flat plate two turbulence model are selected the $k-\omega$ standard and the $k-\omega$ SST because in the present thesis the interest relies on the flow very close to the wall for the flat plate simulations. The $k-\epsilon$ model is left out as it is focus in solving the fully turbulent flow outside the viscous sublayer. $k-\omega$ standard is selected as it is based on the near wall treatment, being able to solve low-Re number problems. The $k-\omega$ SST is also implemented for the simulations since, unlike the the $k-\omega$ standard, it has an adequate treatment of the turbulence interface between near the wall and the free stream of the fluid.

3.2. Flat Plate Meshing

The meshing is performed in ANSYS, a structured grid of hexahedral elements is used for the discretization. The cells are distributed similar in all the grids for the different Reynolds numbers but differing in the first cell size and the thickness of the boundary layer. Inflation was used on the flat plate surface along the z direction to control the values of the y^+ and the boundary layer thickness. Table 3.2 shows the prediction of these values for the different Reynolds numbers at the finest grid. Also, refinement was applied in the x direction around the plane $x = 0$ at the position where the flat plate starts, in order to refine the cells in that zone and have a better capture of the large pressure gradient at the start of the plate. The mesh used for the simulations can be seen at figure 3.2.

Table 3.2.: Flat plate boundary layer meshing characteristics

log10(Re)	**Theoretical flat plate** C_F	**Boundary layer [m]**	**Desired y^+ finest grid**	**First cell size finest grid [m]**	**Grow ratio**	**Number of layers**
6.00	0.0045	0.063	0.018	2.13E-06	1.3	35
6.25	0.0040	0.104	0.018	2.24E-06	1.3	37
6.50	0.0036	0.068	0.018	9.44E-07	1.3	39
6.75	0.0033	0.111	0.018	9.91E-07	1.3	40
7.00	0.0030	0.048	0.018	2.71E-07	1.3	42
7.25	0.0027	0.078	0.018	2.84E-07	1.3	44
7.50	0.0025	0.128	0.018	2.96E-07	1.3	45
7.75	0.0023	0.209	0.018	3.09E-07	1.3	47
8.00	0.0021	0.342	0.018	3.22E-07	1.3	49
8.25	0.0020	0.280	0.050	4.74E-07	1.3	47
8.50	0.0018	0.459	0.050	4.93E-07	1.3	48
8.75	0.0017	0.752	0.050	5.11E-07	1.3	50
9.00	0.0016	1.231	0.050	5.30E-07	1.3	52
9.25	0.0015	2.017	0.050	5.49E-07	1.3	54
9.50	0.0014	1.762	0.050	3.03E-07	1.3	55
9.75	0.0013	2.886	0.050	3.14E-07	1.3	57

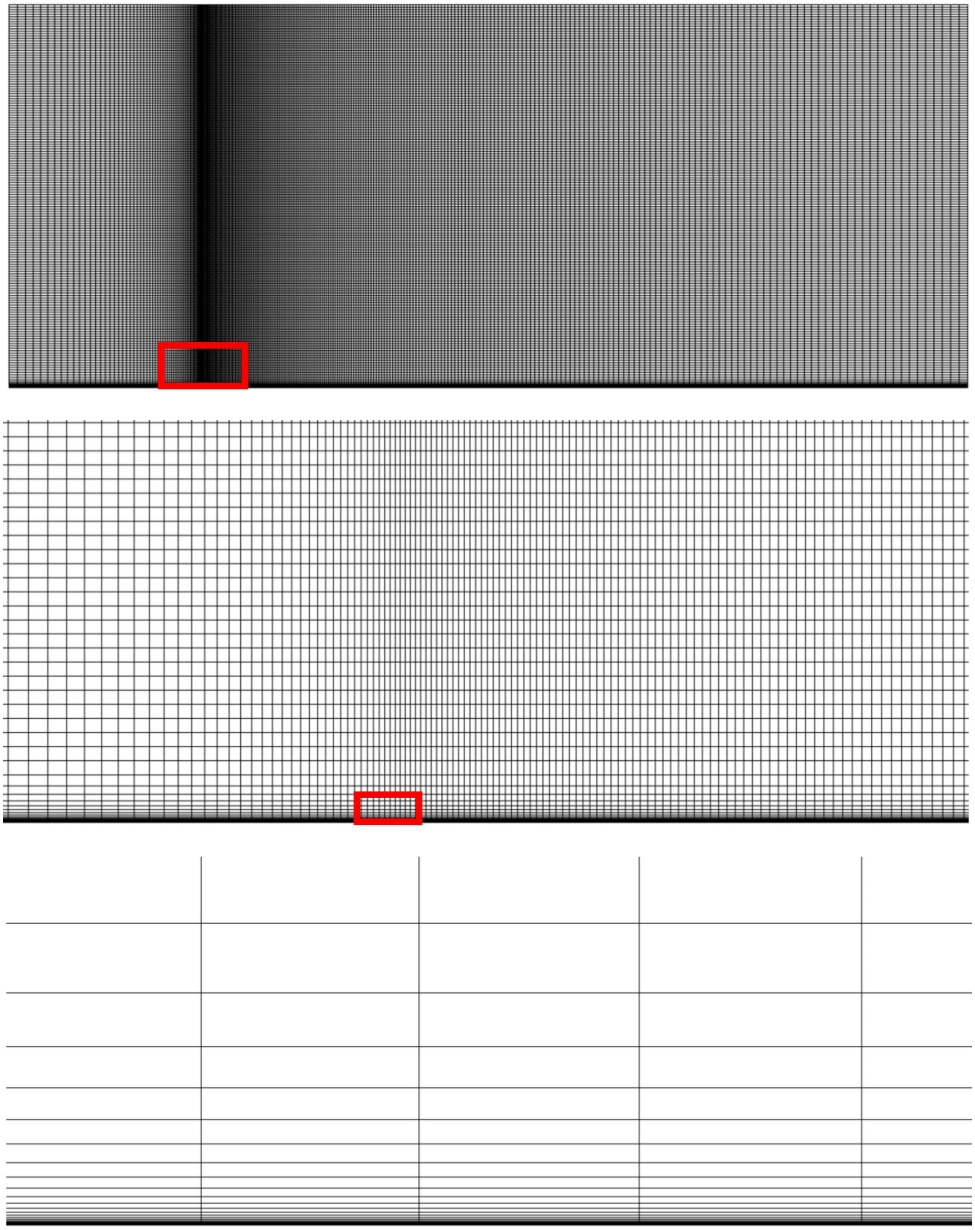

Figure 3.2.: Volume mesh for the CFD simulations

Iterative convergence

In figure 3.3 is shown the residuals of the numerical simulation of the flat plate at $log(Re) = 6.0$ for the finest grid (desired $y^+ = 0.018$). From this figure it can be concluded that the iterative error is negligible as after 40 000 iterations the residuals falls under $10E - 6$. This error is not considered for the calculation of the numerical simulation uncertainty.

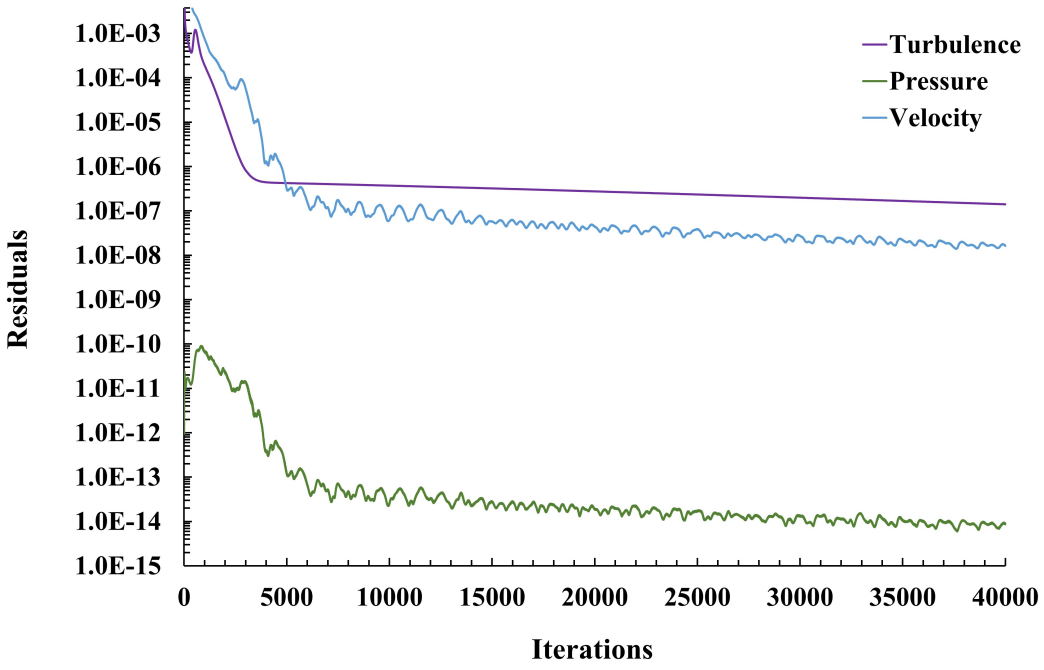

Figure 3.3.: Convergence of residuals in the numerical solution of the flat plate at log(Re) = 6. In the plot, turbulence represents the kinetic energy and dissipation.

3.3. Grid Sensitivity Analysis

In the present work, the estimation of the numerical uncertainty of the total resistance coefficient of the flat plate simulations is based on the discretization error calculated with power series expansions. For each Reynolds number there are 11 grids used in the grid sensitivity analysis. The parameter chosen to vary between the grids, h_i, corresponds to the y^+, with a refinement ratio $h_2/h_1 = \sqrt{2}$, being the same for all the meshes in all the Reynolds numbers. The rest of the parameters are kept constant. The finest y^+ value is chosen differently, from log(Re)=6.0 to log(Re)=8.0, $h_1 = y^+ = 0.018$ and from log(Re)=8.25 to log(Re)=9.75 h_1=0.05 and $h_{11} = 1.6$. Because as the turbulence increase, the boundary layer becomes thicker and the distance to the first cell reduces, this generates oscillation in the results at very thin y^+. The numerical simulations for the grid sensitivity analysis are carried out using the two-equation model $k-\omega$ standard.

The order of grid convergence, p, at each Reynolds is determined following the non linear equations described in the section 2.11. Based on this answer, if 0.5<p<2 or p>2 or p<0.5, the parameters α, ϕ_0, are calculated by power series of the error estimate with or without fixed exponents with one or two terms expansions, δ_{RE}, δ_1, δ_2 or δ_{12} . Table 3.3 shows the p values with their respective equation for the error estimate.

At the lower Reynolds numbers, $6.00 \leqslant log(Re) \leqslant 8.50$, the results of the simulations C_F present a monotonically convergence behaviour with values of the order of grid convergence between $0.5 \leqslant p \leqslant 2$. The error estimate is calculated with the single equation (2.34), δ_{RE}, and

then the uncertainty of this estimation is obtained. Tables 3.4, 3.5, present the values for all the grids at each Reynolds number, reaching around 1% the uncertainties of the total resistance prediction with respect to the finest grid. Within the same Reynolds number the maximum errors occur at the coarser grids, reaching uncertainties of 10%.

At high Reynolds numbers, log(Re)=8.75,log(Re)=9.0, log(Re)=9.5, p values are lower than 0.5 being outside the range of monotonically convergent data, but are not classified as anomalous data as the p values are not less than zero. In these cases, the error estimate is obtained with power series of two terms expansions δ_{12}. The uncertainties of these estimations are shown in table 3.5, where for the majority of high Reynolds numbers the uncertainties are less than 1% except for log(Re)=9.50 with 2%.

Table 3.3.: Order of grid convergence at high Reynolds numbers

Log(Re)	**p**	**Error Estimator**
6.00	0.64	δ_{RE}
6.25	0.65	δ_{RE}
6.50	0.65	δ_{RE}
6.75	0.65	δ_{RE}
7.00	0.66	δ_{RE}
7.25	0.65	δ_{RE}
7.50	0.65	δ_{RE}
7.75	0.70	δ_{RE}
8.00	0.80	δ_{RE}
8.25	0.82	δ_{RE}
8.50	0.58	δ_{RE}
8.75	0.41	δ_{12}
9.00	0.08	δ_{12}
9.25	1.07	δ_{RE}
9.50	0.46	δ_{12}
9.75	1.22	δ_{RE}

Table 3.4.: Percentage of the numerical uncertainty for the total resistance coefficient at Reynolds numbers from log(Re)=6.00 to log(Re)=8.00

Y+	**log(Re)**								
	6.00	**6.25**	**6.50**	**6.75**	**7**	**7.25**	**7.50**	**7.75**	**8.00**
0.018	-0.84	-0.81	-0.76	-0.73	-0.70	-0.70	-0.67	-0.53	-0.34
0.025	-1.05	-1.01	-0.96	-0.91	-0.87	-0.88	-0.81	-0.69	-0.44
0.035	-1.31	-1.26	-1.19	-1.12	-1.08	-1.09	-0.95	-0.85	-0.59
0.050	-1.63	-1.57	-1.49	-1.42	-1.36	-1.36	-1.33	-1.09	-0.82
0.071	-2.05	-1.98	-1.89	-1.80	-1.73	-1.71	-1.68	-1.32	-1.09
0.100	-2.60	-2.52	-2.41	-2.31	-2.22	-2.18	-2.12	-1.78	-1.41
0.141	-3.32	-3.20	-3.06	-2.93	-2.83	-2.79	-2.68	-2.43	-1.87
0.200	-4.19	-4.04	-3.87	-3.71	-3.59	-3.52	-3.39	-3.12	-2.48
0.283	-5.29	-5.11	-4.90	-4.71	-4.55	-4.44	-4.29	-4.01	-3.40
0.400	-6.68	-6.45	-6.20	-5.95	-5.76	-5.61	-5.42	-5.13	-4.58
0.566	-8.24	-7.92	-7.60	-7.31	-7.06	-6.90	-6.66	-6.26	-5.85

Table 3.5.: Percentage of the numerical uncertainty for the total resistance coefficient at Reynolds numbers from log(Re)=8.25 to log(Re)=9.75

Y+	**log(Re)**						
	8.25	**8.50**	**8.75**	**9.00**	**9.25**	**9.50**	**9.75**
0.050	-0.71	-1.01	-0.25	0.47	0.96	1.96	0.15
0.071	-0.92	-1.29	-1.31	4.98	1.07	2.71	0.26
0.100	-1.26	-1.76	-1.13	-0.79	1.07	5.44	0.08
0.141	-1.73	-1.74	-2.46	-1.78	1.70	3.89	0.17
0.200	-2.31	-2.58	-3.73	0.16	1.47	6.64	-0.47
0.283	-3.12	-3.20	-3.79	-4.74	2.31	13.03	0.24
0.400	-4.01	-3.85	-5.57	-6.70	5.45	10.37	-1.35
0.566	-5.62	-4.88	-8.79	-7.62	3.29	15.52	-2.50
0.800		-6.17	-8.92	-7.82	7.01	18.73	-1.70
1.131		-7.78	-10.53	-8.33	9.73	20.32	-5.19
1.600		-8.92	-12.92	0.53	9.37	23.54	-9.20

Figures 3.4, 3.5 and 3.6 show the convergence of the total resistance in terms of the grid refinement ratio y^+. For the majority of Reynolds numbers, visually the monotonically behaviour is confirmed by the plots that contain in addition the respective prediction of the exact solution and the fit values of the resistance coefficients for all the grids. For log(Re)=8.75,log(Re)=9.0, log(Re)=9.5 results of the total resistance from the numerical simulations have oscillatory behavior, which is appreciated in the graphs and was confirmed with p values less than 0.5. The plot of log(Re)=9 shows more scatter in the data than the rest of Reynolds numbers, being the only one that presents $\sigma > \Delta_\phi$, getting the quality of a bad error estimation.

From this section, it can be mention that the convergence of the C_T depends on the Reynolds number and the distance of the first grid cell from the flat plate. There was the need of other error estimators as not all the data fit the standard equation, more specific at high Reynolds numbers. The majority of the uncertainties of the error estimate of the exact solution with respect to the finest grid are below 2%, which allows to continue with further studies. And being this maximum percentage of acceptance normally depending on the complexity of the simulations, grids, turbulent models, etc.

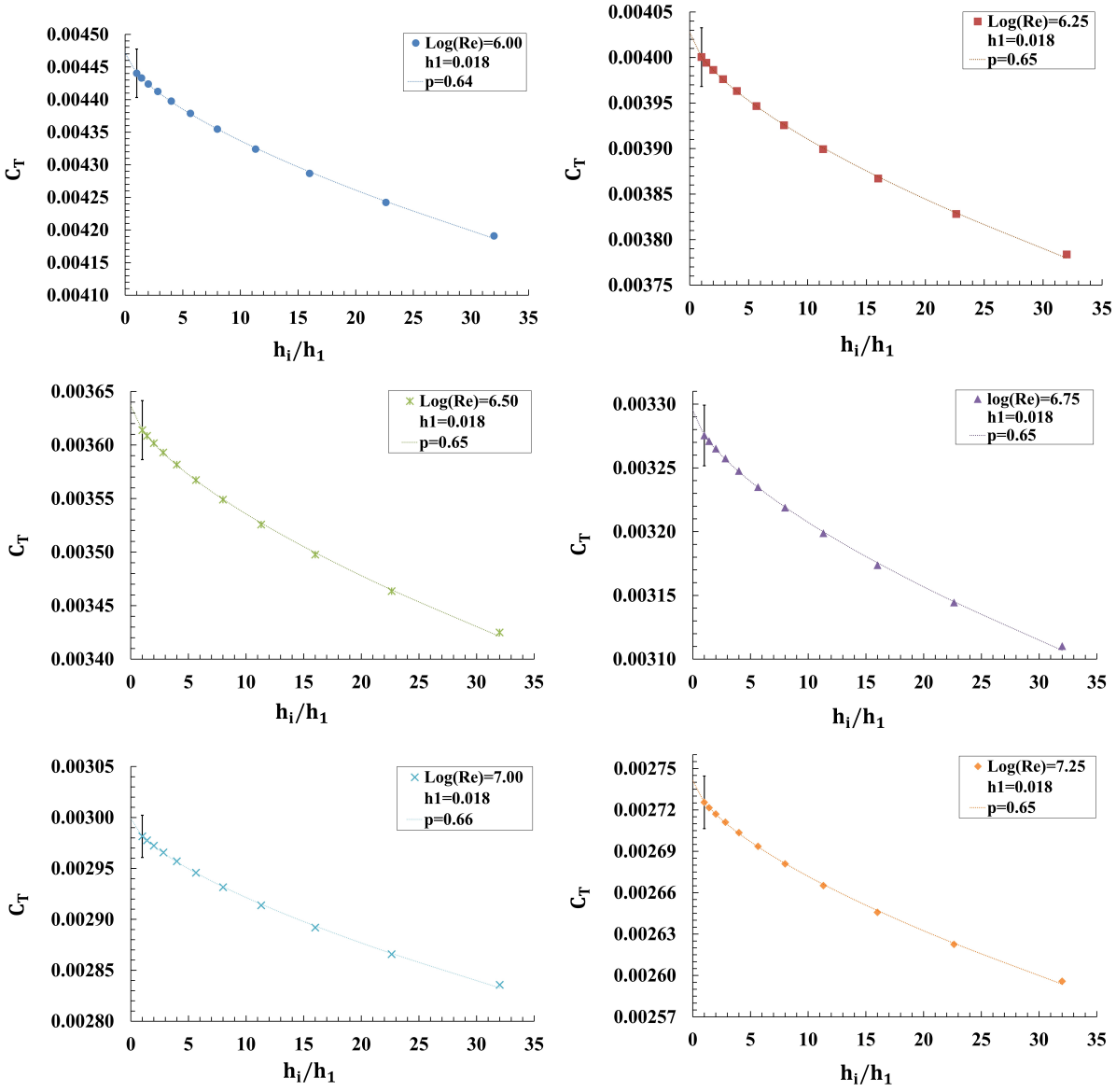

Figure 3.4.: Resistance coefficient with the grid refinement ratio used for the grid convergence analysis of the flat plate numerical simulations varying the y^+ value for a range of Reynolds numbers from log(Re)=6 to log(Re)=7.25

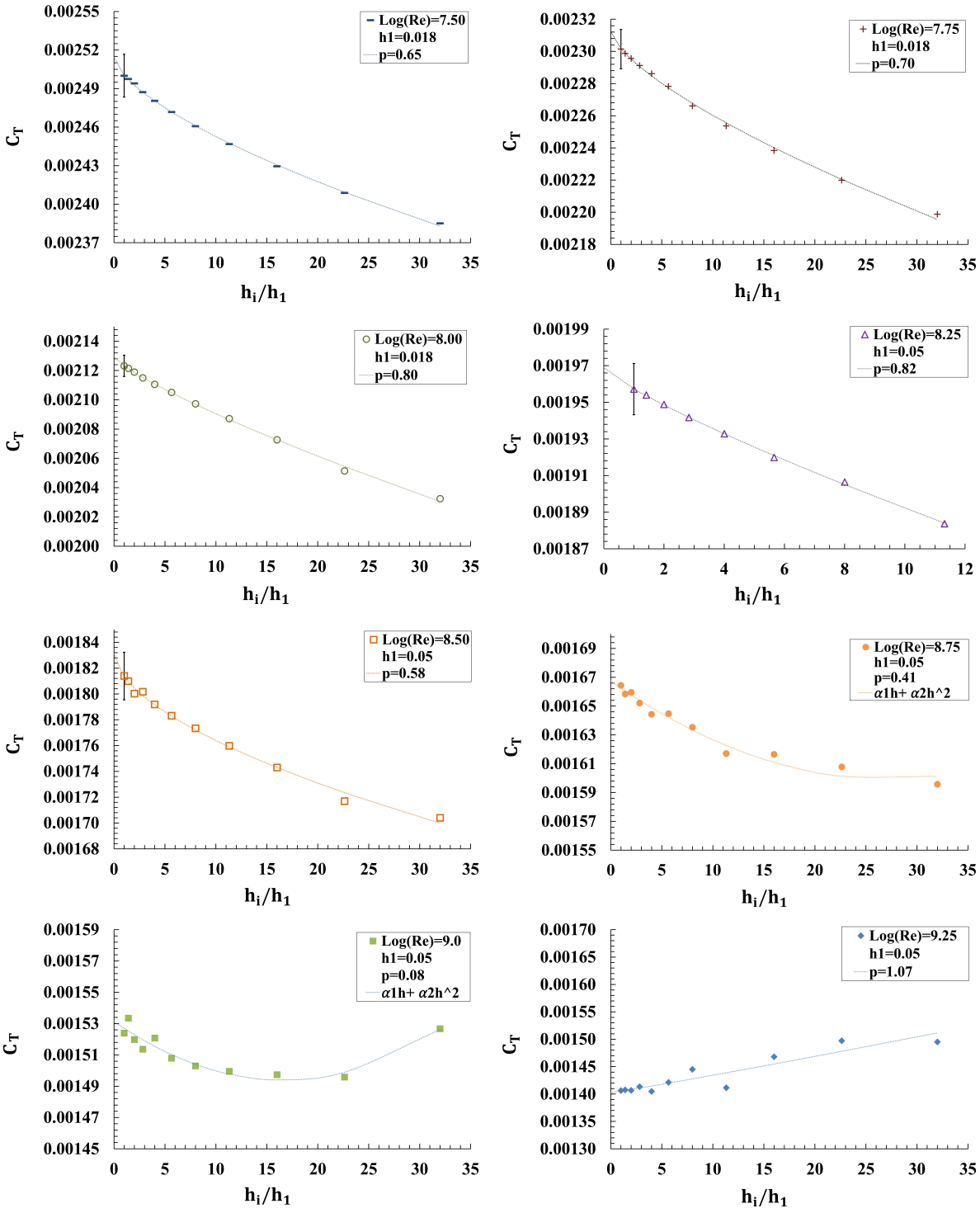

Figure 3.5.: Resistance coefficient with the grid refinement ratio used for the grid convergence analysis of the flat plate numerical simulations varying the y^+ value for a range of Reynolds numbers from log(Re)=7.25 to log(Re)=9.25

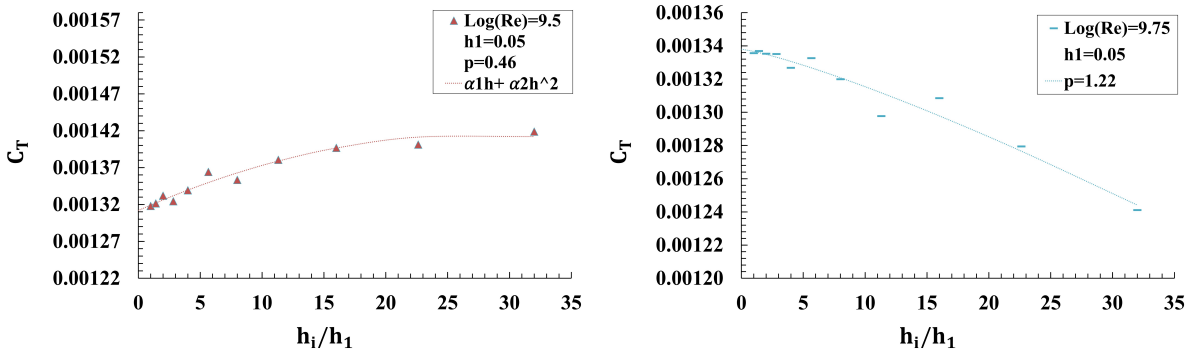

Figure 3.6.: Resistance coefficient with the grid refinement ratio used for the grid convergence analysis of the flat plate numerical simulations varying the y^+ value for a range of Reynolds numbers log(Re)=9.50 and log(Re)=9.75

3.4. Numerical Friction Line

From the results of the numerical simulations, a curve fit is needed to to obtain the numerical friction line. In this study, the ITTC'57 analytical formula (3.1) is used as the function for the curve fitting, a non-linear least squares method is applied to determine the constants a, b, and c of the approximation function. The code used is explained in Appendix A.1

$$C_F = \frac{a}{(\log_{10} Re - b)^c} \tag{3.1}$$

The results of the exact solution predictions of the flat plate frictional resistance coefficient with the $k-\omega$ Standard turbulence model are used to generate the numerical friction line. The curve fit based on the equation 3.1 is applied to this data in order to obtain the curve. Another numerical friction line is generated with the results of the simulations with the turbulence model $k-\omega$ SST, run for the same conditions, using the finest grids at each Reynolds number from the previous grid study. Figure 3.7 shows the data points of the frictional resistance coefficients of the two turbulence models with the respective curve fits. Table 3.6 shows the constants of the model function from the two numerical friction lines.

Table 3.6.: Curve fit coefficients of the numerical friction lines at the two turbulence models

Curve constants	$k-\omega\, Standard$	$k-\omega\, SST$
a	0.814	4.953
b	-0.502	-2.444
c	2.780	3.330

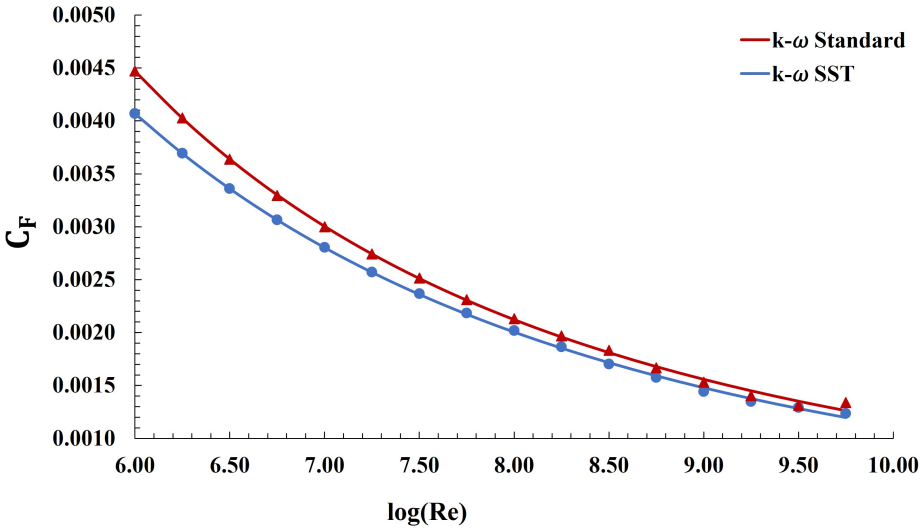

Figure 3.7.: Numerical friction line at two different turbulence models

3.5. Comparison of the numerical friction lines

Figure 3.8 shows the comparison between the numerical friction lines of the $k-\omega$ SST and $k-\omega$ Standard with the analytical equations from the open literature, as the equation for the frictional resistance of a flat plate (2.16) shown in the ITTC [21], and the correlation lines of ITTC'57 [23], Grigson [15] and Katsui [25]. The numerical results are closer to the proposed lines by literature at the highest Reynolds numbers, furthermore it can be seen the great similarity of the $k-\omega$ Standard curve with the one from the analytical line of the frictional resistance of a plat plate (2.16). Figure 3.9 shows the numerical friction lines obtained in this study and the one from Hoeskstra [2] and Korkmaz [27], all of them have the same behavior, getting closer to each other while the Reynolds number increase.

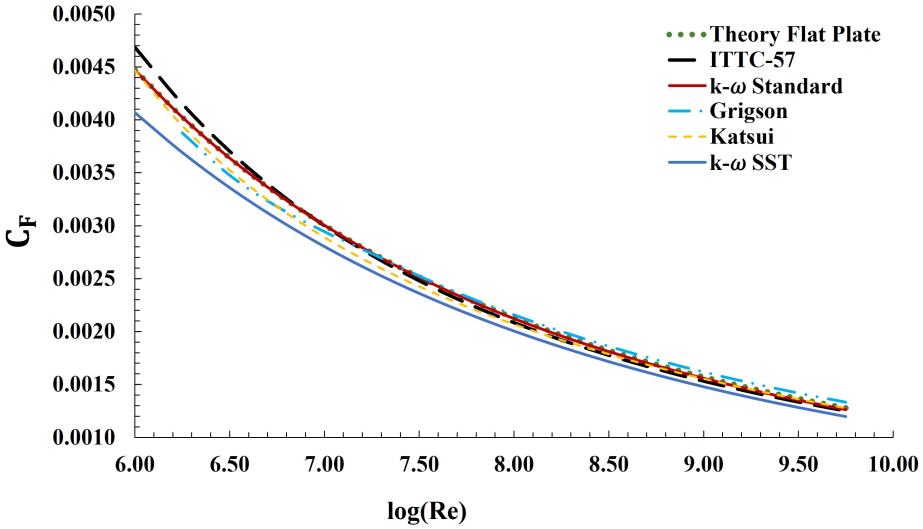

Figure 3.8.: Comparison of the numerical friction lines with the ones from literature by Katsui [25], Grigson [15], Theory Flat Plate [21], ITTC'57 [23]

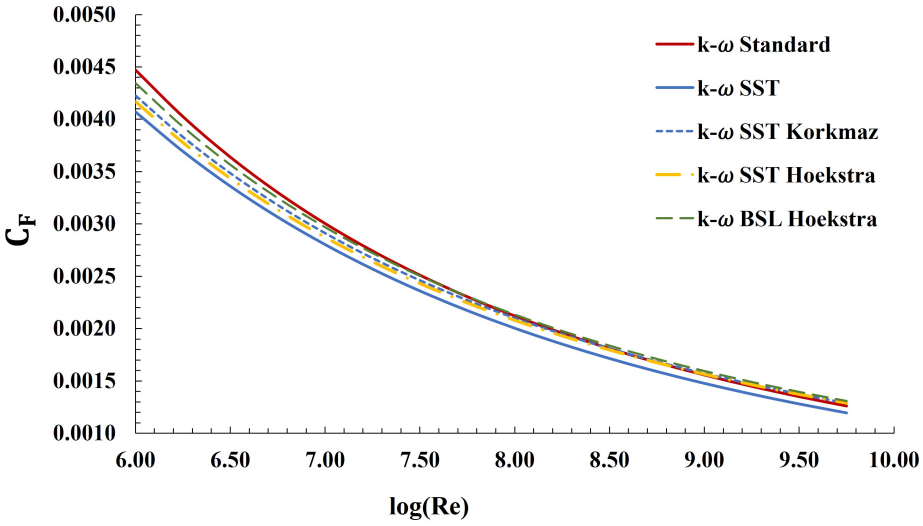

Figure 3.9.: Comparison with other numerical friction lines by Korkmaz [27] and Hoekstra[2]

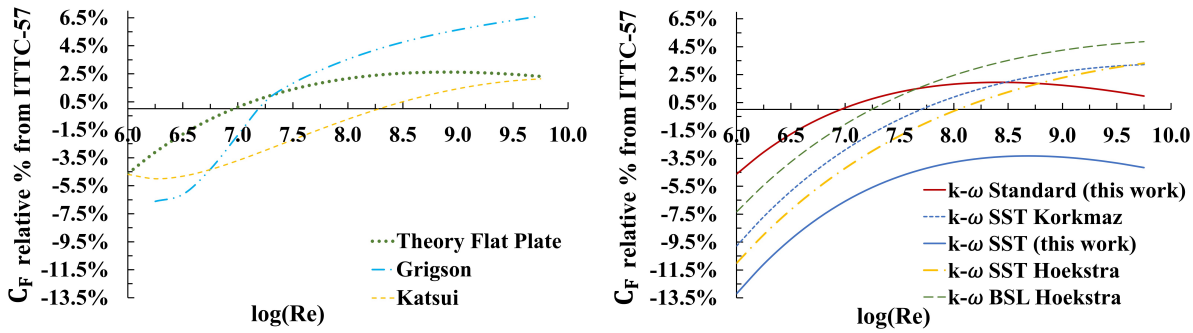

Figure 3.10.: Comparison between the friction lines with respect to the ITTC correlation line

The figure 3.10 from the left shows the difference between three friction lines from the open literature with respect to the ITTC correlation line. It is noticed that at low Reynolds numbers these other curves are lower than the ITTC curve, cross it around log(Re)=7 and log(Re)=8 and is positioned over the curve for the high Reynolds numbers, being the Grigson line with the maximum difference of 6.6% at log(Re)=9.75. The figure in the right show the difference between the numerical friction lines obtained in this study and the ones from the reference papers of Hoekstra [2] and Korkmaz [27] also in comparison with the ITTC correlation line, all the curves follow the same behavior with the exception of the $K-\omega$ SST because its difference from the ITTC line is still negative for the high Reynolds numbers, the rest of the curves have a high negative difference at low Reynolds numbers and cross the ITTC line around log(Re)=7 to log(Re)=8. Comparing the two figures, in general the numerical curves have highest negative difference at the lowest Reynolds numbers than the friction lines proposed in the literature, which means that the C_F, values at low Reynolds numbers predicted numerically are below the ones predicted analytically. Figure 3.11 also shows how the friction lines differ from each other, but in this case with respect to the numerical one proposed by Korkmaz [27], here the same behavior is obtained, the $k-\omega$ SST is below all other numerical curves, and all the analytical curves present higher values for the low Reynolds numbers.

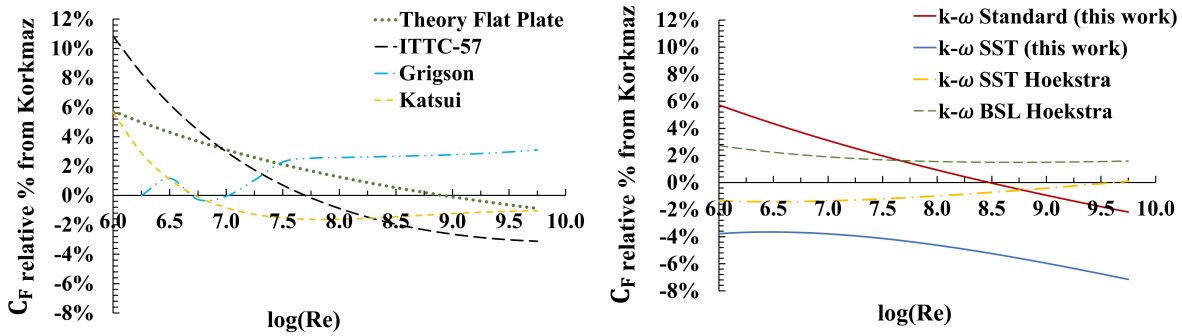

Figure 3.11.: Comparison between the friction lines with respect to the numerical friction line proposed by Korkmaz

4. Form Factor Determination

In this chapter the form factor is determined for 2 HSVA benchmark ship models using the EFD and CFD approaches. For the EFD method, model tests at different speeds and drafts are needed while for the CFD approach simulations at a determined speed at each draft are performed.

4.1. HSVA Towing Tank

The model tests are conducted at the large towing tank at HSVA, illustrated in figure 4.1. A capture during one model test is presented in figure 4.2 where it can be seen the tank, the towing carriage, the ship model, and the platform where the data collection takes place. The dimensions and characteristics of the towing tank are the following:

- Tank length: 300 m
- Tank width: 18 m
- Water depth: 5.6 m
- 30 000 m^3 fresh water
- Maximum speed of 10 m/s
- Model size up to 15 m

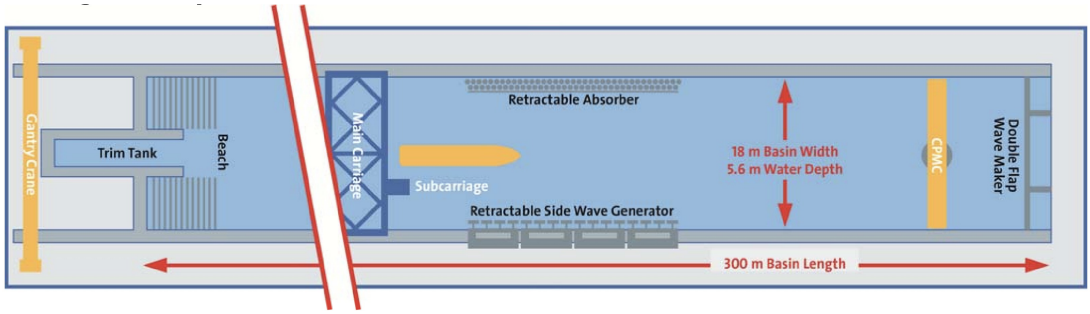

Figure 4.1.: Top view of the HSVA large towing tank [16]

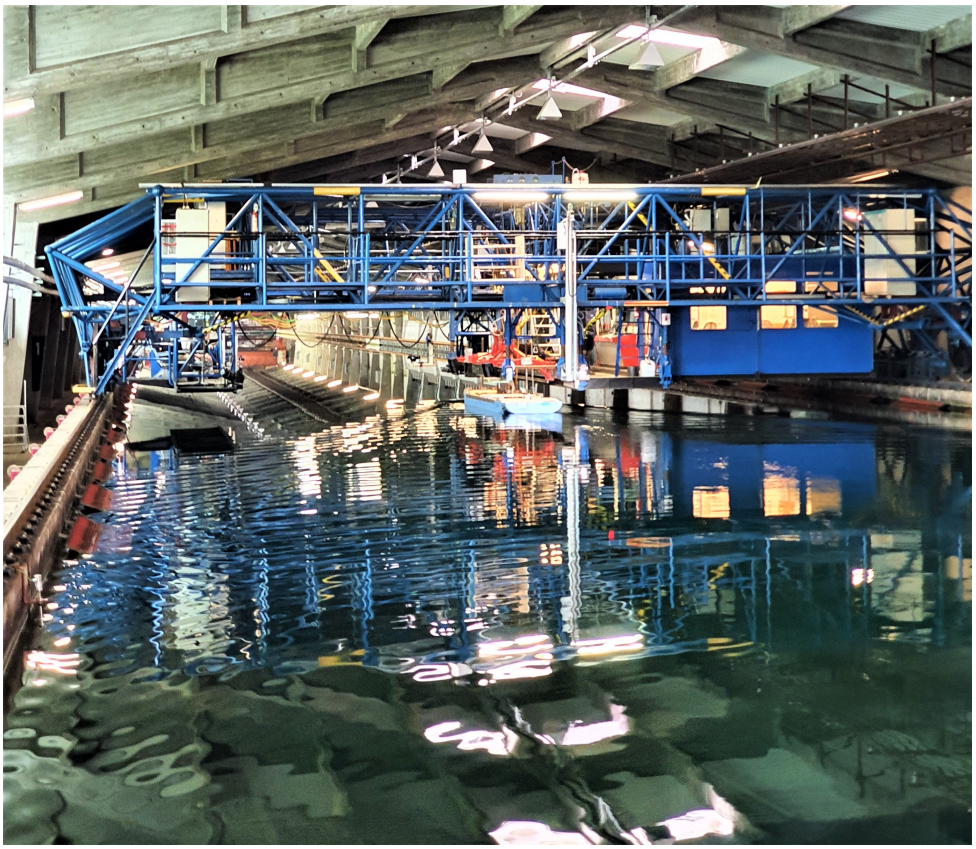

Figure 4.2.: Photograph of HSVA towing tank during a ship model test

4.2. MO5500 HSVA benchmark model

This model ship is selected for the resistance experiments at the towing tank tests. It is a multi-purpose vessel (MPV) with one propeller. The main dimensions of the MO5500 ship model are shown in table 4.1 and its geometry and lines plane are presented in figures 4.3 and 4.4.

Table 4.1.: MO5500 Main dimensions

Length between perpendiculars	L_{PP}	178.8	[m]
Beam on designed waterline	B_{WL}	30.0	[m]
Draft design at Lpp\2	T	10.0	[m]
Draft at FP	T_{FP}	10.0	[m]
Draft at AP	T_{AP}	10.0	[m]
Speed design	V	14.0	[kn]
Block Coefficient	C_B	0.60	
Scale		25.851	

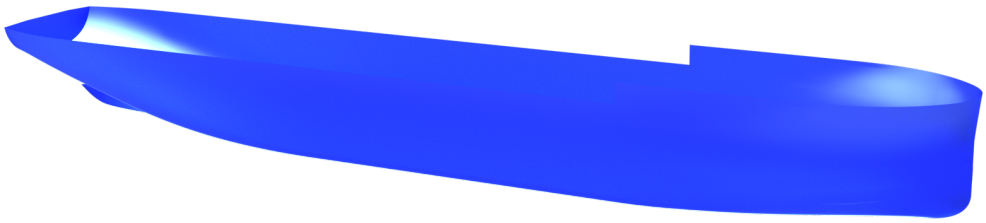

Figure 4.3.: Model Ship MO5500

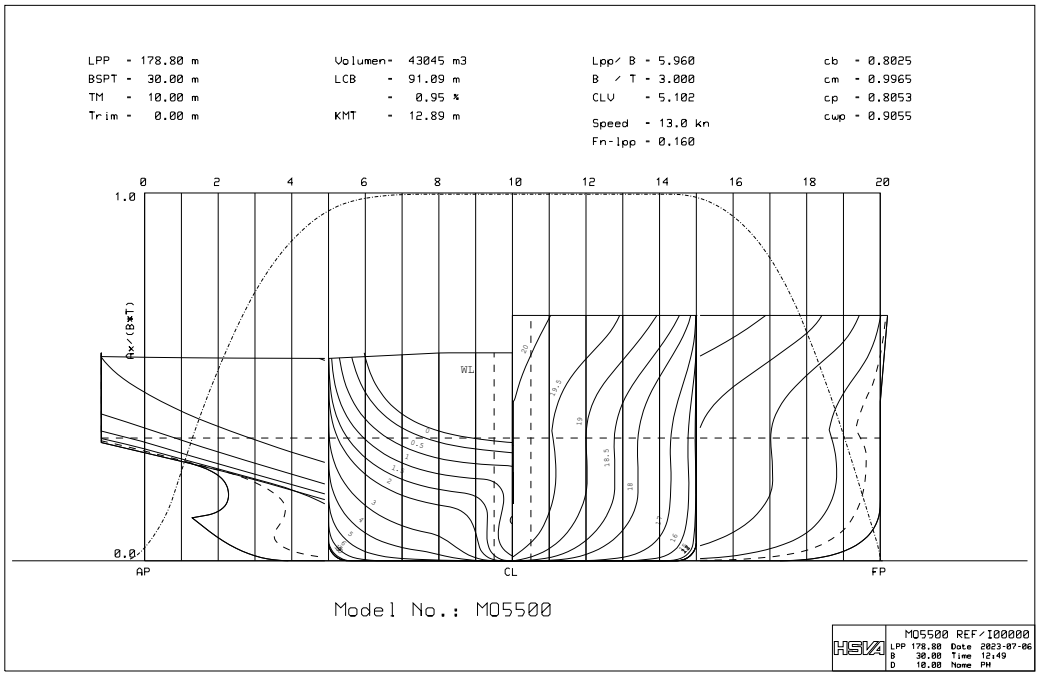

Figure 4.4.: Lines plane of the model ship MO5500. (Find A4 format at appendix A.2)

4.3. MO4500 HSVA benchmark model

The MO4500 corresponds to a model of a single screw container ship with its rudder. The main difference with respect to the previous ship model is that the MO4500 has a prominent bulbous bow. The principal particulars of this ship model are presented in table 4.2 and its geometry with the respective lines plane are shown in figures 4.5 and 4.6.

Table 4.2.: MO4500 Main dimensions

Length between perpendiculars	L_{PP}	252.4	[m]
Beam on designed waterline	B_{WL}	37.3	[m]
Draft design at Lpp\2	T	14.0	[m]
Draft at FP	T_{FP}	14.0	[m]
Draft at AP	T_{AP}	14.0	[m]
Speed design	V	23.0	[kn]
Block Coefficient	C_B	0.80	
Scale		33.15	

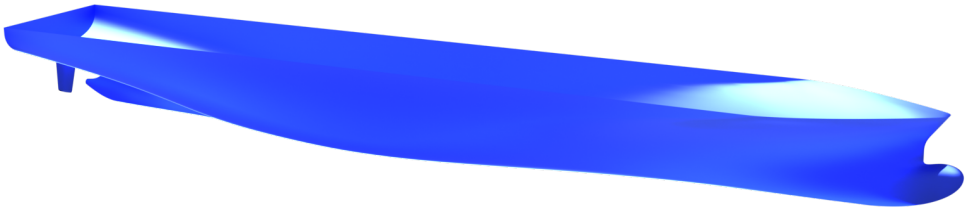

Figure 4.5.: Model Ship MO4500

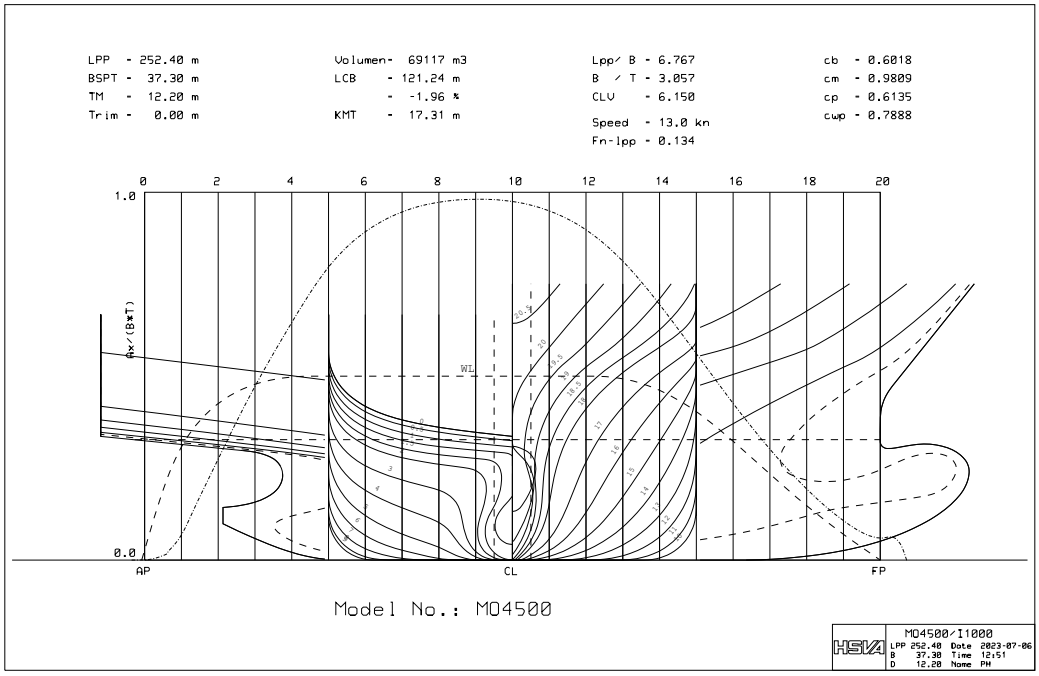

Figure 4.6.: Lines plane of the model ship MO4500. (Find A4 format at appendix A.2)

4.4. Model Tests

Model tests were carried out in order to determine the ship hull resistance at different speeds. With these total resistance coefficients the experimental form factors can be determined by the Prohaska method. To perform the experiments, the scale model of the ship is needed which is similar to the geometry of the full size ship. The scale factor λ, is selected based in the dimensions of the basin, the available stock propeller, the speed range of the carriage and the displacement of the model. The scale factors of the ship models are presented in the following table:

Table 4.3.: MO5500 and MO4500 scale factors

Ship model	λ
MO5500	25.851
MO4500	33.150

Some steps are followed for the model test performance of a resistance test, figure 4.7 show the process of a typical model test carried out at a towing tank. Those steps are followed for the resistance test of the MO5500 and MO4500 ship models. The model are towed while the instantaneous values of the total resistance are recorded when the speed of the carriage is kept constant. After the tests are finished, the instantaneous values are processed to obtain one average value at each speed. The values of the resistance and velocity are the outputs of the resistance tests, and are used for the power prediction. For each test the temperature of the tank is measured as the water properties are needed for the calculations. Table 4.4 shows the properties of the water at the towing tank for each draft condition.

Table 4.4.: Water tank properties at ship model tests

Ship Model	**T [m]**	**Tank temperature [°C]**	**Water density [kg/m³]**	**Kinematic Viscosity [m²/s]**
MO5500	12.00	19.6	998.2	1.01E-06
	10.00	17.5	998.6	1.07E-06
	14.00	16.2	998.8	1.10E-06
MO4500	12.20	16.1	998.8	1.11E-06
	7.75	16.1	998.8	1.11E-06

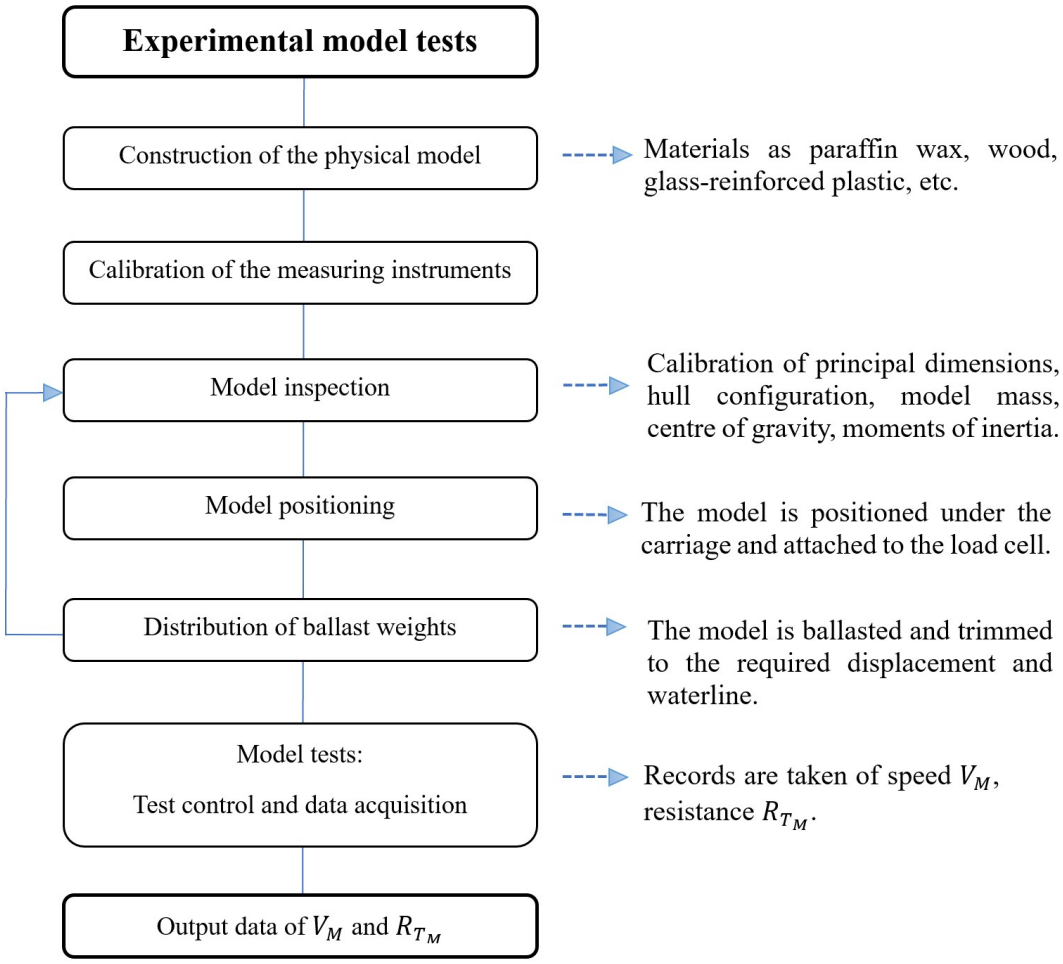

Figure 4.7.: Experimental model test process

Table 4.5 contains at which Froude numbers were performed the model tests for the ship models at the respective draft. Table 4.6 shows the models geometry properties: draft,length, wetted area and volume. Figures 4.9, 4.8 show the total resistance curve as a function of the Froude number from the model tests of the two ship models.

Table 4.5.: Number of tests and range of Froude numbers of the performed experimental models tests

Ship model	**Draft [m]**	**Range of Froude Numbers**	**# Tests**
MO5500	**12.00**	0.10-0.19	17
	10.00	0.02-0.19	23
MO4500	**14.00**	0.05-0.20	8
	12.20	0.05-0.20	7
	7.75	0.05-0.21	8

Table 4.6.: MO5500 and MO4500 main dimensions at each draft

Ship Model	T [m]	T_{aft} [m]	T_{fore} [m]	Wetted Area [m^2]	Volume [m^3]	LPP [m]	LOS [m]
MO5500	12.00	12.00	12.00	8410	52870	178.8	182.3
	10.00	10.00	10.00	7633	43024	178.8	182.3
MO4500	14.00	14.00	14.00	12668	83043	252.4	256.8
	12.20	12.20	12.20	11415	69116	252.4	256.2
	6.00	9.50	7.75	8418	39542	252.4	250.0

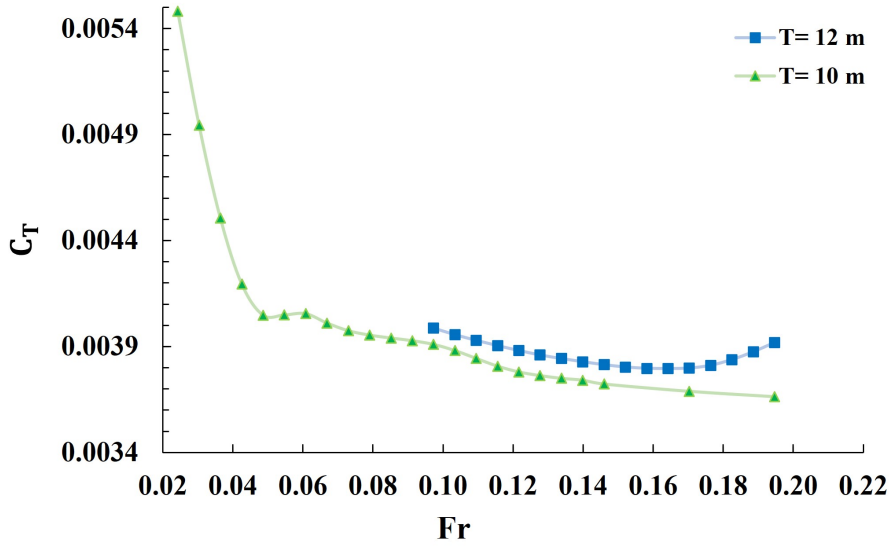

Figure 4.8.: MO5500 total ship resistance coefficient vs Froude number from towing tank tests

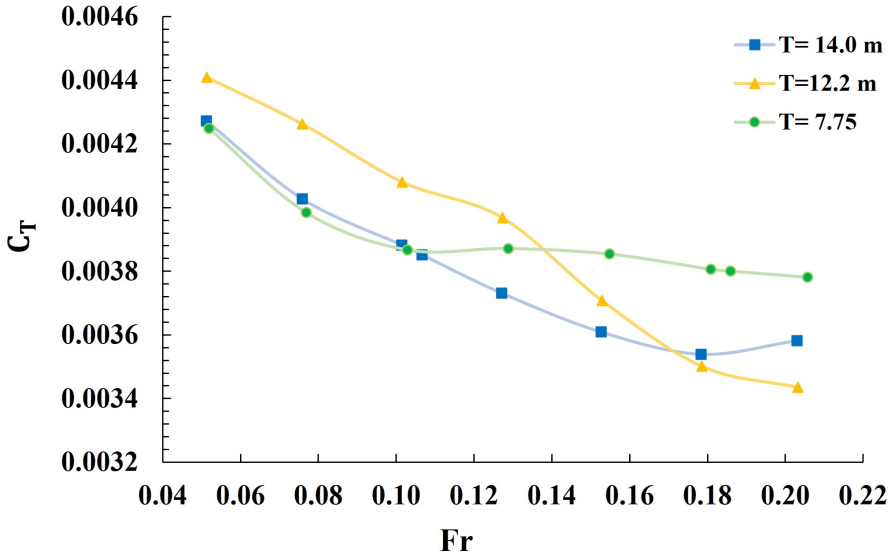

Figure 4.9.: MO4500 total ship resistance coefficient vs Froude number from towing tank tests

4.5. Experimental form factors

Following the ITTC recommendation, the form factors are determined using Prohaska method[18]. The total resistance results from the model tests are used to obtained the form factors, presented in the table 4.7. Even though, these form factor values can vary depending of which points from the results are taking into account for the curve fit. Figure 4.10 to figure 4.14 show Prohaska linear relationship applied for the model tests results at different velocities at each draft. The blue square points correspond to those used in the curve fit, and the yellow points to those not considered for the analysis. Some points were omitted because the Froude number is outside the range recommended by Prohaska of 0.1 to 0.2 or because the results at certain speeds are not considered as a good result of the experiment test.

Table 4.7.: Prohaska form Factors from towing tank tests

Model Ship	T [m]	1+k
5500	12.00	1.194
	10.00	1.169
4500	14.00	1.174
	12.20	1.179
	7.75	1.221

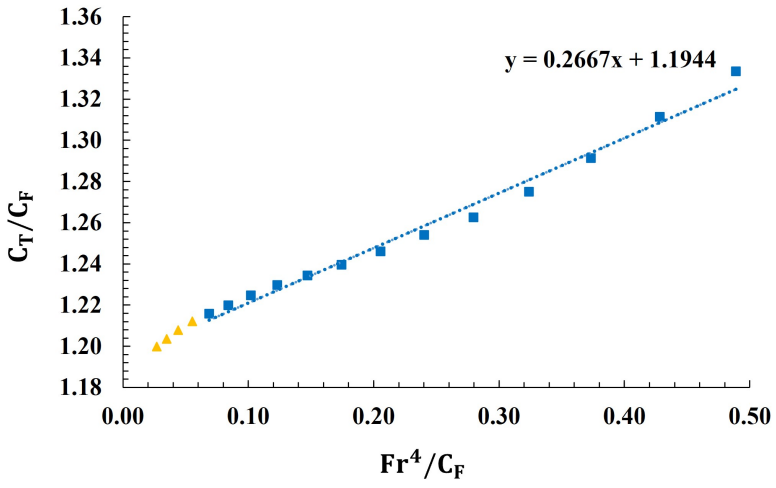

Figure 4.10.: Prohaska plot of MO5500 draft $T = 12\,m$

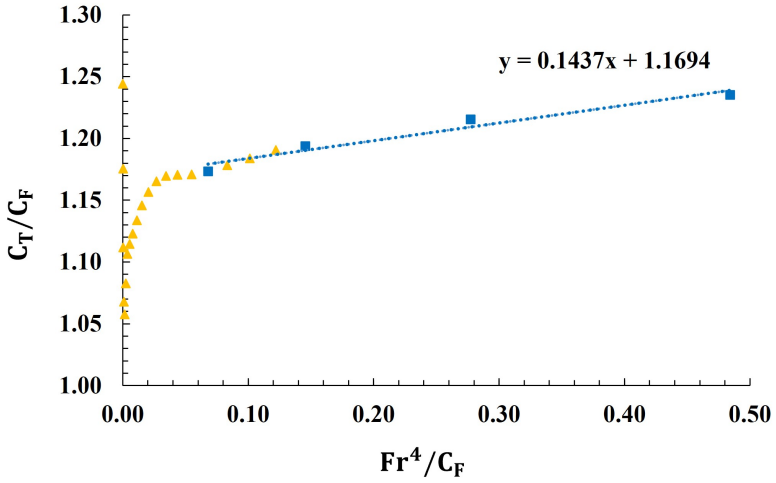

Figure 4.11.: Prohaska plot of MO5500 draft $T = 10\,m$

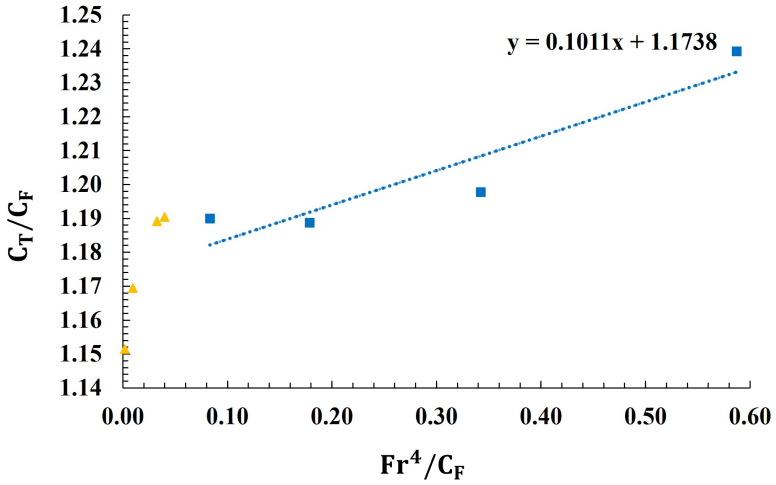

Figure 4.12.: Prohaska plot of MO4500 draft $T = 14.0\,m$

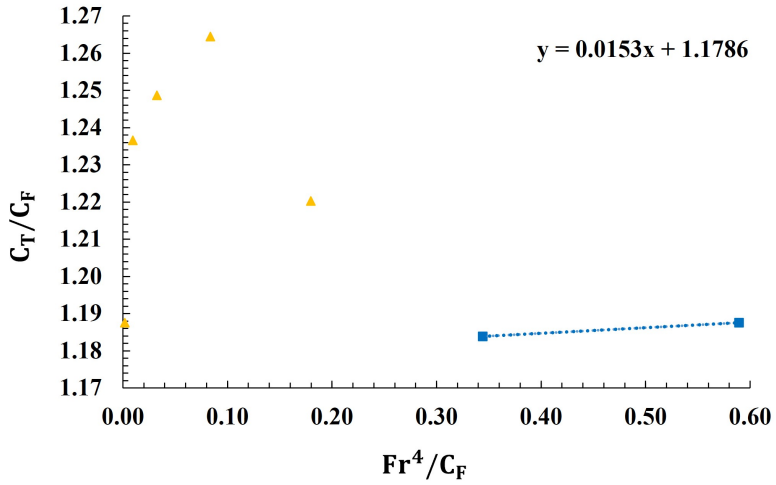

Figure 4.13.: Prohaska plot of MO4500 draft $T = 12.2\,m$

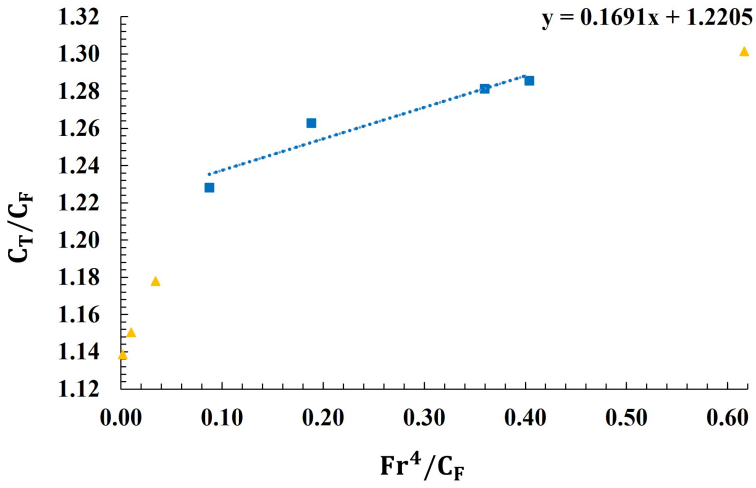

Figure 4.14.: Prohaska plot of MO4500 draft $T_{aft} = 9.5\,m$ $T_{fore} = 6.0\,m$

Prohaska method has been question in many ways, one of them is the effects of the bulbous bow. This was not mentioned by Prohaska because at the dates he proposed the method, the bulbous bow were not an important part of the designs. Nowadays there is the discussion of the influence of the bulbous bow close to the water surface or being partially submerged [28]. It is suggested that the bulbous bow could affect the linearity of the total resistance [34]. In this study the linear relationship of the Prohaska method seams to be affected by the presence of the bulbous. The graphs for the MO4500 model that contains the most prominent bulbous present some scatter points. Figures 4.12, 4.13 do not present a linear behavior and it is in these drafts that the waterline is close to the bulbous bow. However, these results may also be due to uncertainties in the model tests, so further studies are needed.

In order to have greater reliability in the experimental form factors, a careful uncertainty analysis must be carried out in the model tests. Also, each speed should be run at least three times to trust the results and include them all in the curve fit. The results obtained in this study are questionable as in the case of MO4500 at $T = 12.2\,\mathrm{m}$ only two points are used for the form factor determination, but this resulting value is well in line with the other form factors obtained for this vessel at the other drafts.

4.6. Form factor determination by the CFD approach

The CFD simulations were performed also on the two HSVA benchmark models, MO5500 and MO4500. For each model double body numerical simulations are run at model and full scale in order to obtain the form factor at both Reynolds numbers. Double body simulations implies a symmetry boundary condition at the free surface plane, in order to avoid the wave resistance component and be able to apply the concept of the form factor determination based in the CFD approach. For the simulations FRESCO+ solver is used in all cases.

Turbulence model

The simulations are carried out with the two equation $k - \omega$ SST turbulence model with wall functions, for the ship resistance simulations this model is preferred over the standard $k - \omega$ because it presents less sensitivity to the inlet free stream turbulence properties, and has presented a good behaviour in adverse pressure gradients and separating flow. [10]

Computational domain

The computational domain is performed according to HSVA standards for CFD simulations. It is shaped as a rectangular 3D prism. The distance between inlet and fore part of the ship is 1 L_{PP}, the outlet plane is located at 2 L_{PP} behind the stern, the side and bottom boundary are located 1 L_{PP} away from the hull. Figure 4.15 shows the computational domain of the MO5500 ship model, the same shape is done for the MO4500. The symmetry plane at the free surface is given to the domain, also a symmetry plane boundary condition at the ship center plane.

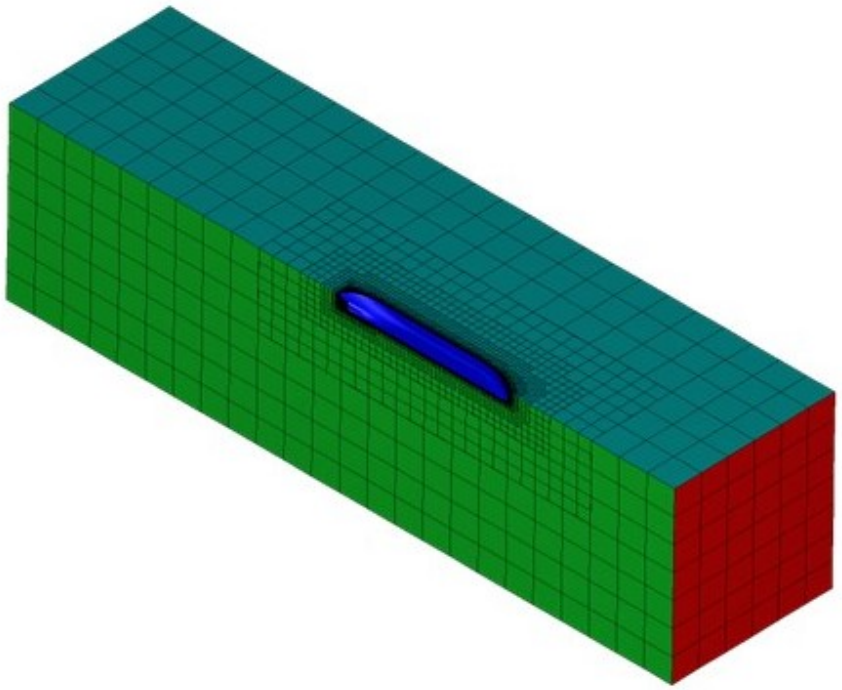

Figure 4.15.: MO550 domain CFD model scale numerical simulation

Mesh

For the ship resistance simulation, the mesh is generated with Fidelity commercial software by Cadence. The mesh contains structured and unstructured elements as the shape of the geometry is more complex and the cells needs to fit the ship form. Structured elements are located around the ship walls in the boundary layer region with a distance associated with the predicted y^+ values. Figures 4.16 and 4.17 show the structure of the distributed mesh in the computational domain around the two ship models respectively, focusing on the areas of greatest change in curvature, in these cases the bow and stern where the mesh has more difficulty to capture the shapes.

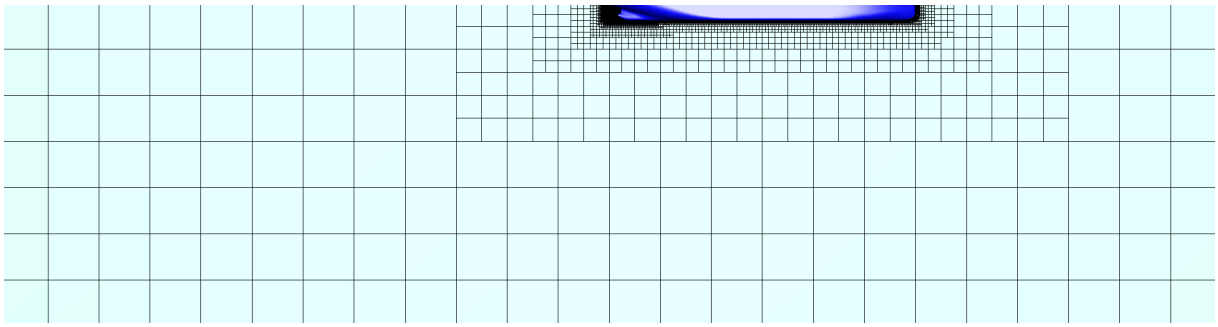

(a) XZ plane view

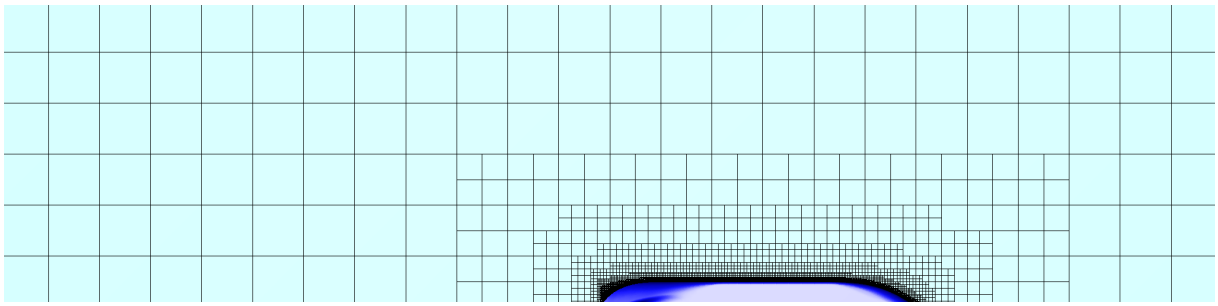

(b) XY plane view

(c) Hull mesh

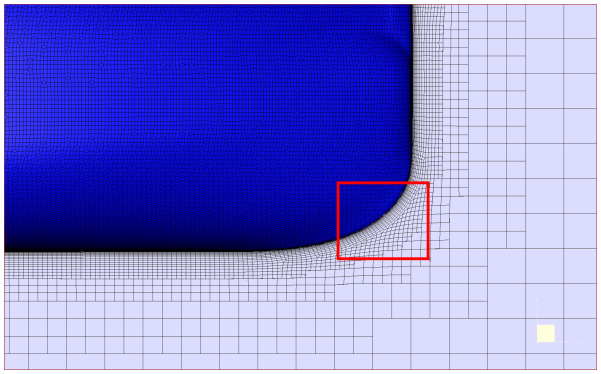

(d) Mesh around the bow

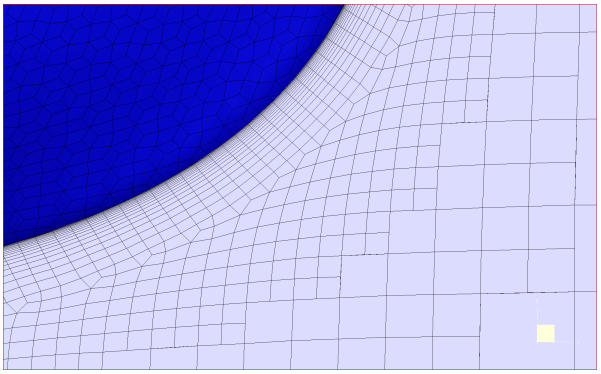

(e) Mesh around the bow (Zoom)

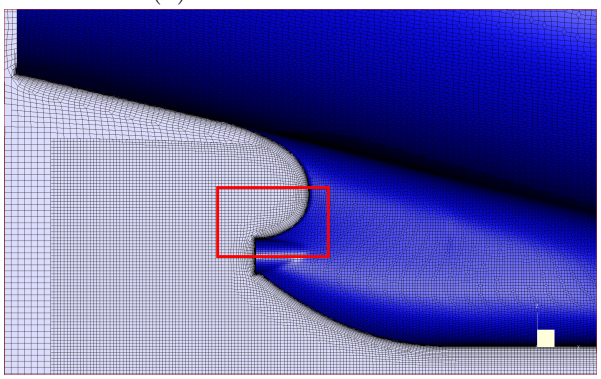

(f) Mesh around the stern

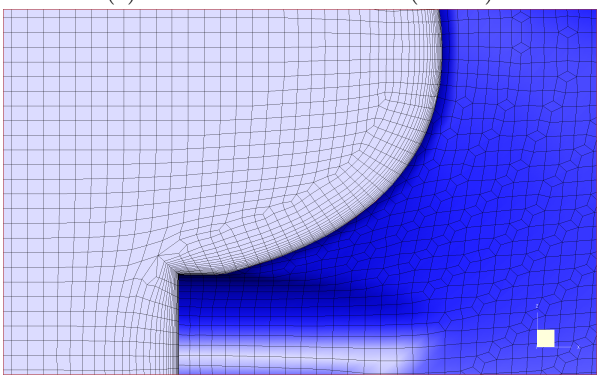

(g) Mesh around the stern (Zoom)

Figure 4.16.: Structure of the finest grid around the MO5500 ship model $y^+ = 50.4$

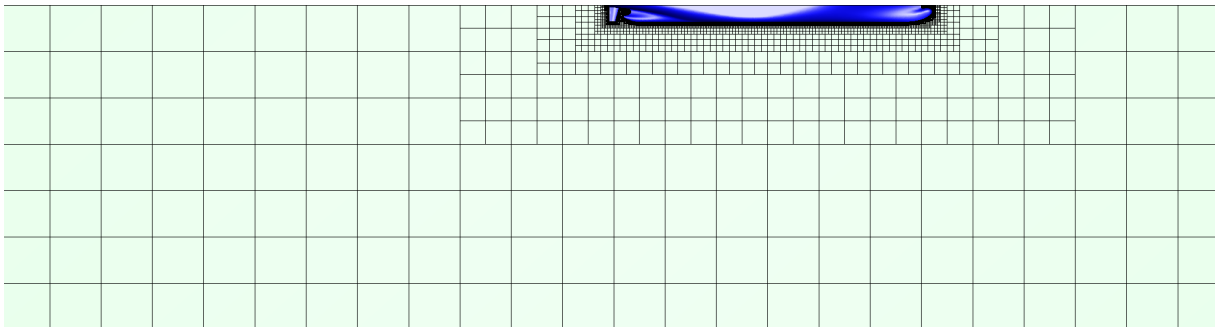

(a) XZ plane view

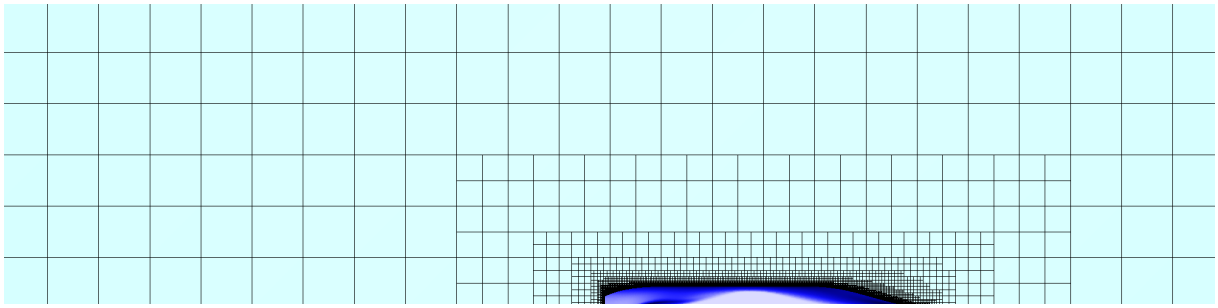

(b) XY plane view

(c) Hull mesh

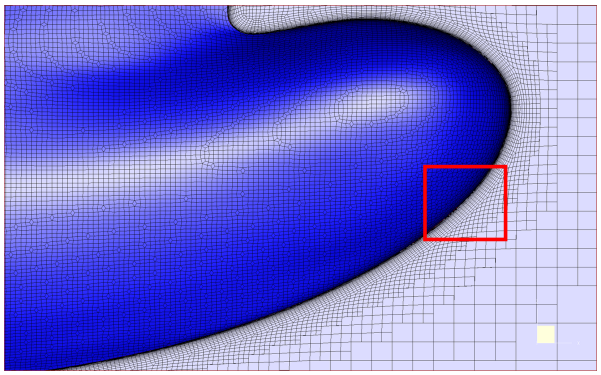

(d) Mesh around the bow

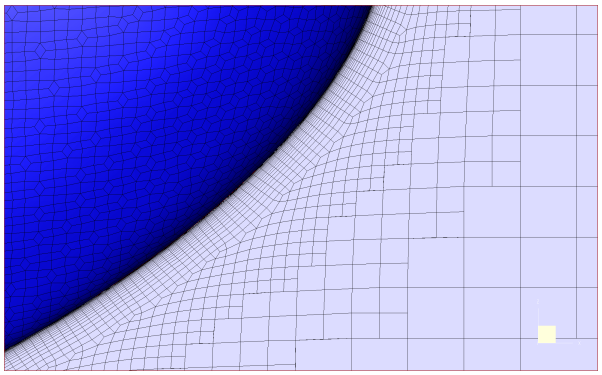

(e) Mesh around the bow (Zoom)

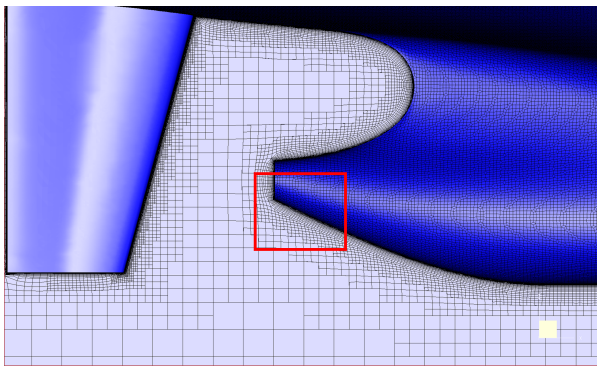

(f) Mesh around the stern

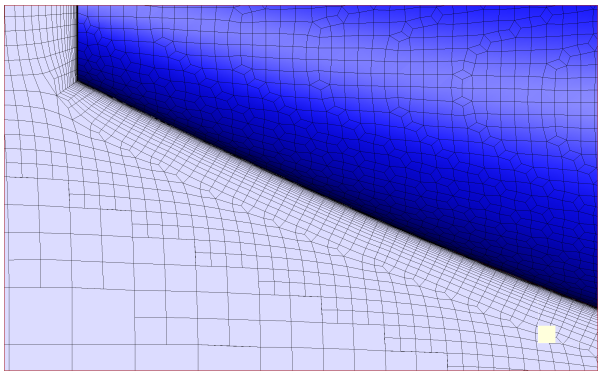

(g) Mesh around the stern (Zoom)

Figure 4.17.: Structure of the finest grid around the MO4500 ship model $y^+ = 50.4$

4.7. Model scale numerical simulations

The simulations for each hull and loading condition are carried out at one speed, following a similar Froude number for all the cases, Fr=0.15. Only the half of the ship hull is used as it is symmetrical with respect to the $x-z$ plane. Table 4.8 contains the non-dimensional quantities, Reynolds number and Froude number for each simulation and the ship properties needed to obtain the undimensioned force coefficients. These non-dimensional quantities are based on LOS. The water properties used in the computations corresponds to a density of 999.01 $[kg/m^3]$ and the kinematic viscosity of 1.14E=06 $[m^2/s]$

Table 4.8.: Ship model properties for model scale numerical simulations

Ship Model	T [m]	Length [m]	Froude Number	Reynolds Number	Velocity [m/s]
MO5500	12.00	7.05	0.146	7.53E+06	1.21
	10.00	7.05	0.146	7.53E+06	1.21
MO4500	14.00	7.75	0.153	9.06E+06	1.33
	12.20	7.73	0.153	9.04E+06	1.33
	7.75	7.54	0.155	8.82E+06	1.33

Convergence simulations

The figure 4.18 shows the residuals of the resistance numerical simulation of the MO5500 ship model at the draft $T = 10\,\mathrm{M}$ and the grid with $y^+ = 50.4$. The simulation reaches the 3000 iterations with residuals less than $1E-6$ for velocity, pressure and turbulence. As a result, the iterative error is considered negligible and the numerical uncertainty is based on the grid sensitivity.

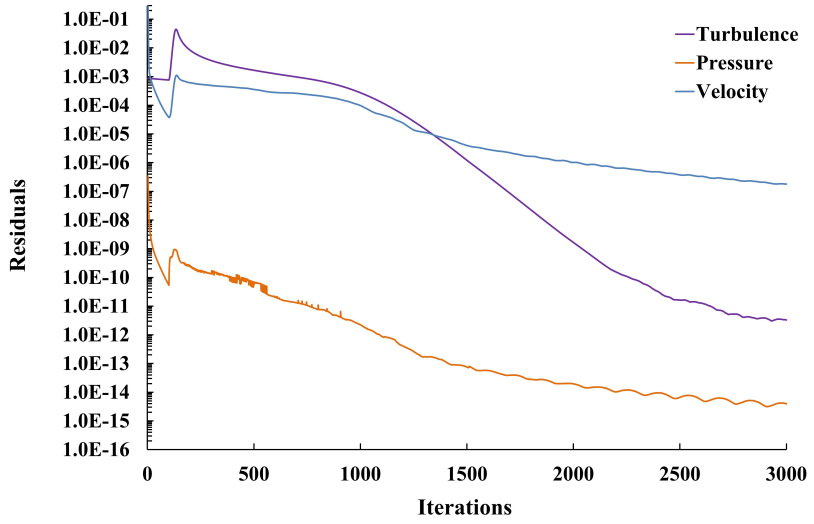

Figure 4.18.: Convergence of residuals in the numerical solution of the MO5500 at model scale $T = 10\,m$ with a grid of $y^+ = 50.4$. In the plot, turbulence represents the kinetic energy and dissipation.

Grid sensitivity Analysis

The grid sensitivity of the numerical simulations of the model ships is analysed using the procedure proposed by Hoekstra, presented in section 2.11. The numerical uncertainty of the total resistance coefficient of the ship model is obtained with the discretizacion error by power series expansions. The MO5500 ship model with a draft of 10 meters and at a Froude number of 0.15 is analysed at 4 different grids, varying the y^+ (h_i), with a refinement ratio h_2/h_1= 1.44 The rest of the parameters are kept constant.

Table 4.9.: MO5500 model scale grid sensitivity

Y+	**hi/h1**	$\mathbf{C_T * 10^3}$	**Uncertainty %**
50.4	1.0	3.699	1.4
72.6	1.4	3.707	1.6
104.5	2.1	3.721	2.2
150.5	3.0	3.723	2.3

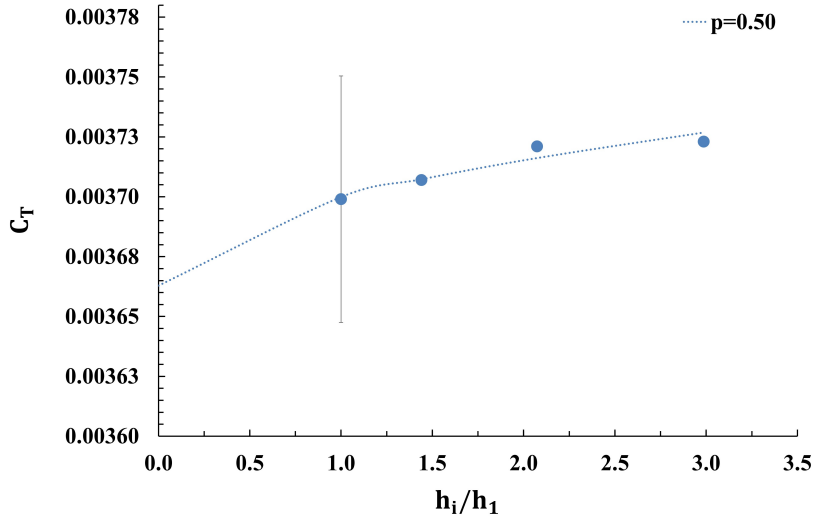

Figure 4.19.: Resistance coefficient with the grid refinement ratio used for the grid convergence analysis of the MO5500 model ship, varying the y^+ value

Model Scale CFD total resistance

The CFD resistance simulations results for the two ships are presented in table 4.10. These results will be used later for the resistance extrapolation to full scale.

Table 4.10.: Ship models total resistance CFD results

Ship model	**Draft [m]**	$\mathbf{R_{T_M}[N]}$	$\mathbf{C_{T_M} * 10^3}$
MO5500	12.00	36.1	3.90
	10.00	31.1	3.70
MO4500	14.00	37.1	3.64
	12.20	32.0	3.48
	7.75	23.7	3.49

4.8. Model scale CFD form factors

The CFD based form factor is determined following the method of Hughes [17] explained in section 2.6, where the total viscous resistance C_V is obtained by double body simulations, and the frictional coefficient $C_{F_{friction\,line}}$ corresponds to results from the flat plate friction resistance, that means the value of the form factor depends on the choice of the friction line, see formula (4.1). The form factors of the two ship models at different drafts are shown in table 4.11. Three different values of the form factor are obtained, each one is calculated with a different frictional coefficient, the one from the ITTC '57 correlation line and the other two from the friction curves obtained numerically in section 3.4 each one by a different turbulence model the $k-\omega$ SST and the $k-\omega$ standard.

$$(1+k) = \frac{C_V}{C_{F_{friction\,line}}} \tag{4.1}$$

with

The form factors for the Reynolds numbers corresponding to the model-scale simulations of the two models MO4500 and MO5500 are around log(Re) 6.9. For this Reynolds number, the ITTC'57 friction line and the numerical $k-\omega$ standard curve are coincident, while the values of the frictional coefficient estimated with the SST curve are below them, consequently generating larger form factor values when using the SST numerical friction line.

Table 4.11.: Form Factors from CFD simulations at model scale

Model Ship	T [m]	ITTC'57 Friction Line	$k-\omega$ Standard Friction Line	$k-\omega$ SST Friction Line
5500	12.00	1.235	1.239	1.330
	10.00	1.173	1.176	1.263
4500	14.00	1.194	1.194	1.280
	12.20	1.141	1.141	1.224
	7.75	1.138	1.139	1.222

4.9. Full scale numerical simulations

Full-scale simulations are becoming more frequent and studied today due to the computational capacity that allows the calculation of large-scale simulations. The importance lies in the fact that the real-scale simulations would avoid the problem of extrapolating the resistance of the towing tanks where it is not possible to have the Reynolds and Froude number similarities simultaneously. The numerical simulations follow the same conditions from the model scale ones. All cases were computed at the same Froude number of 0.15. Table 4.12 contains the non-dimensional quantities, Reynolds number and Froude number for each simulation. The water properties used in the computations corresponds to a density of 1026.20 $[kg/m^3]$ and the kinematic viscosity of 1.19E=06 $[m^2/s]$.

Table 4.12.: Ship properties for full scale numerical simulations

Ship Model	**T [m]**	**Length [m]**	**Froude Number**	**Reynolds Number**	**Velocity [m/s]**
MO5500	12.00	182.33	0.146	9.47E+08	6.17
	10.00	182.33	0.146	9.47E+08	6.17
MO4500	14.00	256.80	0.153	1.65E+09	7.66
	12.20	256.20	0.153	1.65E+09	7.66
	7.75	249.97	0.155	1.61E+09	7.67

Convergence simulations

For full scale numerical simulations, the same ship model was used under the same conditions for the numerical uncertainty analysis. Figure 4.20 shows the residuals of the resistance numerical simulation of the full scale MO5500 ship model at draft $T = 10\,\mathrm{M}$ and grid with $y^+ = 100$. The residuals also fall below $1E-6$ for all parameters analyzed, velocity, pressure and turbulence. Then, the iterative error can be neglected in the calculation of the numerical uncertainty.

Grid sensitivity Analysis

The same procedure is followed for the analysis of the grid convergence of the full scale numerical simulations. The MO5500 ship model is also used for the grid analysis, at the draft of 10 meters and at a Froude number of 0.15. The number of grids is higher than the ones used in the model scale in order to analyse a wider range of y^+ starting from 100 until 1131, with a refinement ratio of h_2/h_1= 1.44, with a total of 8 grids. The rest of the parameters are kept constant.

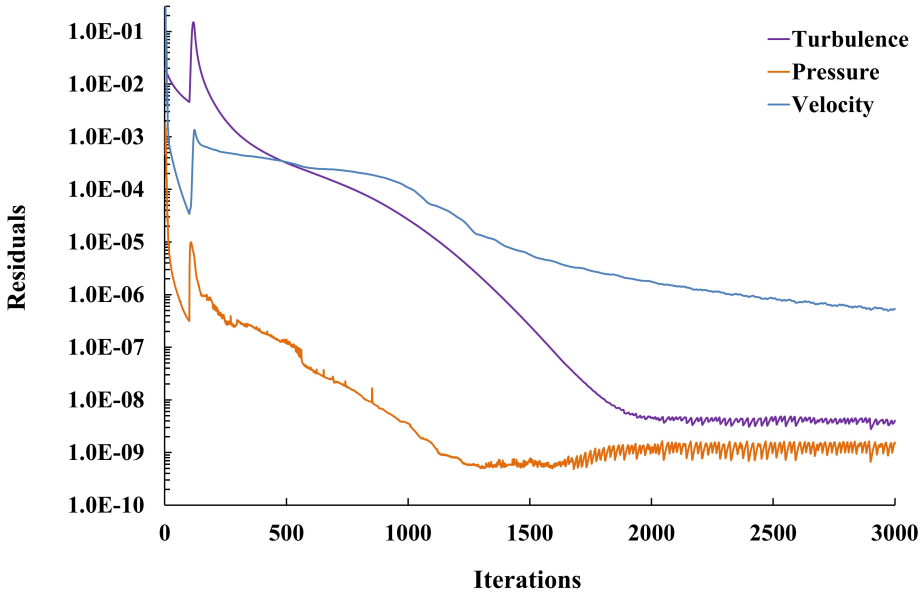

Figure 4.20.: Convergence of residuals in the numerical solution of the MO5500 at full scale $T = 10\,m$ with a grid of $y^+ = 100$. In the plot, turbulence represents the kinetic energy and dissipation.

Table 4.13.: MO5500 full scale grid sensitivity results

$\mathbf{y^+}$	**hi/h1**	$\mathbf{C_T * 10^3}$	**Uncertainty %**
100	1.0	1.915	0.9
141	1.4	1.920	1.1
200	2.0	1.924	1.5
283	2.8	1.928	1.7
400	4.0	1.931	1.9
566	5.7	1.935	2.1
800	8.0	1.939	2.4
1131	11.3	1.943	2.8

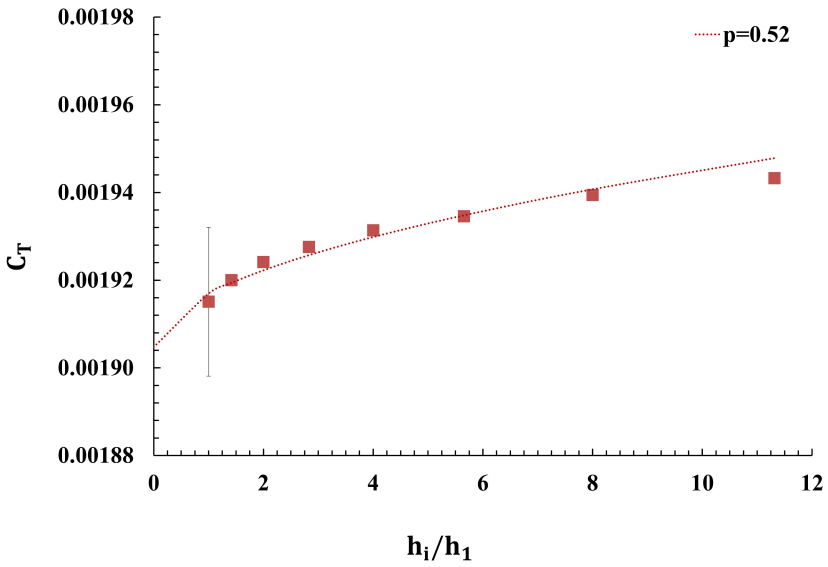

Figure 4.21.: Resistance coefficient with the grid refinement ratio used for the grid convergence analysis of the MO5500 full scale ship, varying the y^+ value

Full Scale CFD total resistance

The CFD full scale resistance simulations results for the two ships are presented in table 4.14. These results will be used later as base for comparison of the extrapolated values of the ship resistance.

Table 4.14.: Ship full scale total resistance CFD results

Ship model	Draft [m]	R_{T_S} [kN]	$C_{T_S} * 10^3$
MO5500	12.00	355	2.16
	10.00	287	1.92
MO4500	14.00	739	1.94
	12.20	630	1.83
	7.75	450	1.77

4.10. Full scale CFD form factors

The form factors obtained from the total resistance values of the full scale CFD simulations of the two ship models at different drafts are shown in table 4.11. The form factors are calculated based on the three different friction lines, the ITTC'57 correlation curve $k-\omega$ SST and the $k-\omega$ standard.

The Reynolds number corresponding to the full scale numerical simulations of the MO4500 is log(Re)=9.2 for the 3 different loading conditions, while for the MO5500 log(Re) is 9. For these Reynolds numbers, the $k-\omega$ standard is slightly above the ITTC'57 friction line, in the other side the $k-\omega$ SST is located below the ITTC'57 curve, this is reason why the estimated form

factors based on the ITTC'57 line stays in the middle with respect to the other two.

Table 4.15.: Form Factors from CFD simulations at full scale

Model Ship	T [m]	ITTC Friction Line	$k-\omega$ Standard Friction Line	$k-\omega$ SST Friction Line
5500	12.00	1.40	1.38	1.45
	10.00	1.25	1.23	1.29
4500	14.00	1.35	1.33	1.40
	12.20	1.27	1.25	1.32
	7.75	1.23	1.21	1.27

4.11. Comparison between EFD vs CFD based form factors

Table 4.16 contains the comparison between the experimentally determined form factors and the CFD based form factors from model scale simulations. In this case the difference from the ITTC'57 form factor present values of percentages lower in comparison with the numerical friction lines. These results depends on the reliability of the experimental determination, no real conclusions will be made respecting these results, for further analysis more experimental tests should be carried out with the respective uncertainty analysis.

Table 4.16.: Comparison in percentages of the EFD form factors vs CFD model scale form factors

Model Ship	T [m]	k_{exp} vs $k_{CFD\,ITTC}$	k_{exp} vs $k_{CFD\,k-\omega Standard}$	k_{exp} vs $k_{CFD\,k-\omega SST}$
5500	12.00	3.4	3.7	11.4
	10.00	0.3	0.6	8.0
4500	14.00	1.7	1.7	9.1
	12.20	-3.2	-3.2	3.9
	7.8	-6.7	-6.7	0.1

Table 4.17 present the difference of the form factors obtained from model scale and full CFD numerical simulations. The difference of the numerical form factors obtained with the ITTC'57 correlation line are in average 10.4%. while the average difference for the $k-\omega$ SST is 6.4%. These results corroborates the scale effects of the ITTC'57 line and a decrease with the use of numerical frictional lines.

Table 4.17.: Comparison in percentages of the CFD model scale vs CFD full scale form factors

Model Ship	T [m]	k_{model} vs k_{ship} ITTC	k_{model} vs k_{ship} $k-\omega\, Standard$	k_{model} vs k_{ship} $k-\omega\, SST$
5500	12.00	13.4	11.1	8.9
	10.00	6.3	4.2	2.2
4500	14.00	12.8	11.0	9.0
	12.20	11.5	9.8	7.8
	7.75	7.9	6.1	4.2
Average		10.4	8.4	6.4

Korkmaz et al [28] stated that the presence of a bulbous bow can affect the form factor at the double body simulations, if there exists a small gap between the top of the bulbous and the still water surface, a flow separation can occur around the top of the bulbous. This behaviour would not happen in free-surface models [28]. Raven et al [39] suggested that this issue can be improved if model ship with bulbous is more submerged at the bow by trimming. From the model MO4500 and MO5500 this behaviour can be seen in the comparison between the form factors of the CFD calculation at model and full scale (Table 4.17). For the MO5500 model the highest difference between the form factors occur at the draft of 12 meters, this draft is located just above the bulbous bow, the frictional resistance distribution on the ship hull obtained from its numerical simulation can be seen in figures 4.22 and 4.23.

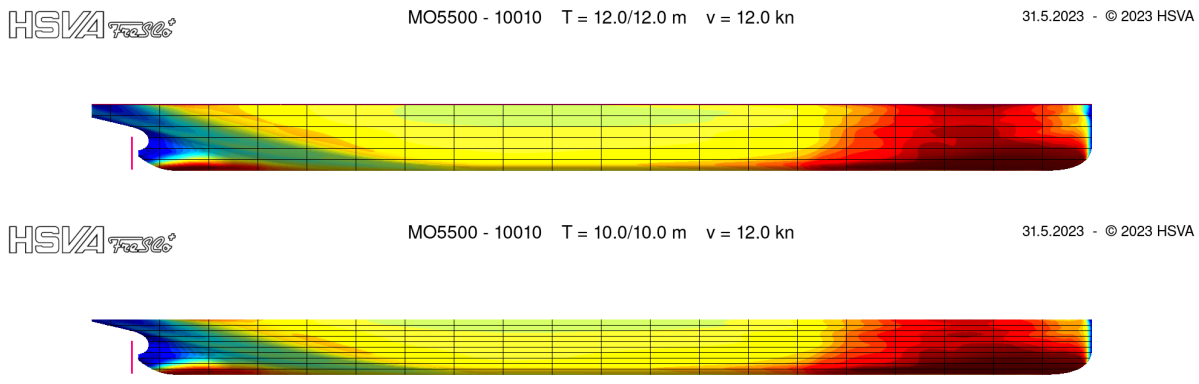

Figure 4.22.: Frictional resistance distribution on the MO5500 ship model at different drafts. (Side view)

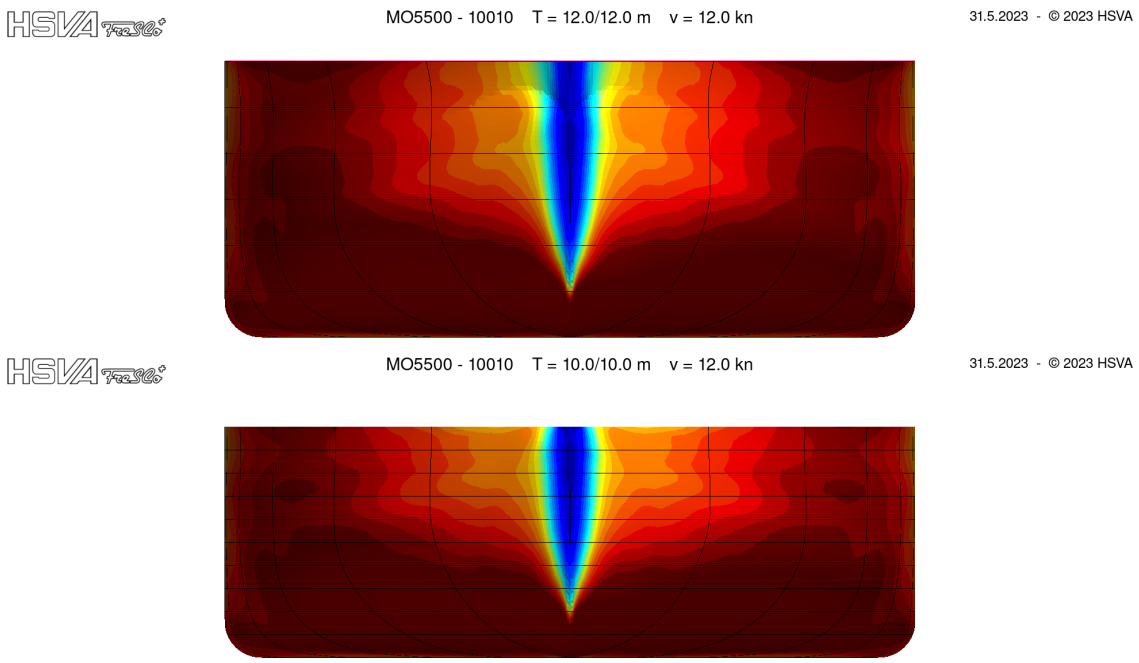

Figure 4.23.: Frictional resistance distribution on the MO5500 model ship at different drafts. (Right view bow)

For the model MO4500 the increment of the difference between the form factors at model and full scale is noticed when it goes from the mean draft of 7.75 to 12.2 meters, being at the 12.2 meters just above the top of the bulbous bow, and being the model with the mean draft of 7.75 trimmed at the bow, which contributes to reduce the percentage. The MO4500 bulbous bow immersion at each draft and the respective frictional resistance distribution are shown in figures 4.24 and 4.25.

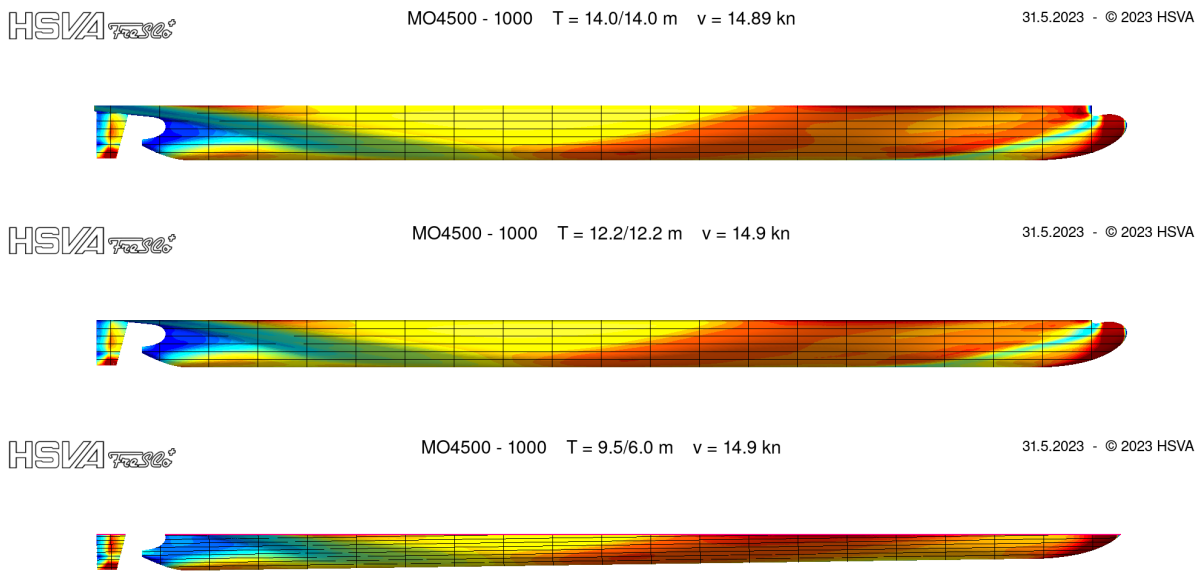

Figure 4.24.: Frictional resistance distribution on the MO4500 ship model at different drafts. (Side view)

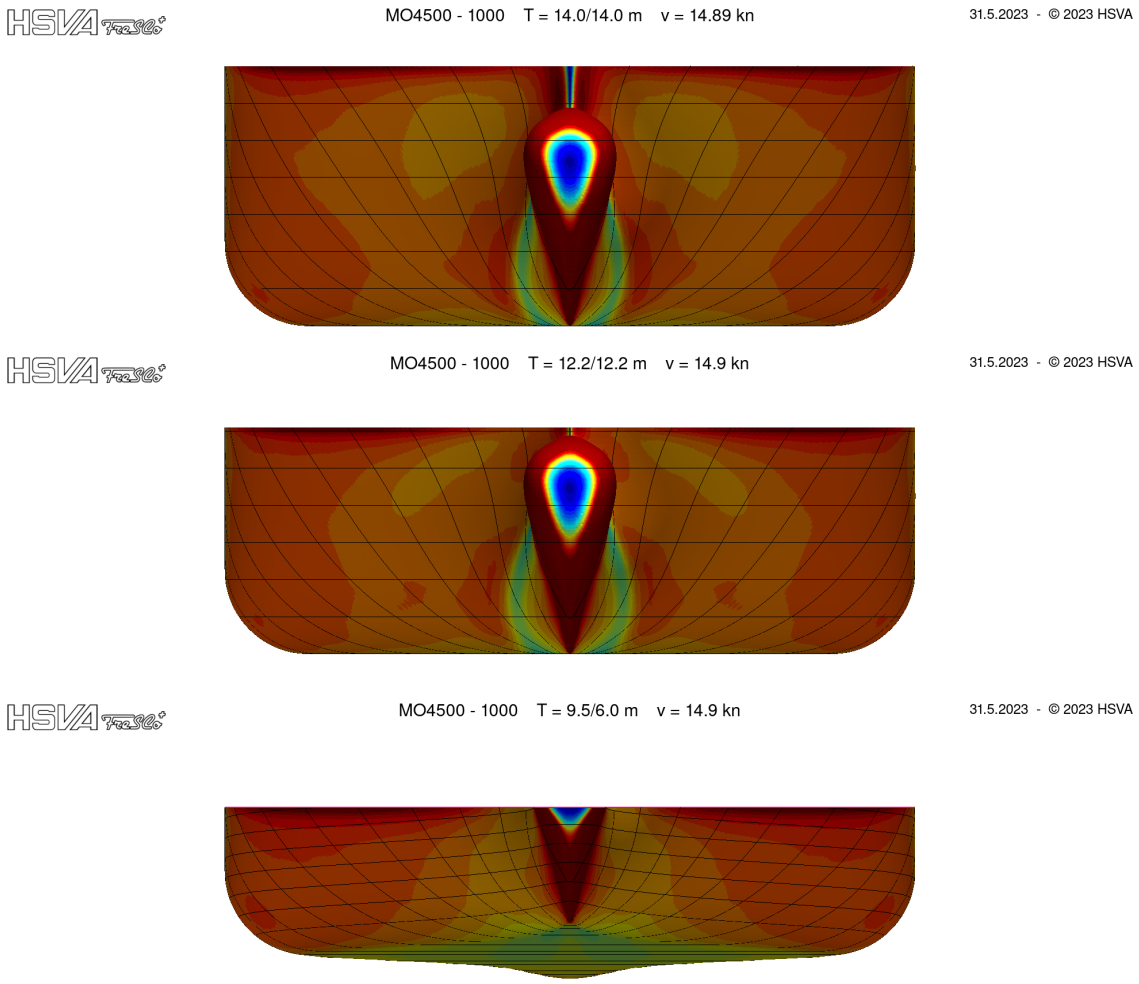

Figure 4.25.: Frictional resistance distribution on the MO4500 ship model at different drafts. (Right view bow)

Also, it is suggested that the transom immersion affects the double-body computations which can also be one of the reasons of the high difference between the form factors for the MO5500 at T=12 m, where part of the transom is submerged in comparison with MO5500 T=10 m where the immersion is minimum, see figure 4.26. For the model MO4500, this can be the explanation why at T=14 m there exists an increment in the percentage difference, even if the bulbous bow is totally submerged and not very close to the water level. At T=14 meters there is the presence of the transom which does not happen for the other drafts, see figue 4.27.

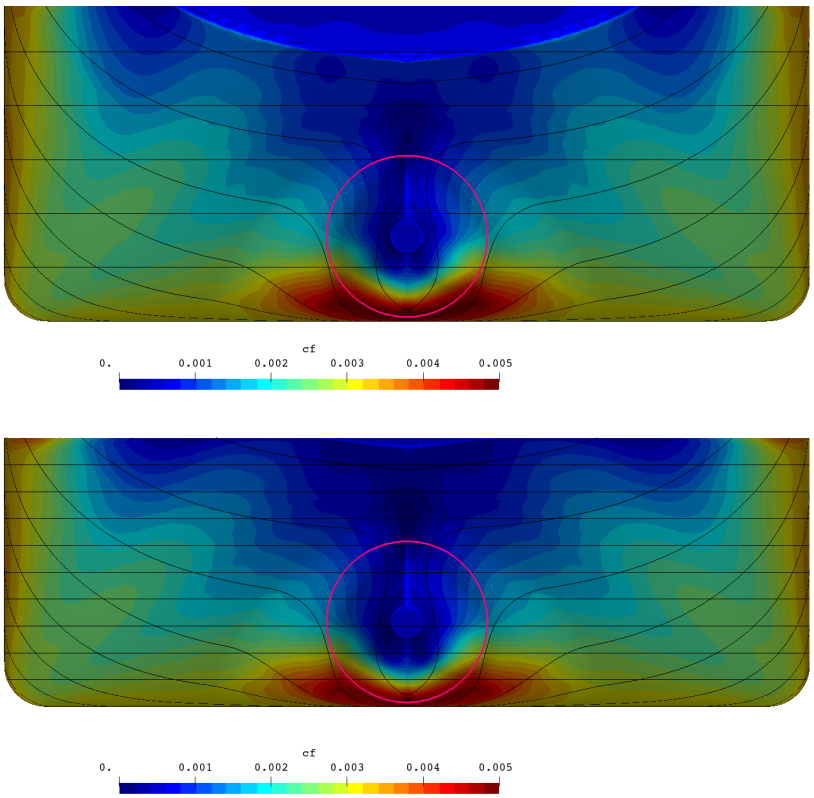

Figure 4.26.: Frictional resistance distribution on the MO5500 ship model at different drafts. (Right view stern)

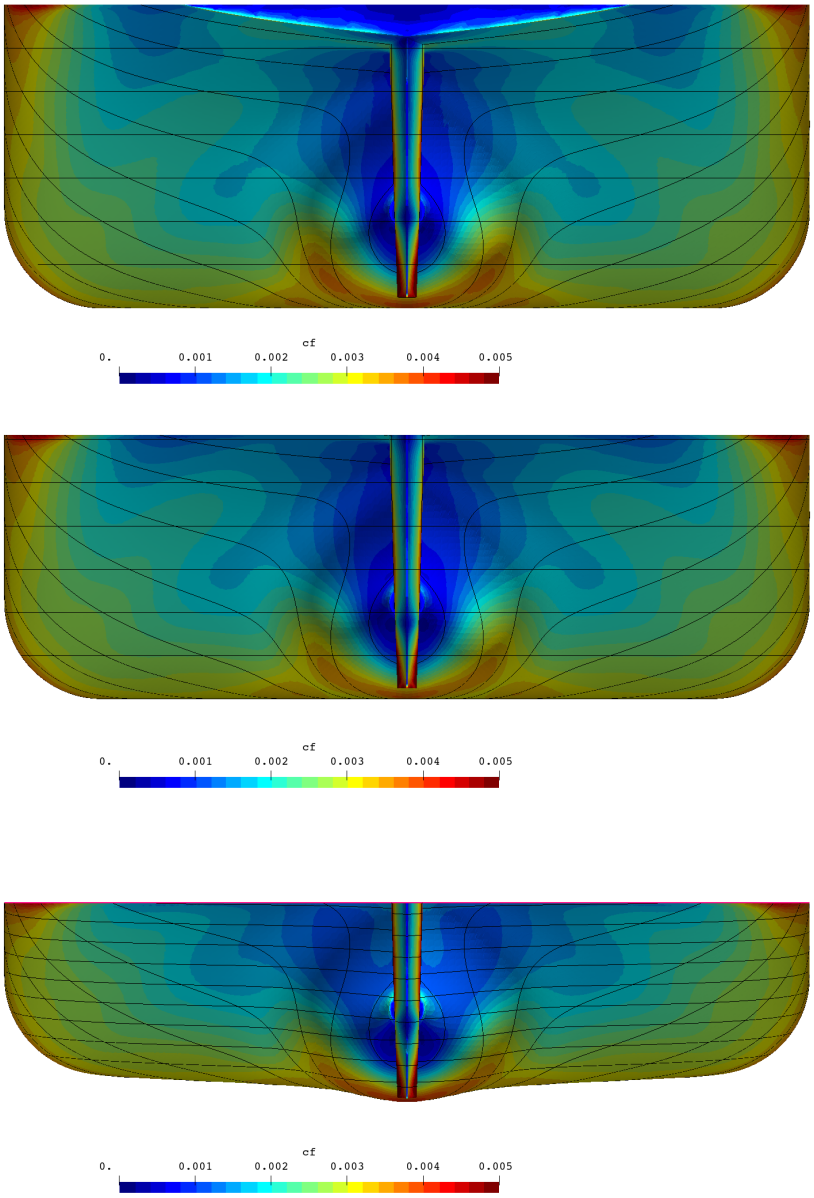

Figure 4.27.: Frictional resistance distribution on the MO4500 ship model at different drafts. (Right view stern)

5. Full scale ship resistance extrapolations based on EFD and combined EFD/CFD methods

5.1. Ship resistance extrapolation using the standard HSVA correlation method

In this section, the power prediction of the full size ships MO5500 ans MO4500 is performed following the standard HSVA correlation method, which does not include the form factor, therefore, only one value of resistance is obtained for each draft. Table 5.1 presents the extrapolated results using the model resistance results from the CFD numerical simulation at model scale and table 5.2 shows the extrapolation based on the resistance values taken from the towing tank model tests.

Table 5.1.: Extrapolated results from the total resistance model scale CFD simulations using HSVA approach

	Draft [m]	**Extrapolated Resistance** [kN]
MO5500	12.00	353
	10.00	295
MO4500	14.00	766
	12.20	643
	7.75	481

Table 5.2.: Extrapolated results from the total resistance model tests using HSVA approach

	Draft [m]	**Extrapolated Resistance** [kN]
MO5500	12.00	339
	10.00	303
MO4500	14.00	759
	12.20	724
	7.75	577

5.2. Ship resistance extrapolation using the ITTC'78 method

Resistance predictions from model to full scale are made by extrapolating the model resistance results, using the ITTC 1978 method. The extrapolations are calculated using 4 different form factors, the one obtained by the Prohaska method from the experimental results. Other 3 form factors obtained with the CFD based method, one using the ITTC'57 correlation line and the other 2 with the numerical friction lines obtained in this thesis, by the $k-\omega$ SST and $k-\omega$ standard turbulence models.

The ITTC'78 method is based on obtaining the components explained in section 2.4. It is important to mention that the air resistance component of the total coefficient is not included in order to compare with the CFD full scale resistance results which are double body simulations. Table 5.3 shows the extrapolated full scale resistance using the model resistance values from the double body CFD model scale numerical simulations. Table 5.4 shows the extrapolated resistance using the model resistance values from the towing tank tests.

The tables 5.3, 5.4 show distant extrapolated results for the MO4500 model at small drafts $T = 12.2\,\text{m}$, $T = 12.2\,\text{m}$. This could happen due to the presence of the rudder in this model. The rudder could cause disturbances in the experimental tests or numerical simulations. The presence in this model ship of a prominent bulbous bow may also be the cause of this difference.

Table 5.3.: Extrapolated results from the CFD model scale simulations using ITTC approach

Ship model	**Draft [m]**	$\mathbf{k_{Prohaska}}$	$\mathbf{k_{ITTC'57}}$	$\mathbf{k_{k-\omega\,standard}}$	$\mathbf{k_{k-\omega\,SST}}$
MO5500	12.00	387	376	375	351
	10.00	333	327	326	305
MO4500	14.00	770	758	758	705
	12.20	638	659	659	613
	7.75	453	487	487	453

Table 5.4.: Extrapolated results from the towing tank resistance model tests using ITTC approach

Ship model	**Draft [m]**	$\mathbf{k_{Prohaska}}$	$\mathbf{k_{ITTC'57}}$	$\mathbf{k_{k-\omega\,standard}}$	$\mathbf{k_{k-\omega\,SST}}$
MO5500	12.00	386	376	375	351
	10.00	342	337	336	316
MO4500	14.00	764	752	752	700
	12.20	720	741	741	696
	7.75	550	584	583	550

5.3. Comparison

Figure 5.1 shows the results of the extrapolated full scale resistance values of the MO5500 ship, using the ITTC'78 method with 4 different form factors. The figure also includes the results of the HSVA approach which does not contain the form factor in the calculations. From the figure, it is observed that the HSVA approach has the closest values to the CFD full scale resistance, for both drafts and using the CFD model results simulations for the extrapolation. The next closest values are the ones obtained by the ITTC'78 method using the form factor with the $k-\omega$ SST friction line. Analysing the extrapolated results, as they just depend on the selected form factor, it is easy to obtain the best option for the power prediction. In this case the $k-\omega$ SST friction line gives the highest values of form factors for the two drafts, and as a consequence the lowest resistance extrapolation that are closer to the CFD full scale results than the obtained by the other CFD based form factors.

Comparing the two drafts, $T = 12\,\text{m}$ is the one with the smallest difference between the extrapolated values and the CFD full scale results. Also at this draft the difference between the results from the extrapolation using the CFD model resistance compared with the extrapolation using the experimental model tests is small. While for the $T = 10\,\text{m}$ the model tests results predict higher values of resistance.

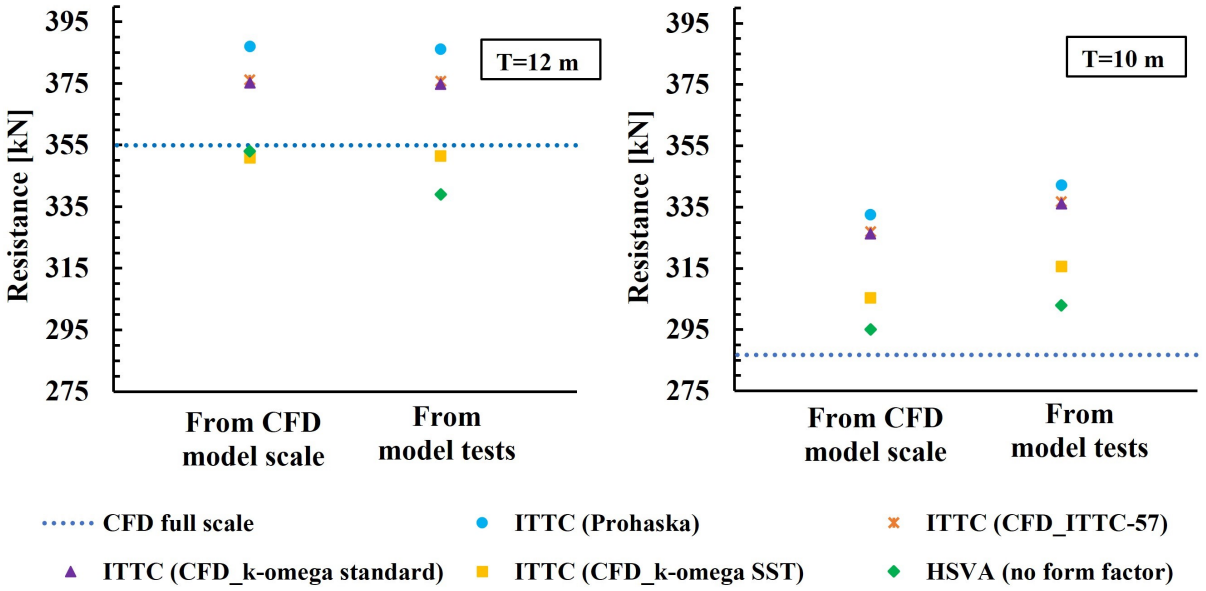

Figure 5.1.: MO5500 extrapolated total resistance to full scale size from CFD model scale and experimental model tests results

Figure 5.2 contains the extrapolated ship resistance of the MO4500 model ship following the same methods used for the MO5500. In this case the HSVA prediction does not present any pattern, while for the ITTC'78 approach the results that come closest to the CFD full scale resistance are still the ones with the form factor from the $k-\omega$ SST friction line. For all drafts the predictions that better approximate the values of the CFD full scale simulations are the ones extrapolated from the CFD model scale resistance simulations, with an average percentage

difference for all cases of 4%. While the extrapolation using the experimental model tests values present an average difference of 15%.

Comparing the results between the drafts, it can be seen that as the draft decreases, the predictions go further from the CFD full scale resistance, this difference is accentuated when it comes to the extrapolations with the experimental results, where for the draft $T = 14\,\text{m}$, for all the extrapolations, the average difference in percentage is 3% and for the smallest draft $T = 7.75\,\text{m}$ the difference is 26%.

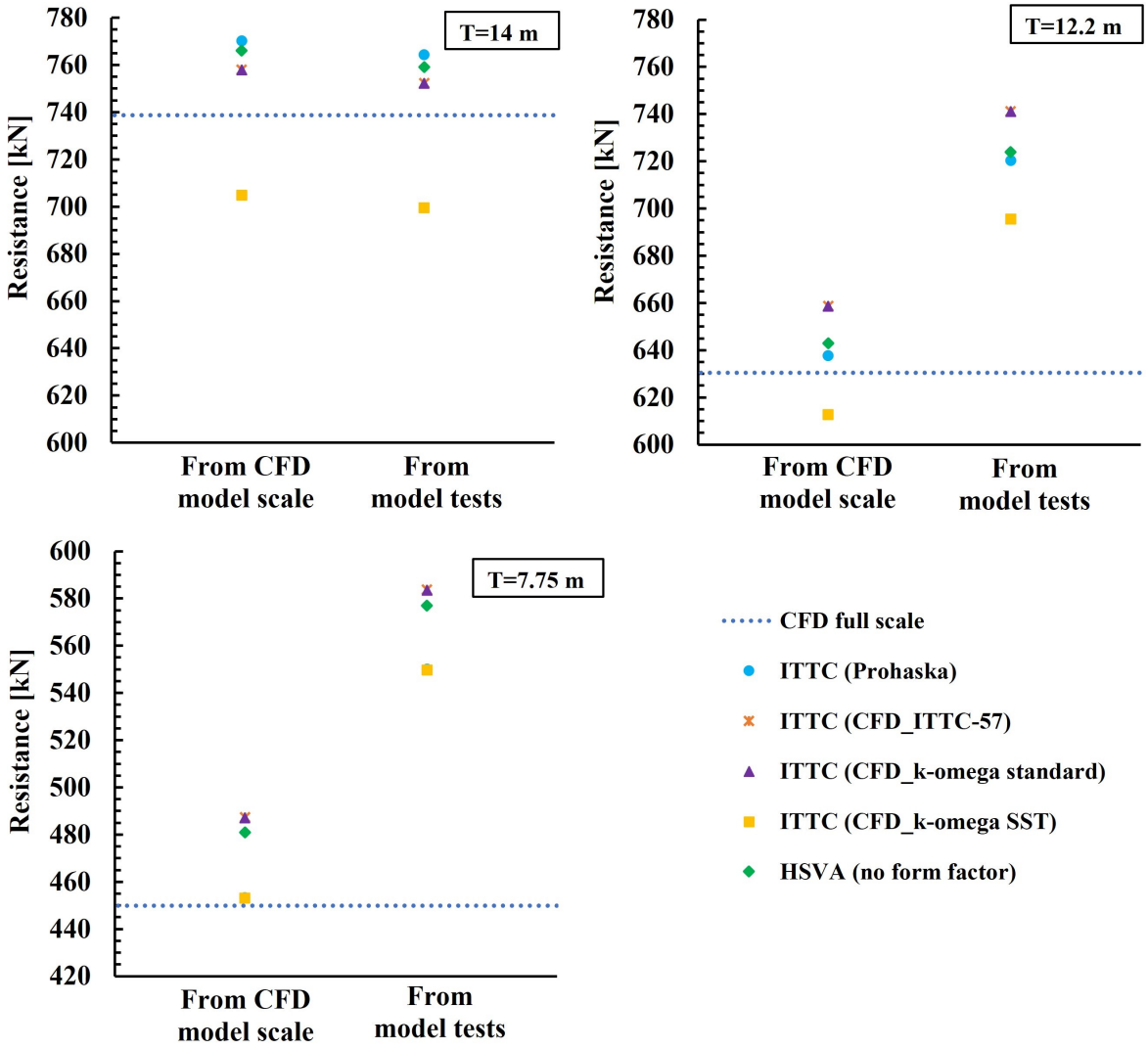

Figure 5.2.: MO4500 extrapolated total resistance to full scale size from CFD model scale and experimental model tests results

Tables 5.5 and 5.6 show the difference in percentage of the total resistance of the full scale ships between the extrapolated results and the CFD full scale total resistance simulations. The first table, presents the extrapolation using the CFD model scale resistance calculations and the second one the extrapolation using the model tests resistance values. It is found that in average for both models, the method that comes closest to the CFD full scale results is the ITTC 1978 using the form factor calculated with the friction line $k - \omega$ SST. In addition, it is observed that

the HSVA approach approximates better using the CFD model tests for the extrapolation, as in average for the two ship models it differs in 3% from the CFD full scale resistance.

It is found that for the ITTC approach, only the case of the form factor $k-\omega$ SST, the predictions for the deepest drafts are lower than the CFD full scale results. For the rest of the predictions with the other 3 form factors, the values are higher than the full scale CFD resistance. The same happens for the HSVA approach, lower predictions are found for the deepest drafts for both models ships. Even though, the results depends purely in the form factors, the ones obtained from the CFD double body simulations present a pattern, while the ones obtained experimentally by Prohaska vary indistinctly between the models ships and drafts.

The extrapolation that contains the highest differences is the one that uses the form factor determined by the ITTC'57 line. This is because in average these form factors are smaller than the ones calculated by the $k-\omega$ standard, $k-\omega$ SST and the experimental results. This is a behaviour expected because of the steepness of the ITTC'57 curve at the model Reynolds numbers.

Comparing the total results from the extrapolation based on the experimental model values with the ones based on the CFD model scale simulations, the differences are lower at the second case, this can be expected as the CFD full scale simulations follow the same settings of the model scale simulations.

Table 5.5.: Difference in percentage between the extrapolated results from the model scale CFD simulation and the full scale total resistance CFD simulations

Ship model		**ITTC approach**				**HSVA**
	Draft [m]	$\mathbf{k_{Prohaska}}$	$\mathbf{k_{ITTC'57}}$	$\mathbf{k_{k-\omega\,standard}}$	$\mathbf{k_{k-\omega\,SST}}$	**approach**
MO5500	**12**	9.0	6.0	5.7	-1.1	-0.5
	10	16.0	14.1	13.8	6.5	2.7
MO4500	**14**	4.2	2.6	2.6	-4.6	3.7
	12.2	1.2	4.5	4.5	-2.8	2.0
	7.75	0.8	8.3	8.3	0.7	7.0
	Average	**6.2**	**7.1**	**7.0**	**3.1**	**3.2**

Table 5.6.: Difference in percentage between the extrapolated results from the model tests and the full scale total resistance CFD simulations

Ship model		ITTC approach				HSVA
	Draft [m]	$k_{Prohaska}$	$k_{ITTC'57}$	$k_{k-\omega\,standard}$	$k_{k-\omega\,SST}$	approach
MO5500	**12.00**	8.8	5.8	5.6	-1.0	-4.5
	10.00	19.3	17.5	17.2	10.1	5.8
MO4500	**14.00**	3.5	1.8	1.8	-5.3	2.8
	12.20	14.3	17.6	17.6	10.3	14.9
	7.75	22.3	29.8	29.7	22.2	28.3
	Average	**13.6**	**14.5**	**14.4**	**9.8**	**11.3**

5.4. Suggestions for improvements of the HSVA CFD standard calculation methods for form factor determination

- It is suggested that the form factor be determined by the CFD based method, as the Prohaska procedure has many aspects to be questioned because it was proposed at a time when actual ship designs such as the bulbous bow were not considered.
- Based on the results of the present thesis, the selected friction line for the form factor calculation is the one using the turbulent model $k-\omega$ SST, because its extrapolated results are the closest to the full scale simulations. However, it is suggested a detailed study of the set up between the solvers used in this thesis and the ones used for other numerical friction lines given by the references in order to understand the reasons of the differences of the results between them.
- Further studies should be carried out on the ITTC'78 prediction method. Whether to continue using the ITTC'57 curve to calculate the frictional coefficients, or to calculate them based on the numerical lines obtained from the simulations around a flat plate.
- The experimental tests must be performed more than once for the same condition in order to have acceptable reliability. The experimental uncertainty may also be a reason of why the extrapolation results using these values are farther from the CFD full scale results.
- It is suggested to obtain the uncertainty of the experimental tests, experimental form factor and extrapolation results, in order to be compared with the CFD based extrapolations and be able to quantify the percentage of reliability gained.
- The extrapolated uncertainties should be also compared with the CFD full scale simulations uncertainties to quantify the accuracy of the results. It would be helpful if there exists a ship with available sea trials to do this study.

6. Conclusions

The CFD based form factor method, can become a reliable method that could replace the experimental form factor determined by the Prohaska method currently used in the ITTC'78 power prediction. It was found that the extrapolation results using the numerical form factor based on the numerical friction line using the $k-\omega$ SST turbulence model has the smallest difference from the full scale ship resistance obtained by CFD full scale simulations. Also the numerically derived full scale values with the largest differences from the CFD full scale resistance have been those with the form factor based on the ITTC'57 curve. The results could be expected because the form factor values based on the ITTC'57 line are smaller than those based on the numerical friction lines, due to the steepness of the curve at the model scale Reynolds numbers.

It was confirmed that the form factor depends on the Reynolds number. When comparing the results for the same loading condition at model and full scale, the values of the form factor were different. The difference obtained with the ITTC'57 curve were in average 10.4%, while for the form factors obtained with the numerical friction line $k-\omega$ SST is 6.4%. These numerical results show that the form factor is less effected by scale effects when using numerical friction lines instead of the ITTC'57 line.

From the grid sensitivity study of the numerical friction lines, it was found that the results of the frictional resistance of a flat plate depend on the non-dimensional wall distance $y+$. The convergence behaviour and uncertainties were not equal when analysing the sensitivity of the grids with same y^+ refinement at different Reynolds number. Furthermore, the friction resistance results vary with the selection of the turbulence model. Even though, in general the resulting numerical friction lines showed a similar behaviour. The numerically predicted C_F values for the flat plate at low Reynolds numbers are below the ones predicted analytically.

The numerical friction lines obtained in this thesis presented the same behaviour than the ones obtained by Korkmaz, Eça and Hoekstra, where the largest differences of the frictional resistance coefficient between each other were found for the lowest Reynolds numbers, while for the highest Reynolds number the differences are significantly reduced. Furthermore, the difference in the obtained numerical friction lines is well in line with the results obtained by Hoekstra who also showed the difference of the numerical friction lines for different turbulence models.

Finally, based on the results of this work, it is recommended to use the numerical calculated form factor instead of the experimental one, since it is indistinct from the ship type avoiding the questionable Prohaska method. The results obtained show that the numerical form factor lead to closer results to the full scale resistance calculated numerically. The level of uncertainty depends in part on the desired confidence range in the grid sensitivity analysis. It is recommended to carry out an study on the uncertainty of the experimental form factor and compare it to the numerical one. Future work should be done to investigate the difference in results obtained using different turbulent models and solvers. To investigate the grid sensitivity not only for each velocity but also for each turbulence model. In addition, if there exists sea trials of a ship, it would help to have an estimate of the accuracy of the CFD full scale simulations.

Bibliography

[1] Darmofal, David: *Aerodynamics: Structured vs Unstructured grids.* MIT Open Course, 2005

[2] Eca, L. and Hoekstra, M. : The numerical friction line. In: *Journal of Marine Science and Technology* 13 (2008), S. 328–345. http://dx.doi.org/10.1007/s00773-008-0018-1. – DOI 10.1007/s00773–008–0018–1

[3] Eca, L. and Hoekstra, M.: A procedure for the estimation of the numerical uncertainty of CFD calculations based on grid refinement studies. In: *Journal of Computational Physics* 262 (20014), S. 104–130

[4] Guerrero, Joel: *A Crash Introduction to the Finite Volume Method and Discretization Schemes in OpenFOAM.* 15th OpenFOAM Workshop, 2020

[5] Tennekes, H. and Lumley, J. L.: *A First Course in Turbulence.* MIT Press, 1972

[6] Wang, Z. and Xiong, Y. and Shi, L. and Liu, Z.: A Numerical Flat Plate Friction Line and its Application. In: *Journal of Hydrodynamics* 25 (2015), S. 383–393

[7] ANSYS: *ANSYS FLUENT Documentation 12.1.* https://www.afs.enea.it/project/neptunius/docs/fluent/index.htm

[8] ANSYS: *ANSYS FLUENT Theory Guide.* 2011

[9] Cengel, Y. ; Cimbala, J. : *Fluid Mechanics, Fundamentals and Applications.* 2006

[10] community, C. : *CFD Online.* https://www.cfd-online.com/. Version: 1994

[11] community, T. S.: *Least-squares and curve fitting.* https://docs.scipy.org/doc/scipy/reference/generated/scipy.optimize.curve_fit.html#scipy.optimize.curve_fit. Version: 2023

[12] Davidson, L. : An Introduction to Turbulence Models. In: *Chalmers University of Thechnology* (2022)

[13] Dogrul, A. ; Song, S. ; Demirel, Y. : Scale effect on ship resistance components and form factor. In: *Ocean Engineering* 209 (2020), Nr. 107428. http://dx.doi.org/https://doi.org/10.1016/j.oceaneng.2020.107428.. – DOI https://doi.org/10.1016/j.oceaneng.2020.107428.

[14] Eca, L. ; Hoestra, M. : On the accuracy of the numerical prediction of scale effects on ship viscous resistance-computational methods in marine engineering. In: *CIMNE Barcelona, international conference on computational methods in marine engineering (MARINE 2005)* (2005)

[15] Grigson, C. : A planar friction algorithm and its use in analysing hull resistance. In: *Transactions of the Royal Institution of Naval Architects, RINA* 142 (2000), S. 76–115

[16] HSVA: *HSVA. The Hamburg Ship Model Basin.* https://www.hsva.de/facilities/large-towing-tank.html. Version: 2023

[17] Hughes, G. : Friction and Form Resistance in Turbulent Flow, and a Proposed Formulation for Use in Model and Ship Correlation. In: *Physical Laboratory: London, UK* (1954)

[18] ITTC: Brief Summary of written contributions. Proceedings of the 11th ITTC (1966)

[19] ITTC: Proceeding of the 24th ITTC. (2005)

[20] ITTC: Practical Guidelines for Ship CFD Applications. No. 7.5-03-02-03 (2011)

[21] ITTC: Practical Guidelines for Ship CFD Applications. No. 7.5-03-02-03 (2014)

[22] ITTC: 1978 ITTC Performance Prediction Method. ITTC Recommended Procedures and Guidelines. No. 7.5-02-03-01.4 (2021)

[23] ITTC: Resistance Test. ITTC Recommended Procedures and Guidelines. No. 7.5-02-02-01 (2021)

[24] Jespersen, D. ; Pulliam, T. ; Childs, M. : OVERFLOW Turbulence Modeling Resource Validation Results. In: *NAS Technical Report: NAS-2016-01* (2016)

[25] Katsui, T. : The proposal of a new friction line. In: *Fifth Osaka colloquium on advanced CFD applications to ship flow and hull form design, Osaka, Japan, 2005*, 2005

[26] Koren, D. : Computational Fluid Dynamics Unstructured Mesh Optimization for the Siemens 4th Generation DLE Burner. In: *School of Engineering Sciences, Department of mechanics, KTH, Royal Institute of Thecnology* (2015)

[27] Korkmaz, K. ; Werner, S. ; Bensow, R. : Numerical friction lines for CFD based form factor determination. In: *VIII Internatinal Conference on Computational Methods in Marine Engineering (MARINE)* (2019)

[28] Korkmaz, K. ; Werner, S. ; Sakamoto, N. ; Queutey, P. : CFD Based Form Factor Determination Method. In: *Ocean Engineering* (2020). http://dx.doi.org/10.1016/j.oceaneng.2020.108451. – DOI 10.1016/j.oceaneng.2020.108451

[29] Korkmaz, S. K.B. a nd W. K.B. a nd Werner ; Bensow, R. : Verification and Validation of CFD Based Form Factors as a Combined CFD/EFD Method. In: *Journal of Marine Science and Engineering* (2021). http://dx.doi.org/https://doi.org/10.3390/jmse9010075. – DOI https://doi.org/10.3390/jmse9010075

[30] Lasminto, U. ; Klasinc, R. : Numerical Modeling of a Y-Bifurcator using Realizable k-Turbulence Model Influence of the boundary layer in the numerical modeling for estimation coefficient losses of Y-Bifurcato. (2011)

[31] Lintermann, A. : *Computational Meshing for CFD Simulations*. Singapore : Springer Nature, 2021

[32] Liu, F. : A Thorough Description of How Wall Functions are Implemented in OpenFOAM. In: *Chalmers University of technology* (2017)

[33] Menter, F. R.: Two-Equation Eddy-Viscosity Turbulence Models for Engineering Applications. In: *AIAA Journal* 32 (1994), Nr. 8, S. 1598–1605

[34] Mewis, F. : Experience in using the form factor method. In: *Schiffbau Versuchsanstalt Potsdam, SVA*

[35] Mishra, P. : A review on selection of turbulence model for CFD analysis of air flow within a cold storage. In: *2nd International conference on Advances in Mechanical Engineering* (2018). http://dx.doi.org/10.1088/1757-899X/402/1/012145. – DOI 10.1088/1757–899X/402/1/012145

[36] Molland, A. ; Turnock, S. ; Hudson, D. : *Ship Resistance and Propulsion. Practical Estimation of Ship Propulsive Power.* United States of America : Cambridge University Press, 1991

[37] Oyan, E. : Speed and powering prediction for ships based on model testing. In: *Norwegian University of Science an Technology* (2012)

[38] Pas, S. ten: The Influence of Y+ in Wall Functions Applied in Ship Viscous Flows. (2016)

[39] Raven, A. ; Ploeg, A. van d. ; Starke, L. ; Eça: Towards a cfd-based prediction of ship performance - progress in predicting full-scale resistance and scale effects. In: *International Journal of Maritime Engineering. Transactions of the Royal Institution of Naval Architects Part A.*

[40] Sforza, P. : *Commercial Airplane Design Principles.* Butterworth-Heinemann, 2014. http://dx.doi.org/https://doi.org/10.1016/B978-0-12-419953-8.00012-7. http://dx.doi.org/https://doi.org/10.1016/B978-0-12-419953-8.00012-7

[41] Terziev, M. ; Tezdogan, T. ; Incecik, A. : A Geosim Analysis of Ship Resistance Decomposition and Scale Effectos with the Aid of CFD. In: *Applied Ocean Research* 92 (2019). http://dx.doi.org/https://doi.org/10.1016/j.apor.2019.101930.. – DOI https://doi.org/10.1016/j.apor.2019.101930.

[42] Tu, J. ; Yeoh, G.-H. ; Liu, C. : *Computational Fluid Dynamics. A Practical Approach.* 3. Katey Birtcher, 12018

[43] Wang, J. ; Yu, H. ; Feng, Y. : Feasible Study on Full-Scale Delivered Power Prediction Using CFD/EFD Combination Method. In: *Journal of Hydrodynamics* 31 (2019). http://dx.doi.org/https://doi.org/10.1007/s42241-019-0075-4.. – DOI https://doi.org/10.1007/s42241–019–0075–4.

[44] Wilcox, D. C.: *Turbulence Modeling for CFD.* La Canada, California : DCW Industries, Inc., 1993

[45] Wimshurst, A. : *Computational Fluid Dynamics Fundamentals.* https://www.fluidmechanics101.com/pages/lectures.html

A. Appendix

A.1. Curve Fitting

The curve fit for the numerical friction line is performed in Python [11] using the following function:

$$scipy.optimize.curvefit(f,\ xdata,\ ydata,\ p0 = None) \tag{A.1}$$

where

- f: is the model functionm in this case corresponds to the ITTC-57 formula for the friction coefficient. f(x, a, b, c) takes the independent value x as the fist argument, and the parameters to determine a, b, c as the remaining arguments)
- xdata: the independent variable, as input data.
- ydata: the dependent input data.
- p0 corresponds to the initial guess for the parameters, a, b, and c.

The output of the curve fit function corresponds to two arrays:

- opt: contains the optimal values for the parameters, a, b, and c.
- pcov: a 2-D arrays which diagonal provides the variance of the parameters estimate.

Python Curve Fit Code

```
1  import numpy as np
2  import matplotlib.pyplot as plt
3  import pandas as pd
4  import math
5  from scipy.optimize import curve_fit
6
7  df = pd.read_csv(r'MSST.csv')
8  df.head()
9
10 x_data = df['Log_Re'].to_numpy()
11 y_data = df['CF'].to_numpy()
12
13 def model_function(x, a, b, c):
14     return a/((x-b)**c)
```

```
15
16 popt, pcov = curve_fit(model_function, x_data, y_data, p0=[0.6,0,3])
17
18 a, b, c = popt
19 print("a:", a)
20 print("b:", b)
21 print("c:", c)
```

A.2. Model Ships Planes

LPP - 252.40 m	Volumen- 69117 m3	Lpp/ B - 6.767	cb - 0.6018
BSPT - 37.30 m	LCB - 121.24 m	B / T - 3.057	cm - 0.9809
TM - 12.20 m	- -1.96 %	CLV - 6.150	cp - 0.6135
Trim - 0.00 m	KMT - 17.31 m	Speed - 13.0 kn	cwp - 0.7888
		Fn-lpp - 0.134	

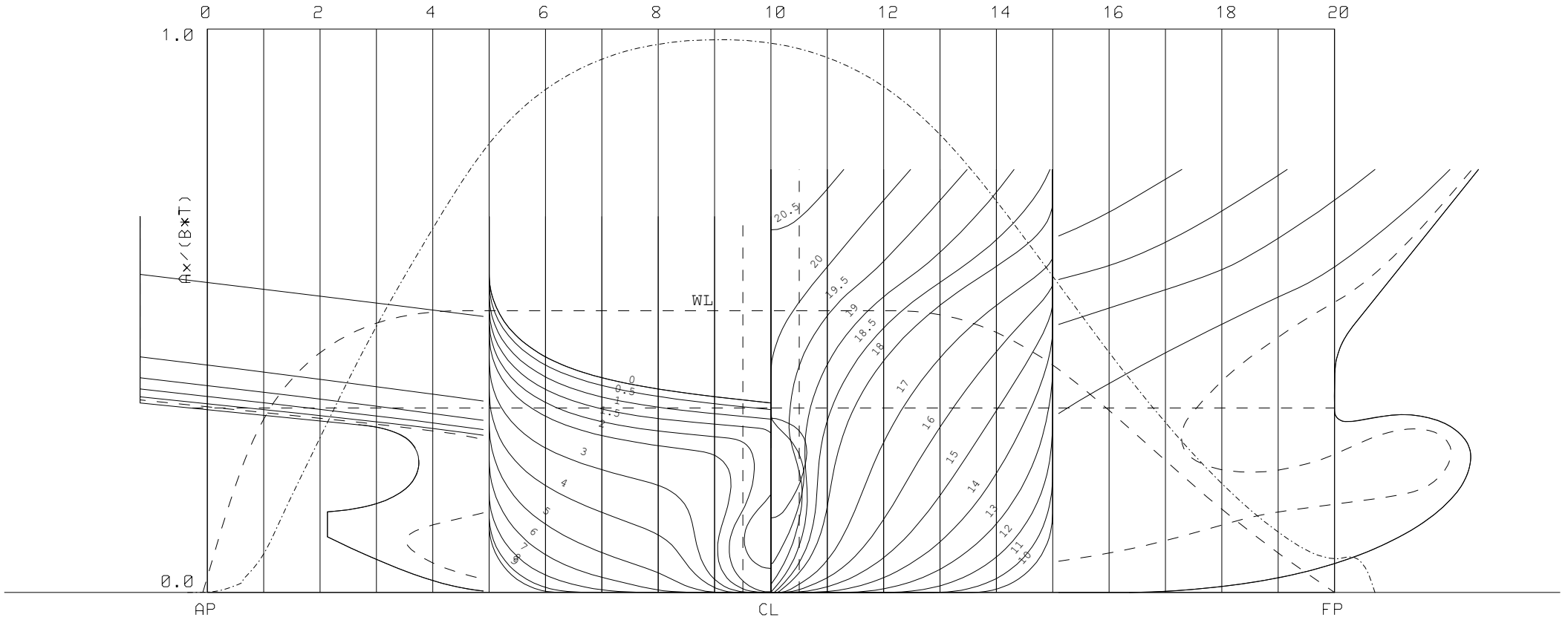

Model No.: M04500

HSVA	M04500/I1000
LPP 252.40	Date 2023-07-06
B 37.30	Time 12:51
D 12.20	Name PH

LPP	- 178.80 m	Volumen-	43045 m3	Lpp/ B	- 5.960	cb	- 0.8025
BSPT	- 30.00 m	LCB	- 91.09 m	B / T	- 3.000	cm	- 0.9965
TM	- 10.00 m		- 0.95 %	CLV	- 5.102	cp	- 0.8053
Trim	- 0.00 m	KMT	- 12.89 m	Speed	- 13.0 kn	cwp	- 0.9055
				Fn-lpp	- 0.160		

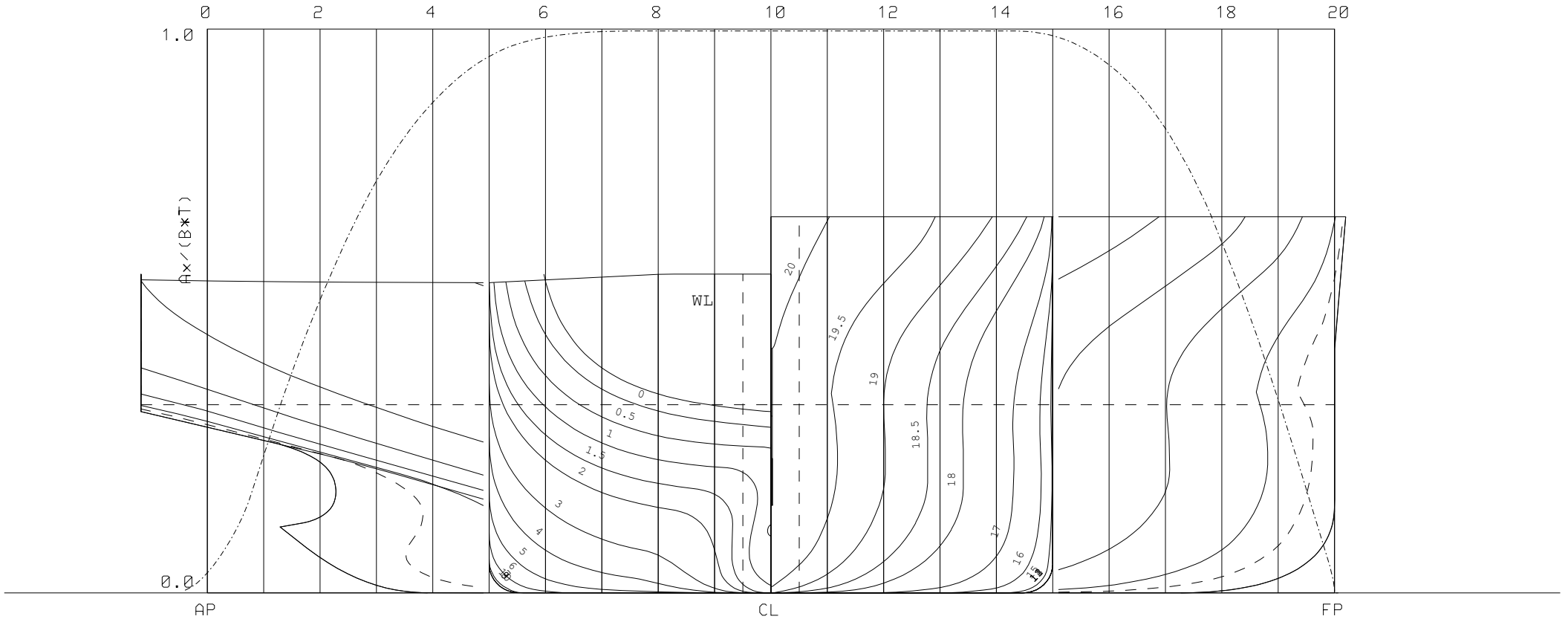

Model No.: M05500

HSVA	M05500 REF/I00000		
	LPP 178.80	Date	2023-07-06
	B 30.00	Time	12:49
	D 10.00	Name	PH

Declaration of authorship

I declare in an official manner by handwritten signature that I have written this thesis independently and without the use of any other resources than those indicated. All passages taken literally or in substance from other publications have been indicated. This also applies to drawings, sketches, illustrations and sources from the Internet.

I further declare that I have not submitted or will not submit the present work in any other examination procedure. (The submitted written version is identical to the electronically submitted version). I understand that if I submit an incorrect assurance, the thesis has to be considered as failed.

Rostock, July 31, 2023

María Tadea Quintuña Rodríguez